POLISH
ACADEMY
OF SCIENCES

COMMITTEE
OF MACHINE
ENGINEERING

SCIENTIFIC PROBLEMS OF MACHINES OPERATION AND MAINTENANCE

ZAGADNIENIA EKSPLOATACJI MASZYN

TRIBOLOGY • RELIABILITY • TEROTECHNOLOGY
DIAGNOSTICS • SAFETY • ECO-ENGINEERING

TRIBOLOGIA • NIEZAWODNOŚĆ • EKSPLOATYKA
DIAGNOSTYKA • BEZPIECZEŃSTWO • EKOINŻYNIERIA

4 (164)
Vol. 45
2010

Institute for Sustainable Technologies – National Research Institute, Radom

Mailing address: Scientific Problems of Machines Operation and Maintenance
Institute for Sustainable Technologies – National Research Institute
ul. Pułaskiego 6/10, 26-600 Radom, Poland
Phone (48-48) 364 47 90
E-mail: ewa.szczepanik@itee.radom.pl

The figures have been directly reproduced from the originals submitted by the Authors.

Publishing House of Institute for Sustainable Technologies – National Research Institute
26-600 Radom, K. Pułaskiego 6/10 St., phone (48-48) 364-42-41, fax (48) 364-47-65
www.tribologia.org

SCIENTIFIC PROBLEMS
OF MACHINES OPERATION
AND MAINTENANCE
4 (164) 2010

CONTENTS

SPIS TREŚCI

SCIENTIFIC PROBLEMS
OF MACHINES OPERATION
AND MAINTENANCE
4 (164) 2010

TOMASZ STAWICKI*, PAWEŁ SĘDŁAK*, ADAM KONIUSZY*

The testing of the influence of the roughness of the crankshaft journal upon the durability of the crankshaft bearing in engines of agricultural machines

Key words

Tribological tests, linear wear, durability, reliability, roughness.

Słowa kluczowe

Badania tribologiczne**,** zużycie liniowe, trwałość, niezawodność, chropowatość.

Summary

In the process of the operation of agricultural tractors and harvesters, it is necessary to perform periodical technical service related to the repair of the crankshaft bearings in Diesel engines. The solutions applied in machine finishing of crankshaft journals regenerated by grinding, make it necessary to run the same in operation, which results from the fact that working surfaces are not suitable for the conditions of use. Therefore, testing was initiated in order to establish whether the roughness of working surfaces of crankshaft journals obtained as a result of the repairs may have a considerable influence upon the limitation of durability of the journal-bushing sliding joint. Wear tests were performed in the model arrangement constituting material representation and, in the case of crankshaft journals, also the geometrical representation of real parts. The wear tests were performed for established sliding and load values with the assumption

* Agrotechnical System Engineering; Szczecin University of Technology; Papieża Pawła VI 1 Street, 71-459 Szczecin, Poland; e-mail: tomasz.stawicki@zut.edu.pl.

of variable roughness of roller modelling the crankshaft journals. On the basis of the statistical evaluation of the test results, it was shown that there is a significant relationship between the initial condition of microgeometry of the rollers as described by values of average arithmetic deviation of the profile from the medium line (parameter Ra) and the measure of linear use of the bush material of the sample.

Introduction

Slide bearings of the crankshaft of Diesel engines in agricultural machines constitute examples of sliding joints subject to complicated operating effects. Due to such conditions as the variability of loads and relative speeds as well as various conditions of use and operation, it is difficult to forecast the durability and reliability of the slide bearings. This also means that indicated service intervals and repair activities as well as the expected time of normative and inter-repair courses may be burdened with a considerable degree of uncertainty. In considering the above and the observed practice of users' failure to comply with due dates for technical inspections as well as errors relating to interpretation of the operation manual [Bujak 2003], it may be concluded that discrepancies between manufacturers' forecasts and the needs conditioned upon technical condition of the machines are even greater. A significant problem is connected with agricultural machines subject to post-guarantee repairs. As results from the tests performed indicate, as many as 50% of farmers decide to make repairs on their own [Płocki 2005]. In the event of the absence of appropriate knowledge and technical support in most cases, it is justified to suspect that the quality of such repairs is rather poor [Tomczyk 2009].

Results of the author's tests indicated that the use of regenerative grinding and smoothing of crankshaft journals during repairs does not fulfil the condition for adjustment of the part for the acceptance of the full range of operating loads from the start of the process of use [Stawicki 2006]. It was established that microgeometry of the technologically obtained roughness of the journals does not correspond to the surfaces obtained in the process of operating run-in. The condition of the surface of the journals following finishing machining during repairs mostly corresponded to the roughness of Class 8 according to PN 87/M04251, i.e. *Ra* within the range of 0.33-0.63 μm (frequently $Ra > 0.63$ μm), where the tested run-in parts were characterised by average the arithmetic deviation of the profile from the average line below 0.20 μm. This may be opposed to the proposal of the optimisation of use of the normative durability of sliding joints, which provides that shaping of technological roughness, which is possibly close to the microgeometry typical of the operating top layer, and should result in shortening of the time of the adjustment of working surfaces to the conditions of use, the limitation of intensity of use during running in and, as a consequence, larger reserves of the part material for normal wear and tear [Burakowski; Marczak 2000; Legutko, Nosal 2004].

A possible favourable variant of repair should result in the susceptibility of working surfaces to the shaping of balanced roughness during the short period of operating running-in. It is thought that the balanced condition of the surface ensures minimum values of potential energy and the least dissipation of energy in given conditions of friction cooperation [Kombałow 1974], which, in turn, is identified with thermodynamic stability and the resistance of the top layer to tribological wear [Sadowski 2009]. From the current testing experience, it appears that the presently applied technological solutions (structural, materials, and machining) do not comply with the above-mentioned proposal of the preparation of the working surfaces. This is confirmed by the results of tests of the microgeometry of surfaces of the crankshaft journals that, after the recommended periods of operating running-in, were characterised by greater roughness than after machining during the process of repair [Śliwiński 1990, Wanke 1997].

As it has already been shown, it is difficult to obtain recurrent and optimum machining effects with respect to shaping of microgeometry of working surfaces of crankshaft journals in the repair practice. The question is, whether the initial condition of surfaces of journals may have significant effects upon the durability of the entire sliding joint. If the answer to the question is yes, the current methods of the repair of sliding joints should be verified and the adopted criterion of their evaluation should involve the possibility of the standardisation of the initial condition and the standard may also involve the balanced condition of friction surfaces.

Materials and methods

The author's own tests aimed at the verification of the influence of the roughness of working surfaces of journals in regenerated crankshafts upon the durability of the journal-bushing sliding joint. Therefore, laboratory wear tests were performed in the model arrangement, which constituted the material representation and, in the case of the journal, a geometrical representation of the real system of the sliding joint. The tested sliding joint is presented in Fig. 1. The rollers (1) were made of 40 HM steel in accordance with the technology of the shaping of utility properties of crankshaft journals: tempered on 51÷53 HRC and then subject to the grinding process with the parameters corresponding to machining finishing of such parts as the roller. The grinding parameters used made it possible to select two groups of rollers with roughness parameters corresponding approximately to limits of Classes 8 and 9 (selection on the basis of the value of *Ra* parameter). The other ground rollers were subject to smoothing or roughing with the use of sandpaper with appropriate grit size. This made it possible to select another two groups of rollers that were characterised by roughness corresponding to limits of Classes 10 and 9 (Table 1 shows the results of measurements of *Ra* parameter of surfaces of the rollers used in the tests). Samples (2) in the form of plates with measurements of 7.5x20 mm were made of bimetal tape before shaping them in the form of semi-bushings of bearing slides of the crankshaft in engines of agricultural tractors.

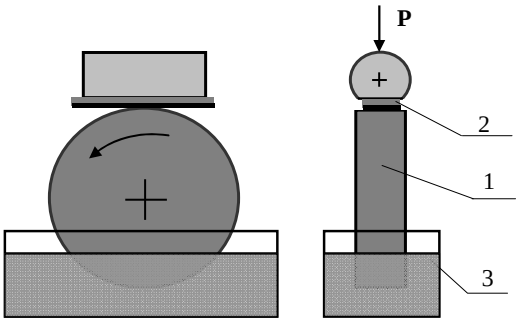

Fig. 1. Accepted configuration of the tested joint: 1 – sample of steel 40HM, 2 – sample of bearing alloy, 3 – engine oil
Rys. 1. Przyjęty układ węzła testowego: 1 – rolka ze stali 40 HM, 2 – próbka ze stopu łożyskowego, 3 – olej silnikowy SUPEROL CC 30

Table 1. Roughness of rollers used in the wear tests
Tabela 1. Chropowatości rolek zastosowanych w badaniach zużyciowych

Roller No.	Average roughness according to Ra [μm]	Standard deviation s [μm]	Limits of roughness classes according to PN 87/M04251 [μm]	Rollers qualified for roughness classes
1	0.17	0.04	0.16	10
2	0.14	0.02		
3	0.17	0.03		
4	0.15	0.03		
5	0.18	0.03		
6	0.32	0.11	0.32	9
7	0.27	0.04		
8	0.27	0.05		
9	0.31	0.09		
10	0.32	0.06		
11	0.61	0.08	0.63	8
12	0.59	0.07		
13	0.57	0.06		
14	0.61	0.04		
15	0.69	0.08		
16	1.15	0.09	1.25	7
17	1.12	0.10		
18	1.28	0.15		
19	1.21	0.07		
20	1.13	0.11		

The friction tests were made with the use of the following determined forced values:

- Load P = 368 N,
- Sliding speed v = 1 m/s,
- Wear test time t = 1800 s.

SUPEROL CC 30 engine oil was used as a lubricant used in agricultural industry.

During the friction tests, linear wear of the bushing material (measurements of the depth of wear trace in the sample), the temperature of the lubricant, and the resistance of roller movements were recorded. After each testing run, measurements of the surface of rollers were made with the use of a profiler in order to determine the influence of operating parameters of the tested joint upon qualitative and quantitative changes of the initial roughness of the counter-samples.

Presentation and evaluation of the test results

Table 2 includes the results of tests on linear wear of Z_i samples as compared to the values of the parameter *Ra* roughness of rollers used in subsequent friction tests. The results of measurements with the use of a profiler are also presented. The results are related to the evaluation of the condition of the surface of counter-samples and were obtained following the wear tests.

Table 2. The comparison of results of measurements of the rollers with the use of a profiler and linear wear of the samples
Tabela 2. Zestawienie wyników badań profilografometrycznych rolek oraz zużycia liniowego próbek

Friction pair No.	Data relating to roughness of counter-samples (rollers)		Data relating to wear of the samples	
	Before the test *Ra* [μm]	After the test *Ra* [μm]	Z_i [mm]	$Z_{i\,śr}$ [mm]
1	0.17	0.38	0.021	
2	0.14	0.33	0.042	
3	0.17	1.04	0.122	0.047
4	0.15	0.36	0.022	
5	0.18	0.33	0.028	
6	0.32	0.30	0.029	
7	0.27	0.36	0.104	
8	0.27	0.38	0.020	0.071
9	0.31	0.29	0.101	
10	0.32	0.49	0.103	
11	0.61	0.52	0.200	
12	0.59	0.76	0.143	
13	0.57	0.56	0.299	0.233
14	0.61	0.57	0.153	
15	0.69	0.65	0.370	
16	1.15	1.08	0.495	
17	1.12	1.03	0.583	
18	1.28	1.24	0.638	0.600
19	1.21	1.22	0.658	
20	1.13	1.22	0.600	

On the basis of the statistic evaluation of the *Ra* value, it was found that operating conditions of the tested joint in the case of friction pairs numbered from 1 to 5 resulted in a significant increase of the roughness of counter-samples. The greatest degree of roller roughness and, at the same time, the greatest degree of sample wear, applied to the Friction Pair 3. The tests confirmed that the value of *Ra* increased six times (from 0.17 to 1.04 μm), and the measure of wear of the sample bushing material increased approximately three times as compared to wear of the remaining samples cooperating with rollers of the same roughness class. The observed relationships are reflected in the course of changes of the friction moment in the function of time of the testing run (Fig. 2) – the third pair is characterised by greatest resistance of movements.

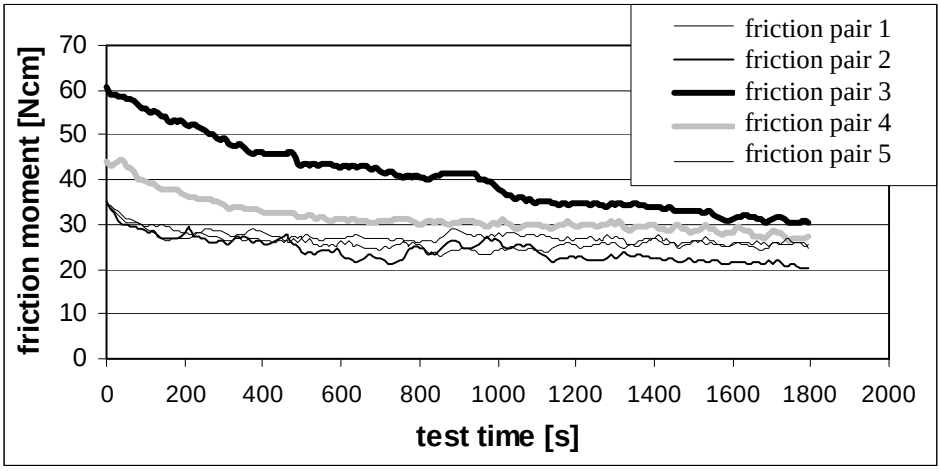

Fig. 2. The course of changes of the friction moment $M_t = f(t)$ for applied rollers of Class 10
Rys. 2. Przebieg zmian momentu tarcia $M_t = f(t)$ dla zastosowanych rolek klasy 10

In the event of rollers qualified as roughness Classes 7, 8 and 9, no significant changes in microgeometry as described by *Ra* values were observed after the wear tests. However, the quantitative evaluation of the roughness of the rollers does not explain the differences in the measure of the wear of the rollers and, in particular, in the case of tests, for which rollers qualified as roughness Class 9 were used. In order to identify the cause of the above, qualitative evaluation of the microgeometry of the surface of rollers was performed following the wear tests. Roughness profiles as well as corresponding courses of the curve of the material ratios were evaluated. It was established that the qualitative differences in the topography of particular rollers might have affected the degree of sample wear. In order to confirm that this observation is justified, the comparison of Roller 6 roughness profiles (Z_i = 0.29 mm) and Roller 7 roughness profiles (Z_i = 0.104 mm) as well as corresponding material

ratios are presented in Fig. 2. Roller 7 is characterised by a steeper course of the curve of material ratio as compared to counter-sample 6, which proves lesser bearing of its surface. As for the determined values of external forces, lesser bearing share means greater unit pressures, and this could result in the observed intensification of destructive effects in the area of the friction contact.

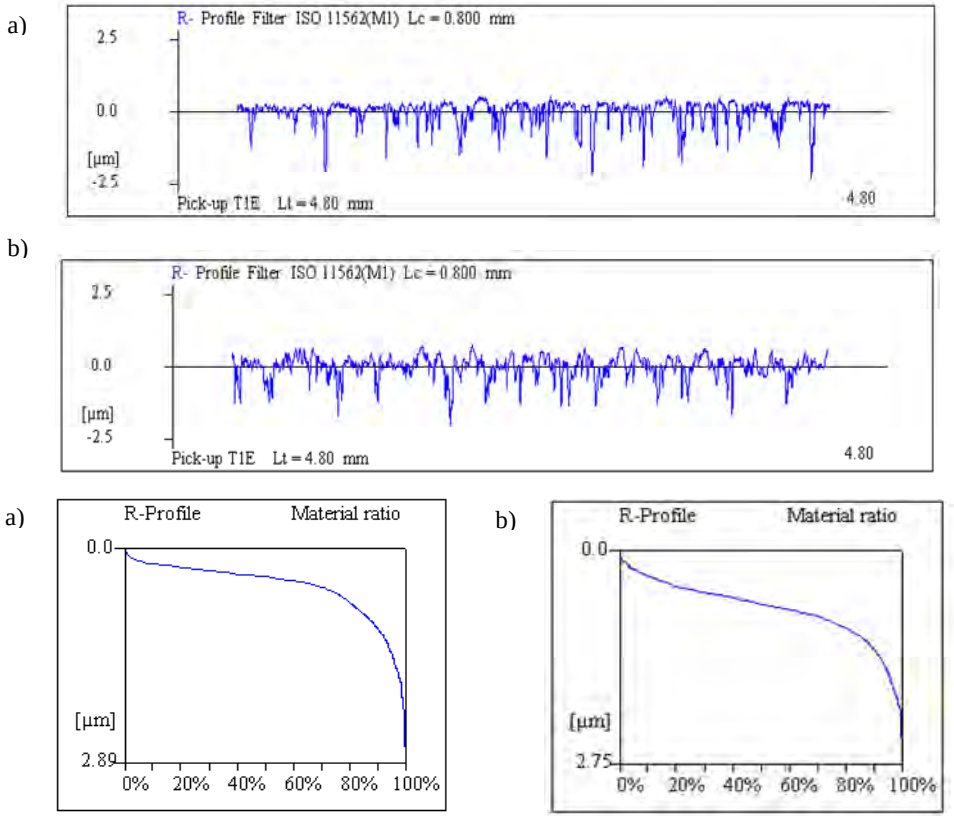

Fig. 3. Comparison of roughness profiles and material ratios of surfaces of selected rollers: a – Roller 6, b – Roller 7
Rys. 3. Porównanie profili chropowatości i udziałów materiałowych powierzchni wybranych rolek: a – rolka 6, b – rolka 7

Despite the discrepancies shown with respect to the wear of particular samples cooperating with counter-samples of a given roughness class, it may be concluded that wear depends on roughness classes of the rollers. This relationship was interpreted in the form of characteristics of $Z_I = f(Ra)$, presenting average values of linear wear of samples depending on roughness of the rollers (Fig. 4). The model of linear regression was chosen for the

description of the measure of the wear of samples as a function of condition of roller surfaces, because this model ensures best adjustment to empirical data. On the basis of the statistical evaluation of the adopted regression model, a significant relationship between the linear wear of samples and the value of the roughness of the rollers was shown (Student and Fischer-Snedecor tests were used – relevance level $\alpha = 0.01$). The obtained adjustment of the trend line to the experimental data (determination coefficient $R^2 = 0.98$) also indicates the possibility to forecast the value of linear wear of samples depending on a given value of the *Ra* parameter of the roller surface. This proves the practical suitability of the *Ra* parameter as a criterion of the evaluation of the quality of repair of real part working surfaces.

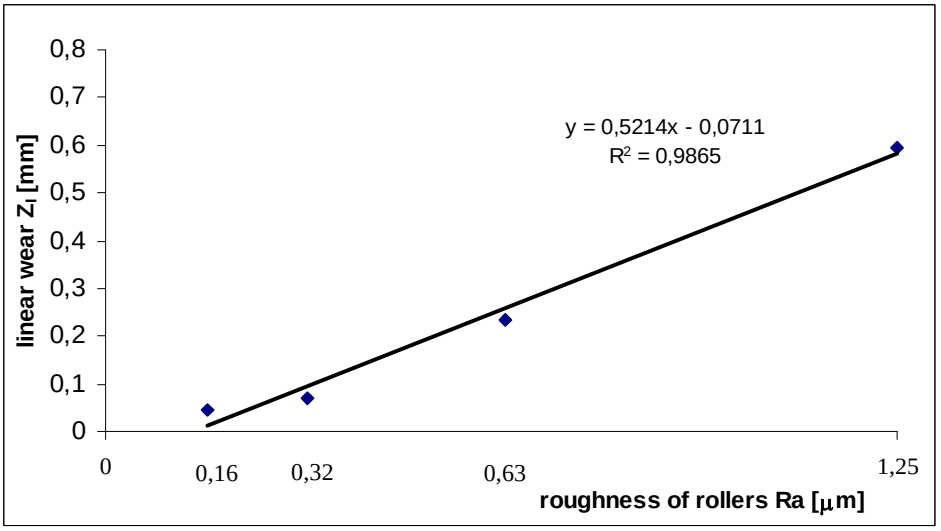

Fig. 4. The relationship between the measure of wear of the samples and average values of roller roughness surface – *Ra*
Rys. 4. Zależność miary zużycia próbek od średnich wartości *Ra* chropowatości powierzchni rolek

On the basis of the analysis of the course of wear tests, it was found that changes of the parameters of various intensity describing the cooperation of the tested joint element, i.e. temperature of the lubricant (T), friction moment (M_t) and wear (Z_i) in the function of time of the testing course corresponded to particular tribological tests. On the basis of the comparative analysis, it was found that there is a correlation between the condition of the microgeometry of the rollers and the recorded characteristi cs $Z_i = f(t)$, $T = f(t)$ and $M_t = f(t)$, and we may talk about a typical variability of the tribological parameter values for a given class of roughness of the rollers. In order to confirm this observation, Fig. 5 shows the comparison of test results for selected and representative friction pairs.

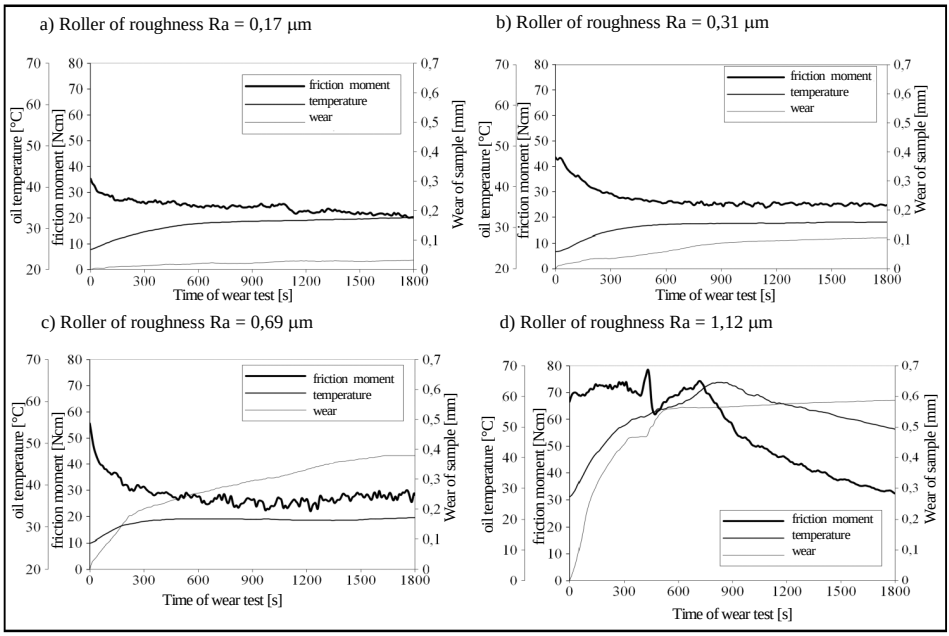

Fig. 5. The comparison of research test results for selected friction pairs, for which rollers of various roughness classes were used

Rys. 5. Porównanie wyników testów badawczych wybranych par tarcia, w których stosowano rolki różnych klas chropowatości

The presented results prove the significance of microgeometry of the rollers for the intensity of mechanical and power engineering effects occurring within the friction area. The greater degree of roughness corresponds to the increase of sample wear and to the less stable conditions of friction cooperation.

Summary and conclusions

Referring the obtained test results to the journal-bushing friction joint, one has to consider the different character of the friction contact of cooperating elements and different range of external force values in real conditions (relative speeds and loads) as compared to the prescribed test conditions. However, this does not mean that the indicated real relationship between the wear of the bushing material and condition of roughness of the roll modelling the crankshaft journal is not applicable to operating practice. There are two main arguments in favour of this as follows:

− Technologically shaped roughness of working surfaces of the journals does not correspond to the microgeometry of the part running-in during a long period of time.

− In undetermined (start up, stop, operating overload) conditions typical of agricultural machines, we may deal with the contact of friction counter-surface and, in the case of failure to adjust to acceptance of external forces, with accelerated wear of part materials.

Having considered the above and the results of the statistical evaluation of the wear tests performed, it may be concluded that there is a significant dependency of durability of the journal-bushing sliding joint on the initial condition of the top layer of crankshaft journals in agricultural engines. This means that the shaping of the technological roughness of the journal, which is different from the optimum condition obtained during the operating running-in process, proves that the sliding joint is not adjusted to conditions of cooperation and, consequently, has effects upon the limitation of its operation time until reaching admissible wear.

References

[1] Bujak T.: Gdy nowy ciągnik szwankuje. Rolniczy Przegląd Techniczny, 10/2003, s. 47.
[2] Płocki K.: Serwis ciągników. Rolniczy Przegląd Techniczny, 4/2005 s. 32.
[3] Tomczyk W.: Obsługi techniczne maszyn i urządzeń rolniczych w praktyce. Inżynieria Rolnicza 6(115)/2009, s. 295–300.
[4] Stawicki T.: Wpływ modyfikacji powierzchni roboczych na cechy użytkowe łożysk ślizgowych wybranych maszyn rolniczych. Rozprawa doktorska, Szczecin 2006.
[5] Burakowski T., Marczak R.: Badania eksploatacyjnej warstwy wierzchniej, [w:] Tribologia I tribotechnika, Wydawnictwo Instytutu Technologii Eksploatacji, Radom 2000.
[6] Legutko S., Nosal S.: Kształtowanie technologicznej i eksploatacyjnej warstwy wierzchniej części maszyn, Ośrodek Wydawnictw Naukowych PAN, Poznań 2004.
[7] Kombałow W.: Wlijanie szepochowatosti twierdych tieł na trienie i iznos. Nauka, Moskwa 1974.
[8] Sadowski J.: Dyssypacja i akumulacja energii jako czynniki warunkujące trwałość par tarciowych. Tribologia 2009, vol. 40, nr 3, s. 219–226.
[9] Śliwiński W.: Proces docierania metalowych par trących w warunkach smarowania. Zeszyty Naukowe Politechniki Krakowskiej. Mechanika, z. 71, Kraków 1990.
[10] Wanke P., Dreszczyk E.: Wytwarzanie wielostrefowych warstw tribologicznych na czopach w fazie docierania. Zbiór prac konferencyjnych „Problemy Niekonwencjonalnych układów łożyskowych". 15–16 maja 1997.

Badanie wpływu chropowatości czopa na trwałość łożyskowań mechanizmu korbowego silników maszyn rolniczych

S t r e s z c z e n i e

W procesie eksploatacji ciągników rolniczych i kombajnów zbożowych zachodzi potrzeba okresowego wykonania obsługi technicznej w zakresie naprawy łożyskowań mechanizmu korbowego silników spalinowych. Stosowane rozwiązania techniczne w zakresie obróbki

wykańczającej, regenerowanych szlifowaniem czopów wałów korbowych wymuszają jednak potrzebę ich docierania eksploatacyjnego, co jest efektem nieprzystosowania powierzchni roboczych do warunków użytkowania. W związku z tym podjęto badania zmierzające do ustalenia, czy uzyskiwany w naprawach stan chropowatości powierzchni roboczych czopów wałów korbowych może istotnie wpływać na ograniczenie trwałości węzła ślizgowego czop––panewka. Wykonano badania zużyciowe w układzie modelowym stanowiącym odwzorowanie materiałowe, a w przypadku czopów również geometryczne części rzeczywistych. Testy zużyciowe realizowano przy ustalonych wartościach prędkości ślizgania i obciążenia, przyjmując za zmienną chropowatość powierzchni rolek modelujących czopy wały korbowego. Na podstawie oceny statystycznej wyników badań wykazano, że istnieje istotna zależność między stanem początkowym mikrogeometrii rolek, opisanym wartościami średniego arytmetycznego odchylenia profilu od linii średniej (parametr Ra), a miarą liniowego zużycia materiału panewkowego próbki.

SCIENTIFIC PROBLEMS
OF MACHINES OPERATION
AND MAINTENANCE
4 (164) 2010

STANISŁAW ŚCIESZKA*, WOJCIECH GRZEGORZEK*,
MARCEL ŻOŁNIERZ*

Laboratory methods for combined testing of abrasiveness, grindability and wear in coal processing systems

Key words

Abrasiveness, grindability, wear resistance.

Słowa kluczowe

Własności ścierne, kruszalność, odporność na zużycie.

Summary

Laboratory methods were developed which involved the use of the three new rigs simulating the grinding action found in the majority of existing types of coal mills. All three rigs combine abrasion and erosion in comminution process. The objective of this investigation was to develop a tests procedure that would be suitable for general use in estimating the abrasiveness of particular coal, and to study the abrasive wear in various grinding systems. Three separate industrial problems involving coal grinding were investigated by means of the novel apparatus. The results from the relatively simply laboratory procedures, designed and operated according to the principles of similarity, may be used to predict the service life of grinding machine elements. The tribo-testing procedure and apparatus can be used to evaluate the abrasiveness of any granular coal and for testing the wear resistance of any material in abrasive or erosive action.

* Silesian University of Technology, Faculty of Mining and Geology, Institute of Mining Mechanisation, Akademicka 2A Street, 44-100 Gliwice, Poland; e-mail: stanislaw.scieszka@polsl.pl.

Introduction

The operating cost of a coal milling plant is directly affected by the throughput rate of a fossil fuel through a mill, the power requirements of the mill, and the wear rate of the internal components of the mill. Thus, the coal properties that affect wear, such as abrasiveness, grindability, and the wear resistance of materials used for the manufacture of the grinding element, are of direct interest in this investigation. The presently available indices do not adequately describe coal properties in terms of the required information.

It is clear that there is no such thing as an intrinsic friction property of a material [1]. The same applies to other tribological material properties such as wear resistance and abrasiveness. These properties are system properties in which the given material is only one of the parameters. A carefully designed simulation in which isolated mechanical components undergo similar processes as in a complex engineering environment can only determine material performance in such a system. If the engineering environment includes processes such as abrasion and comminution, both of them must be incorporated into simulation [2], see Appendix A.

There is a complicated energy balance inside the mills during a mechanical crushing process. Crushing results in energy conversion from one form to another, including such primary energy absorbing processes as the creation of new surfaces, plastic deformation, elastic deformation, vibration and noise. In secondary energy dissipation processes, most of the energy expended in internal and external friction is converted to heat. Other factors influencing size reduction and wear processes are the distribution of coal internal weaknesses [3-6], e.g. cracks, the concentration and size of hard particles such as quartz and environmental effects, such as moisture, and the presence of chemically active gases which affect the fracture process [7-13]. Parameters affecting the grinding process can be summarised under three headings [3, 4, 14]:

1. Mineral:
   – hardness,
   – abrasiveness,
   – particle size, shape,
   – mineralogy, etc.
2. Mill:
   – mechanical properties of components,
   – microstructure of components,
   – size of mill,
   – speed of moving elements, etc.
3. Mill environment:
   – water chemistry and pH,
   – slurry rheology,
   – temperature,
   – chemically active gases, etc.

The effective action in breaking appears to be almost always tensile or shear, since compressive strength is usually greater than tensile strength, and some minerals are brittle under tension and ductile under compression. Elementary forces acting on a single grain within the majority of mills are predominantly compressive and shear. The use of compressive force in grinding machines is one of the sources of inefficiency in the comminution processes. A large number of different mills can be classified according to many criteria but the most common is classification according to purpose and principal comminuting action [3].

For the purpose of simulative testing of coal performance in comminution and abrasive/erosive interaction with grinding elements, the following classification is proposed (Fig. 1):

1. Static three-body interaction by means of direct static stressing-nipping machines, e.g. ball-race mills;
2. Low speed three-body interaction by means of inertial forces in the presence of grinding media, produced by gravity-tumbling machines, e.g. ball and rod mills; and,
3. High-speed direct impact interaction by means of inertial forces produced by mechanical means-impacting machines, e.g. hammer and beater mills.

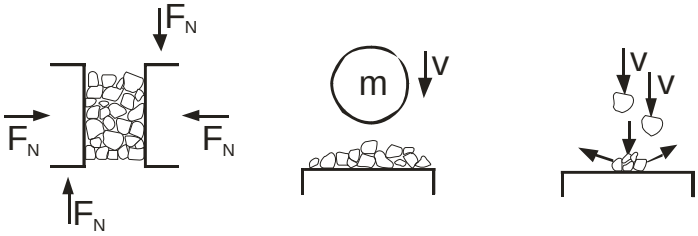

Fig. 1. Simple representation of three kinds of interactions between coal particles and grinding elements in comminution
Rys. 1. Uproszczone przedstawienie trzech rodzajów oddziaływań między cząstkami węgla a elementami mielącymi w procesie rozdrabniania

In all three classes of equipment with different mechanics of action, the tribological conditions are described by the pressure distribution, peak pressure, gradient of sliding velocity, impact speed, temperature inside the grinding zone of the mineral [15-24] and many other factors.

The procedure for adjusting the operating variables in simulated tribotesting is shown in Figs. 2-4. More accurate modelling procedures for the grinding and wear processes in all three classes of mills are presented in Refs. [22-25].

Basic mechanical properties of particulate material

The comminution process continues until all individual coal particles are small enough to leave the mill. The time taken for such a particle to be produced from the initial charge is a function of the efficiency of the mill and a property of

the coal that determines the ease with which it is broken up. Empirical factors which are used at present to determine the rate at which comminution proceeds are known as the Hardgrove Index (*HGI*) and Bond Work Index, *Wi* [3, 26, 27].

The abrasiveness of a coal can be determined in a number of ways, and the traditional method for coal is based on the procedure given by Yancey, Geer, and Price [28] and described more fully in British Standard [29] as the Index of Abrasion (*AI*).

Each of these indices measures a given property of the coal, but the wear in a mill is a composite of these two separate factors, since the easier it is to crush a mineral, the less time the particle will spend in the wear process inside the mill, and the lower the abrasiveness of the mineral, resulting in a lower overall wear rate. The methods of testing presented in Figs. 2-4 combine both comminution and wear, but only in the method presented in Fig. 2 is any particle which reaches a predetermined size ejected from the grinding area through the annulus between the grinding bar holder and the stationary cylinder. In this method, the shear process is accompanied by wear of the bar. The grains of mineral become ground to a greater or lesser degree that can be determined by the index of comminution (*IC*). This index characterises the ease of pulverisation of coal. A prepared sample of coal receives a given amount of grinding energy (energy input), and the change in size is determined by sieving. The index of comminution (*IC*) of coal, for example, is expressed in milligrams of pulverised coal (fraction below 75 μm particle size) per Joule of energy input.

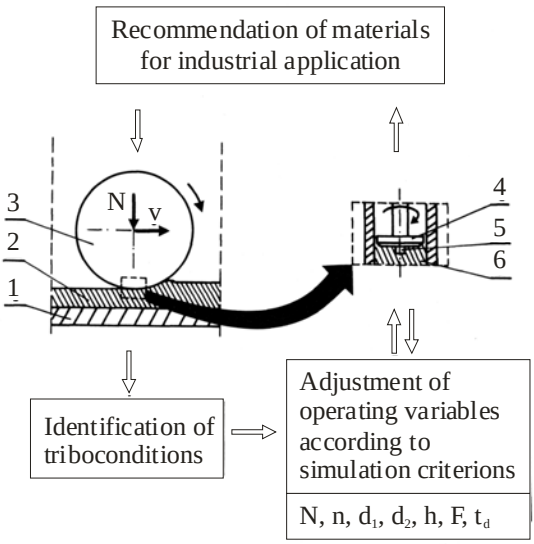

Fig. 2. Simulative tribo-testing of phenomena inside nipping mills such as ball-race within which static three-body interaction by means of direct static stressing prevails, where: 1 – bottom ring or pan; 2 – bed of coal; 3 – ball or roller; 4 – disc; 5 – bar; 6 – bed of coal

Rys. 2. Tribologiczne badanie symulacyjne zjawisk zachodzących wewnątrz młynów kulowych, w których przeważa statyczne ściskanie warstwy węgla poprzez toczące się kule, gdzie: 1 – pierścień dolny; 2 – warstwa węgla; 3 – kula albo wałek; 4 – tarcza; 5 – próbka; 6 – warstwa węgla

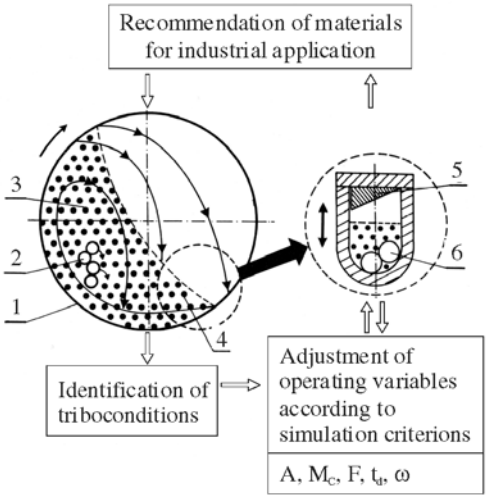

Fig. 3. Simulative tribo-testing of phenomena inside tumbling mills such as ball and rod mills within which low speed three-body interaction by means of inertial forces produced by gravity prevail, where: 1 – mill shell and lining; 2 – mill charge; 3 – tumbling zone; 4 – impact zone; 5 – lining; 6 – balls

Rys. 3. Tribologiczne badanie symulacyjne zjawisk zachodzących wewnątrz młynów bębnowych, takich jak młyny kulowe i prętowe, w których dominujące oddziaływania na warstwę węgla pochodzą od siły bezwładności ładunku w polu grawitacji, gdzie: 1 – osłona i wykładzina młyna; 2 – ładunek młyna; 3 – strefa rozdrabniania; 4 – strefa uderzenia; 5 – wykładzina; 6 – kulki

The relative displacement between the layers of particulate coal and the bar's surface provides the abrasion wear of the bar material due to coal particles sliding across the surface. They may also move relative to one another, and they may rotate while sliding across the wearing surface. In a ball-mill grinding situation, as well as in a laboratory test apparatus, the high stress abrasion occurs where the hard particles are crushed. The abrasion factor (AF) and the intensity of abrasion (IA) represent the abrasion property of coal. The abrasion factor (*AF*) is the mass of metal lost by abrasion from a carbon steel bar when rotated in a specified mass of mineral under specified conditions, expressed in milligrams of metal lost per kilogram of pulverised coal. The second parameter, intensity of abrasion (*IA*), does not include the mineral size reduction effect during the tests and is expressed in milligrams of metal lost in one second from one square meter of the bar's surface exposed to abrasive wear. Wear resistance (*WR*) and relative resistance (ε) give the best indication of the material's resistance to wear. Wear resistance (*WR*) is represented as the energy input required to wear the bar when rotated in a specified mass of coal under specified conditions expressed in megajoules of energy input per gram of metal lost. Relative wear resistance (ε) is the ratio between the wear resistance of the testing material and the wear resistance of a standard material (carbon steel). For experimental results presentation the following set of calculation formulae are used:

Wear of blade $$\Delta W = m_1 - m_2 \tag{1}$$

Energy input $$EI = 2\pi Ti \quad \text{or} \quad EI = 0.3\omega^3 A^2 M_C t_d \tag{2}$$

where $$T = \frac{1}{t_d}\int_0^{t_d} T(t)dt \tag{3}$$

Abrasion and erosion factor $$EF = AF = \frac{\Delta W}{PC}10^6 \tag{4}$$

Intensity of abrasion $$IA = \frac{\Delta W}{St_d} \tag{5}$$

where S is the area of blade surface exposed to wear (m^2)

Work index $$W_i = W\left(\frac{F}{F-P}\right)^{0.5}\left(\frac{P}{75}\right)^{0.5} \tag{6}$$

Index of comminution $$IC = \frac{PC}{EI}10^3 \tag{7}$$

Wear resistance of material $$WR = \frac{EI}{\Delta W}10^{-6} \tag{8}$$

Relative wear resistance of material $$\varepsilon = \frac{WR_{specimen}}{WR_{standard}} \tag{9}$$

A series of tests have been performed on nineteen coals in order to determine the parameters of interest in comminution and wear [17, 18]. Additional targets of the investigation were the comparison between various methods of testing grindability and abrasiveness of minerals, including the standard methods, and the proposed new method, as well as the determination of the properties of the most abrasive coal which was used in the following wear resistance investigation (Table 1).

The abrasiveness of the coals (*AF* and *IA*) tested in the various material configurations (standard carbon steel and chrome cast iron) show relatively different results (Table 1). Therefore, the abrasive property of a mineral should be tested with bars made from materials currently used for the balls and the races. Only those results from tests that completely simulate operational and material conditions in industrial mills can be applied directly to design calculations.

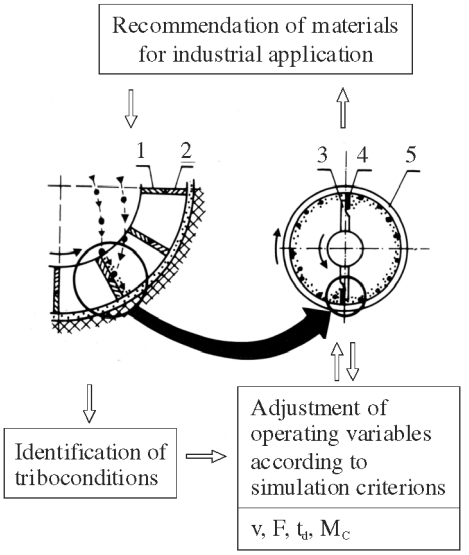

Fig. 4. Simulative tribo-testing of phenomena inside impacting mills, such as beater mills, within which high speed impact interaction by means of mechanical inertial forces prevail, where: 1 – inner beater plate; 2 – outer beater plate; 3 – rotating paddle; 4 – specimen; 5 – rotating drum
Rys. 4. Tribologiczne badanie symulacyjne zjawisk zachodzących wewnątrz młynów udarowych, takich jak młyny bijakowe, w których dominuje oddziaływanie pochodzące od dużych prędkości uderzenia i towarzyszących im sił bezwładności, gdzie: 1 – wewnętrzna płyta bijaka; 2 – zewnętrzna płyta bijaka; 3 – wirująca łopatka; 4 – próbka; 5 – wirujący bęben

Table 1. Basic mechanical properties of tested coals
Tabela 1. Podstawowe własności mechaniczne badanych węgli

No Of Coal	Quartz	Pyrite	*HGI*	*AI*	*IC*	*Wi*	Standard carbon steel		Chrome cast iron	
							AF_S	IA_S	AF_C	IA_C
	%	%	-	mg/kg	mg/J	J/g	mg/kg	mg/m^{2}s	mg/kg	mg/m^{2}s
1	0.5	0.5	60.8	5.2	0.682	1724	45	31	3.8	3.8
2	3.0	0.5	77.3	13.9	0.711	1482	141	101	12.6	12.6
3	6.2	1.5	63.9	70.2	0.895	1149	1468	1590	105.0	105.0
4	4.0	1.3	61.4	14.6	0.740	1657	181	142	16.2	16.2
5	9.0	1.5	71.0	151.5	0.876	1140	3530	3594	193.0	193.0
6	4.8	0.0	77.1	54.0	0.740	1423	903	720	81.7	81.7
7	2.6	2.5	64.6	16.1	0.452	1416	206	68	22.5	22.5
8	6.5	1.5	60.4	98.9	0.631	1343	2209	1175	152.0	152.0
9	2.7	1.5	62.2	57.6	0.806	1350	1621	1463	168.0	168.0
10	1.7	0.0	55.8	10.8	0.704	1602	92	66	13.2	13.2
11	4.3	0.0	73.5	46.0	0.816	1264	1557	1424	80.4	80.4
12	10.0	0.0	52.7	93.6	0.715	1599	1192	827	46.8	46.8
13	2.2	5.5	62.5	38.5	0.700	1469	440	328	28.5	28.5
14	6.0	1.2	68.2	67.2	0.776	1297	2027	1684	47.2	47.2
15	5.4	0.0	65.7	58.5	0.892	1150	1092	1126	82.4	82.4
16	5.7	0.0	66.4	48.1	0.759	1452	1153	840	45.0	45.0
17	15.5	70.1	70.1	55.0	0.741	1244	660	492	45.4	45.4
18	7.0	68.1	68.1	31.5	0.844	1255	719	679	66.6	66.6
19	8.0	49.0	49.0	18.8	0.747	1522	135	110	10.7	10.7

Some considerations on abrasive wear in comminution

Abrasive wear is the major form of wear on mill components. This form of wear is usually caused by hard mineral particles that produce no significant adhesion and seizure phenomena during the course of wear. The large variety of shapes and mechanical properties of the abrasive particles (e.g. quartz and pyrite particles in coal) and diverse loading conditions give rise to variable stresses at contact [30-32].

Wear debris is generated as a result of a single or multiple action of the abrasive agents, i.e. microploughing, microcutting, microcracking, and microfatigue [33-37]. This diversity of wear processes and conditions results in various combinations of the elementary processes involving the disintegration and loosening of the surface layers.

Since the abrasive wear process is complex and varies from one situation to another, it is impossible to design a universal abrasive wear tester. Consequently, many specialised testers have been developed. For abrasive wear, testers have been designed by Khruschov [34] and others [37-40].

In spite of the wide variety of testers, there was a demand for a new apparatus simulating conditions in various mill designs which combine both abrasion and comminution processes. The objective of this investigation was to develop a test procedure that would be suitable for general use in estimating the abrasiveness of particular minerals, and to study the abrasive/erosive wear in various grinding systems (Figs. 2-4).

Three separate industrial problems involving coal grinding were undertaken by means of three novel design apparatus. The results from tests and discussion are presented below.

Testing Wear Resistance of Materials in a Predominantly Static Three-Body Interaction

Conditions within a large-size vertical ball-race mill were simulated in this series of tests by means of the apparatus (Figs. 2 and 5) designed by Ścieszka [17], [18]. The highly abrasive coal No 5 (Table 1) was used in all tests. The group of materials tested consisted of five hard cemented tungsten carbides, one standard carbon steel, and one high chrome cast iron, CI (Table 2) currently used for rings in ball-race pulverises. The decision to select this set of materials was based on significant success achieved in a casting process that metallurgically bonds exceptionally hard cemented tungsten carbides to tough 4330 base steel [41]. This casting process reduced excessive wear problems in some severe operating conditions and could be applied to the manufacture of the grinding elements.

The tribological conditions, which are generated on the bottom surface of the rectangular bar (Fig. 5), simulate conditions on the ball-coal layer interface inside ball-race mills [22] and [23]. Hence, the results obtained from the tests can be applied directly to predict the material performance in industrial pulverises. The results are summarised in Table 2. Most of the cemented tungsten carbides gave excellent wear resistance.

With material grade No 3, wear resistance was increased 658 times compared with the standard material and 26 times compared with the high chrome cast iron presently used for casting race.

Table 2 includes additional parameters such as hardness, relative impact resistance, and optional parameter β.

$$\beta = \varepsilon \, \alpha \, 10^{-3} \tag{10}$$

where: ε is relative wear resistance
α is relative impact resistance. (The data presented in Table 2 were taken from Ref. [41] that includes the drops weight test method definition).

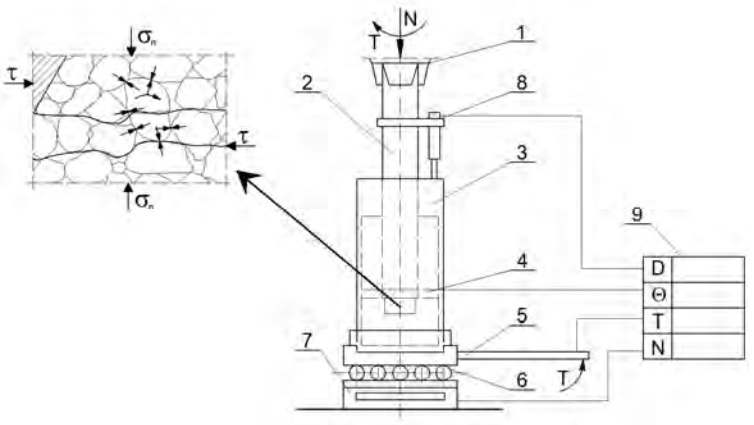

Fig. 5. Schematic diagram of apparatus, and interpretation of interaction between the particulate mineral and the bar within the shear zone, where: 1 – drill chuck; 2 – drive shaft; 3 – cylindrical chamber; 4 – thermocouple; 5 – torque indicator; 6 – thrust bearing; 7 – force indicator; 8 – displacement indicator; 9 – recorder
Rys. 5. Schemat urządzenia i objaśnienie oddziaływania między cząstkami mineralnymi a próbką w strefie ścinania, gdzie: 1 – uchwyt wiertarski; 2 – wałek napędowy; 3 – komora cylindryczna; 4 – termopara; 5 – wskaźnik momentu obrotowego; 6 – łożysko oporowe; 7 – wskaźnik siły; 8 – wskaźnik przemieszczenia; 9 – rejestrator

Parameter β is based on the assumption that the relative wear resistance and relative impact resistance are an equally important property of material when considering the application of materials for casting mills' race. Applying

parameter β as a criterion, the grade No 3 was chosen and recommended as a filler for the composite cemented tungsten carbide 4330 base steel rings. This indicates that the optimal percentage of binder for a given range of sintered carbides and tribo-conditions was about 12 percent (Table 2).

Table 2. Mechanical properties of bar materials
Tabela 2. Własności mechaniczne próbek materiałów

No	Material composition		Wear	Wear resistance MJ - 9	Relative wear resistance	Vicker's hardness HV_{30}	Relative impact resistance α	β
	Material grade	Co Binder						
		%	µg/rev					
1	Carbon Steel, CS	-	74.00	1.18	1.0	134	188	0.2
2	Cast Iron, CI	-	3.10	29.10	24.7	746	125	15.6
3	Cemented WC-Co	12.2	0.14	776.00	658.0	1210	100	65.8
4	Cemented WC-Co	8.8	0.18	623.00	528.0	1310	71	37.5
5	Cemented WC-Co	20.0	0.78	128.00	108.0	897	100	10.8
6	Cemented WC-Co	6.0	0.13	808.00	685.0	1501	25	17.1
7	Cemented WC-Co	7.0	0.16	666.00	564.0	1717	12	6.8

Testing Grinding Properties of Coal in a Predominantly Tumbling Condition

In tumbling mills, the predominant mechanism of comminution is crushing, due to the low speed impact and tumbling action of the charge. In the simplified horizontal tube mill arrangement shown in Fig. 3, the mechanical conditions are described by the interaction between the charge and the mill's inner surface and also by the interaction within the charge. Considering the origin of wear and size reduction processes in the impacting machine, the peak maximum pressure p_{max}, similarity criterion was used.

$$p_{max} = 0.265(E^9\ R^{-6}\ V^4\ m^2)^{1/10} \tag{11}$$

where: E – reduced modulus (GPa)
R – radius of curvature (m)
V – speed of collision (ms^{-1})
m – mass of ball (kg)

The applied model is based on the Hertz impact theory [43].

The proposed method, which simulates the impact action in the tube mill, involves the use of an electromagnetic vibrator (EMV) and chamber with the two balls inside, shown in Fig. 3. The energy input absorbed by the grinding system is given by Equation [44]:

$$EI = 0.3\ \omega^3\ A^2\ M_c\ t_d \tag{12}$$

In each test, a charge of 30 g of coal sieved through a 600-1200 μm sieve, together with two steel balls, was placed inside the chamber. The grinding action was performed by the balls impacting against the sides of the chamber and against each other. In order to create a sliding component of the compound impact action, the chamber cover, simulating a mill liner, was tilted as shown in Fig. 3.

Since the grindability and abrasiveness of minerals are not their inherent properties but a grinding system property, it is necessary to obtain a set of suitable conditions in which to run the tests, and to keep them constant for each test on all the mineral samples. In this way, the final results can be directly compared to obtain the order of grindability, abrasiveness, and wear resistance of materials used for the production of balls and liners. In this part of the investigation, the frequency (n = 50Hz) and the amplitude (A = 0.005 m) were fixed based on the similarity of the kinematic collision energy in the laboratory rig and the actual mill.

A series of tests was conducted on the five coals. The results are presented in Figs. 6 and 7. Figure 6 is of special interest, because it shows that coal samples respond inversely to the two grinding methods (nipping and tumbling) with a high correlation coefficient of 0.983. Those coal samples poorly ground by nipping could be ground better by tumbling, because they respond well in comparison with the other samples to this kind of grinding.

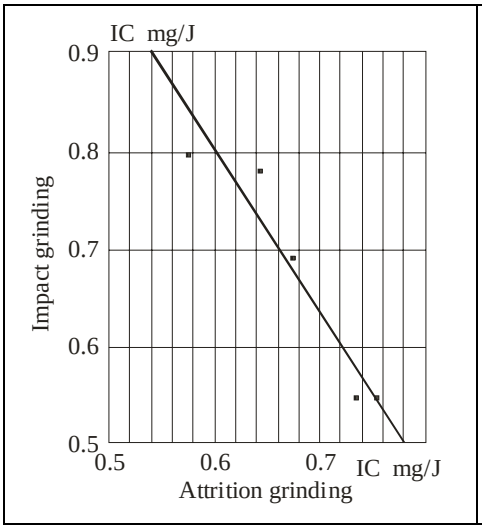

Fig. 6. The correlation between the index of comminution (IC) in two different grinding systems for five coals

Rys. 6. Zależność między wskaźnikiem rozdrabniania w dwóch różnych systemach mielących dla pięciu węgli

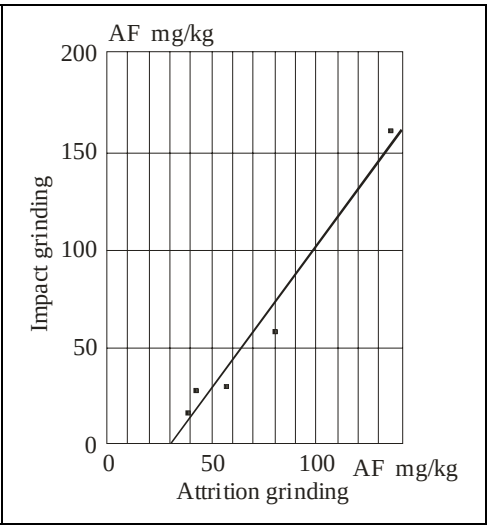

Fig. 7. The correlation between the abrasion factor (AF) in two different grinding systems for five coals

Rys. 7. Zależność między współczynnikiem ścieralności w dwóch różnych systemach mielących dla pięciu węgli

Testing Wear Resistance of Materials in a Predominantly High Speed Impact Interaction

In order to simulate as closely as possible the tribological conditions inside a coal impact beater mill, a high-speed erosion tester was constructed [25]. The construction of this tester is shown in Fig. 4. In the type of impact mill that this rig simulates, the coal enters axially and changes its flow direction to a radial one inside the mill. The area of impact of coal grains with the beater plate depends on the position of the coal entry to the mill. The area of direct impact is equivalent to the inner beater plate in Fig. 4.

The grinding intensity depends mainly on the impact stress in the coal grain contact area with the beater plate and on the number of contacts. The impact stress depends on the impact velocity. In the full-scale mill analysed, the peripheral speed was about 100 m/s, which was sufficient for grinding soft coals such as lignite. Wear during the comminution of lignite was characterised by deep grooving due to hard mineral impurities such as quartz and pyrites.

Although erosive wear has a stochastic character determined by random particle dynamics, the worn material is removed by a combination of simple local processes such as cutting, ploughing, cracking and surface and sub-surface fatigue. The relative contribution of each process to the overall wear rate depends mainly on the material hardness and fracture toughness, and it can be classified as either brittle or ductile wear.

In the region equivalent to the outer plate, wear is less intense, because it is caused only by sliding erosion without direct impact. In this region, the predominant wear mode is low stress scratching, mainly cutting or ploughing, by hard mineral fragments of coal below their crushing strength. It was postulated that the two distinct regions of predominantly impact, and predominantly sliding erosion, together with the size reduction process could be modelled in relatively simple laboratory experiment.

The rig shown in Fig. 8 consists of two counter-rotating components, a shaft onto which two specimens are attached, and a drum. The rotational speed of the drum and the shaft were 3000 revolutions per minute giving a relative velocity of 6000 rpm and peripheral speed of about 100 m/s. The specimen front faces were worn by impact erosion, the external face being worn predominantly by sliding erosion. The test duration was selected to simulate the time taken for the coal in the full-size mill to be comminuted to the desired size. The test duration was five minutes for all tests.

The erosion was determined by the erosion factor EF that was calculated from the following equation:

$$EF = (\Delta W/PC)\ 10^6\ mg/kg \tag{13}$$

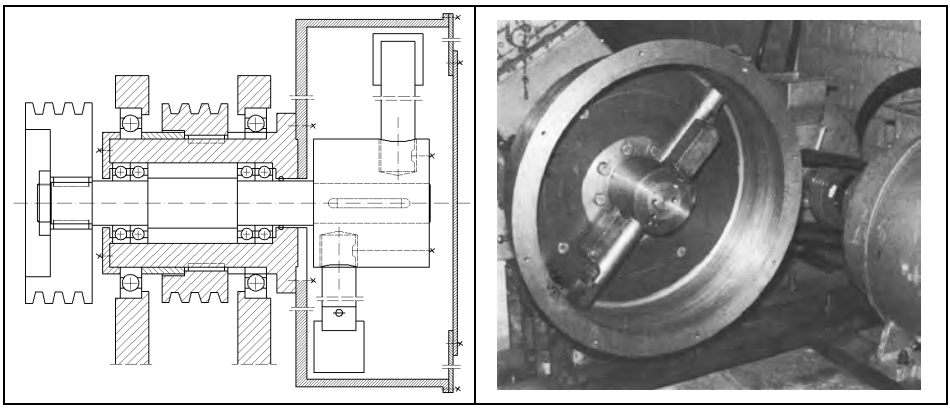

Fig. 8. Overall view of the high speed impact tester
Rys. 8. Ogólny widok testera o dużej prędkości uderzenia

The relative erosion resistance (ε) of each material was calculated by dividing the erosion factor for the least erosion resistant specimen by the erosion factor of the material considered.

The results are summarised in Table 3. These results allow the specimens to be classified according to their resistance to the type of wear that takes place on the beater plates.

Table 3. Relative erosion resistance of various metals tested in the impact rig
Tabela 3. Względna odporność na ścieranie różnych metali badanych w urządzeniu udarowym

Spec. No	Material	*EF* mg/kg	E
1	25Cr cast iron (martensitic)	51.7	14.20
2	12Cr tool steel	275.9	2.66
3	12Mn steel	540.2	1.36
4	Carbon tool steel	734.9	1.00

The results suggest that the life expectancy of the beater plate could be increased by up to 14 times by using the 25 percent chrome cast iron instead of the carbon tool steel originally used or by a factor of 2.5 by using the 12 percent chrome steel.

Conclusions

Three types of apparatus have been developed to study the abrasive wear of materials in friction contact with mineral particles during the comminution process and grinding properties of granular coal. The equipment has a wide pressure and velocity range and can be used to simulate tribo- conditions inside various types of mills.

The test procedure developed in the course of this work may not be refined sufficiently in its present form for general use, but it may serve as a starting point from which an acceptable test procedure can be developed. So far this method has been used on nineteen coals. Only wider use of the procedure by other investigators and correlation with many plant experiences can determine to what extent the method will have to be modified to render it suitable for general application.

The abrasion factor and intensity of abrasion can be applied in the calculation of the service life of the rings. In this case, the results from a relatively simple laboratory apparatus, designed and operated according to the principles of similarity, may be used to predict the service life of machine elements in industry. The simulative tribo-testing procedure and rig can be used to evaluate the abrasiveness of any granular mineral and for testing the wear resistance of any material in any abrasive action.

The rigs described are an attempt to simulate as accurately as possible the wear mechanism and size reduction processes inside the full-scale equipment in a laboratory size rig.

References

[1] Godet M.: Tribo-Testing. Trib. Tech., Senholzi P.B. ed., Martinus Nijhoff Publishers. The Hague (1982), pp. 535-609.
[2] Godet M.: Extrapolation in Tribology. Wear, 77 (1982), pp. 29-44.
[3] Lowrison G.C.: Crushing and Grinding. Butterworths, London, pp. 49-55 (1974).
[4] Berkowitz N.: An Introduction to Coal Technology. Academic Press, London (1979) pp. 69-75.
[5] Van Krevelen D.W.: Coal-Typology-Chemistry-Physics-Construction. Elsevier, Amsterdam (1981) pp. 127-141.
[6] Millard D.J.: The Apparent Strength of Extensively Cracked Material. Proc. Phys. Soc. Section B. 68, p. 1184 (1955).
[7] Lytle J.M.: Concentration of Mineral-Rich Component in Coal Particle. Am. Chem. Soc. Dm. Fuel. Chem. Prepr., 27, p. 307 (1982).
[8] Lytle J.M., Prisbrey K.A.: Size and Shape of Coal Particles During Comminution. Powder Technol. 38, 1. p. 93 (1984).
[9] Evans I., Pomeroy G.: The Strength, Fracture and Workability of Coal. Pergamon Press, London (1966) pp. 55-65.
[10] Misra A., Finnic I.: Erosion of Solid Particles. Wear, 68, p. 41 (1981).
[11] Hutchings I.M.: Wear by Particulates. Chem. Eng. Sri., 42,4, pp. 869-878 (1987).
[12] Raask E.: Flame Imprinted Characteristics of Ash Relevant to Boiler Slagging, Corrosion and Erosion. Trans. ASME, Jour. Eng. Power. 164, p. 858 (1982).
[13] Rehbinder P.A., Shchukin E. D.: Surface Phenomena in Solid During Deformation and Fracture Processes. Pergamon Press, London (1973).
[14] Moore J., Perez R., Gangopadhyay A., Eggert J.: Factors Affecting Wear in Tumbling Mills: Influence of Composition and Micro- structure. Intl. Jour. of Mineral Proc., 22, pp. 313-343 (1988).
[15] Krause H., Senuma T.: A Contribution Towards Improving the Applicability of Laboratory Wear Tests in Practice. Proc. Int. Conf. on Wear of Materials. ASME, New York, pp. 753-763 (1981).

[16] Czichos H.: Tribology. Elsevier, Amsterdam (1978) pp. 264-277.
[17] Ścieszka S.F.: New Concept for Determining Pulverizing Properties of Coal. Fuel, 64, pp. 1132-1142 (1985).
[18] Ścieszka S.F.: A Technique to Investigate Pulverizing Properties of Coal. Powder Tech.. 43, pp. 89-102 (1985).
[19] Austin L.G., Rogers R.S.: Powder Technology in Industrial Size Reduction. Powder Tech.. 42, pp. 91-109 (1985).
[20] Austin L.G.: Coal Preparation and Comminution. Handbook of Powder Sri. and Tech.. Van Nostrand Reinhold, New York, pp. 562-606 (1984).
[21] Rose H.E., Sullivan R.M.: Tube and Rod Mills. Constable, London (1958) pp. 107-141.
[22] Ścieszka S.F.: Modelling Durability of Coal Grinding Systems. Wear, 114, pp. 29-39 (1987).
[23] Ścieszka S.F.: A Technique to Study Abrasive Wear in Contacts With Particular Materials. Wear, 119, pp. 237-249 (1987).
[24] Ścieszka S.F.: Grinding Behavior of Coal in Different Size-Reduction Systems. Powder Tech. 49, pp. 191-192 (1987).
[25] Ścieszka S.F.: Methods for the Determination of Sliding and Impact Erosion Wear in Equipment. SA Mech. Eng., 40, pp. 248-259 (1990).
[26] Standard Test Method for Grindability of Coal by the Hardgrove-Machine Method. ASTM D409-71 (1978).
[27] Yancey H.F., Geer M.R., Price J.D.: An Investigation of the Abrasiveness of Coal and its Associated Impurities. Trans. Metall. Soc. AIME, pp. 262-268 (1951).
[28] British Standard 1016, Part 19: Determination of the Index of Abrasion of Coal, (1980).
[29] Norman T.: Wear in Ore Processing Machinery. Wear Control Handbook. Peterson M.B., Winer W.O., eds., ASME, New York (1980) p. 1015.
[30] Eyre T.S.: Wear Characteristics of Metals. Trib. Intl., 10, pp. 203-212 (1976).
[31] Rabinowicz E.: Friction and Wear of Materials, J. Wiley, New York (1965) pp. 167-197.
[32] Misra A., Finnie I.: A Review of the Abrasive Wear of Metals. Trans. ASME, Jour. Eng. Materials and Tech., 104, pp. 94-101 (1982).
[33] Moore M. A.: A Review of Two-Body Abrasive Wear. Wear, 27, pp. 1-17 (1974).
[34] Khruschov M.M.: Principles of Abrasive Wear. Wear, 28, pp. 69-88 (1974).
[35] Czichos H.: Tribology. Elsevier, Amsterdam (1978), pp. 112-118.
[36] Rabinowicz E., Dunn L.A., Russell P.G.: A Study of Abrasive Wear Under Three-Body Condition. Wear, 4, pp. 345-355 (1961).
[37] Neale M.J. and Gee M.: Guide to Wear Problems and Testing for Industry. Professional Eng. Publ. London 2000.
[38] Roebuck B., Gee M. Bennett E.G. and Morrell R.: Mechanical Tests for Hardmetals, NPL Good Practice Guide, No 20, Teddington 2000.
[39] Hutching I.M.: Tribology, Friction and Wear of Engineering Materials, Arnold, London 1992.
[40] Stachowiak G.W. and Batchelor A.W.: Engineering Tribology, Butterworth-Heinemann, Woburn 2001.
[41] Tough, New, Economical, Wear-resistant Materials. Kennametal Report B82-175/5/L2, pp. 1-10 (1982).
[42] Zum Gahr K.H.: Microstructure and Wear of Materials. Elsevier, Amsterdam (1987) pp. 93-99.
[43] Engel P.A.: Impact of Materials. Elsevier, New York (1978).
[44] Rose H.E., Sullivan R.M.: Vibration Mills and Vibration Milling. Constable, London (1961) pp. 107-141.

APPENDIX A

Concomitant Effects in Comminution

Simple tests were conducted on a specially designed apparatus to determine a correlation between particle comminution and abrasion wear. A comparison was made between results obtained without the bar and with the bar fixed to the underside of the disk (Fig. Al). Highly abrasive coal No 5 and low abrasive coal No 1 are described elsewhere and were used for the analysis shown in Table 1 were used. In all tests, the same normal load, N=2000N, number of revolutions, i=400 and rotational speed, n=100 min^{-1} were applied. Every test was repeated four times. The average values are presented in Table Al.

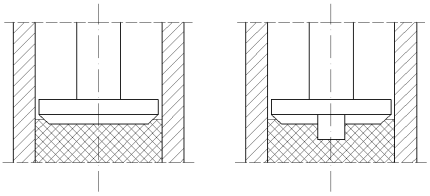

Fig. A1. Shaft-disc assembly with and without a bar
Rys. A1. Układ wałek-tarcza z próbką i bez próbki

Results indicate that wear was significantly affected by the presence or absence of the bar. The tests conducted without the bar closely represent two-body abrasion in which interlocked particles under compression are sliding upon a rotating disc with only little shearing, rotation, and consequently, little particle crushing.

The test with the bar, on the other hand, represents three-body abrasion in which particles in contact with the bar are being continuously redistributed by shearing action. This action guarantees that, in every revolution, a different particle layer is in contact with the bar, and the bar surface is attacked by new sharp edges just created in the shearing/crushing process.

It is clear from parameters such as AF (Table Al) that wear is closely correlated with the size reduction processes.

Table A1. Comparative results from grindability-abrasion test
Tabela A1. Wyniki porównawcze z badania kruszalności i ścierności

Property	Highly Abrasive Coal		Low Abrasive Coal	
	Without Bar	With Bar	Without Bar	With Bar
ΔW [g]	0.002	0.0472	0.0001	0.0016
PC [g]	0.760	16.80	0.45	10.80
EI [J]	17700.0	36260.0	25200.0	31500.0
AF [mg/kg]	2631.0	2809.0	222.0	148.0
IA [mg/m^2g]	63.0	1479.0	3.0	50.0

This correlation can be attributed to the creation of new sharp edges during the crushing of particles, as well as, but to a lesser degree, to sudden release of elastic energy after particle collapse. This simple experiment shows the inter-relation between abrasion and comminution and emphasises the difference between two-body and three-body abrasion. If, in a practical tribo-engineering system, three-body abrasion prevails, it must not be simulated by means of a laboratory two-body abrasive test system.

Nomenclature

A	– amplitude (m)	p	– pressure (MPa)
AF	– abrasion factor (mg/kg)	P	– product size modulus (μm)
AI	– index of abrasion (mg/kg)	PC	– pulverized fraction of coal below 75μm (g)
d_1	– diameter of disc (m)	R	– radius (m)
d_2	– diameter of cylinder (m)	S	– area of surface (m^2)
EF	– erosion factor (mg/kg)	t	– time (s)
EI	– energy input (J)	t_d	– duration of test (s)
F_N	– normal force (N)	T	– average integral value of torque (Nm)
F_T	– tangential force (N)	v	– velocity (m/s)
F	– feed size modulus (μm)	W	– work input (J/g)
H	– height of bar (m)	W_i	– work index (J/g)
i	– number of revolutions	ΔW	– wear of blade (g)
IA	– intensity of abrasion ($mg/m^2 \cdot s$)	WR	– wear resistance (MJ/g)
IC	– index of comminution (mg /J)	α	– relative impact resistance
m	– mass (g)	ε	– relative wear resistance
m_1	– initial mass of blade (g)	σ_c	– compressive strength (MPa)
m_2	– final mass of blade (g)	σ_n	– normal stress (MPa)
M_C	– mass of charge (kg)	τ	– shear strength (MPa)
N	– rotational speed (min^{-1})	ω	– angular velocity (rad/s)
N	– normal force (N)		

Scientific work executed within the Strategic Programme "Innovative Systems of Technical Support" for Sustainable Development of Economy Operational Programme.

Metody laboratoryjne do łącznego badania własności ściernych, kruszalności i zużycia w systemach przeróbki węgla

Streszczenie

Opracowano metody laboratoryjne, które dotyczą wykorzystania trzech nowych testerów symulujących proces mielenia, jaki zachodzi w większości typów istniejących młynów węglowych. Wszystkie trzy testery łączą ścieranie i erozję z rozdrabnianiem. Przedmiotem tego badania było opracowanie procedury badań, która nadawałaby się do powszechnego stosowania w szacowaniu własności ściernych określonego węgla i do badania zużycia ściernego w różnych systemach mielących. Za pomocą nowej aparatury badano trzy odrębne problemy przemysłowe dotyczące kruszalności węgla. Wyniki z relatywnie prostych procedur laboratoryjnych, zaprojektowanych i przeprowadzonych zgodnie z zasadami podobieństwa, mogą być wykorzystane do prognozowania trwałości eksploatacyjnej elementów młynów węglowych. Tribologiczne procedury badawcze i aparatura mogą być wykorzystane do oceny własności ściernych dowolnego węgla i do badania odporności na zużycie dowolnego materiału konstrukcyjnego pracującego w warunkach dominującego procesu zużycia ściernego lub erozyjnego.

SCIENTIFIC PROBLEMS
OF MACHINES OPERATION
AND MAINTENANCE
4 (164) 2010

STANISŁAW ŚCIESZKA*, WOJCIECH GRZEGORZEK*,
MARCEL ŻOŁNIERZ*

Simulative tribo-testing of erosive wear for coal impact mills

Key words

Abrasion and erosion wear, grinding action.

Słowa kluczowe

Zużycie ścierne i erozyjne, proces mielenia.

Summary

In some lignite-fired power stations, very high wear appears in the impact mills and in related processing equipment such as classifier flaps, splitters, and fuel pipe bends. In the power industry, abrasion and erosion wear are important cost generating factors during the conveyance of raw coal, during the coal grinding process, during the conveyance of pulverised fuel, and during the conveyance of ash. Three laboratory methods were developed that require the use of three separate rigs to simulate the following: a) grinding action and erosion wear in the coal impact mills, b) classifier flap erosion wear by solid coal fuel particles impingement, and c) coal fuel pipe bends and splitters erosion wear.

Definition of problem

Very high wear appears in the coal pulverises and in related processing equipment such as classifier flaps, splitters, and fuel pipe bends at the lignite-fired power stations. The intensity of abrasion and erosion wear experienced in some impact mills is particularly severe. The impact mill presented on Figure 1

* Silesian University of Technology, Faculty of Mining and Geology, Institute of Mining Mechanisation, Akademicka 2A Street, 44-100 Gliwice, Poland; e-mail: stanislaw.scieszka@polsl.pl.

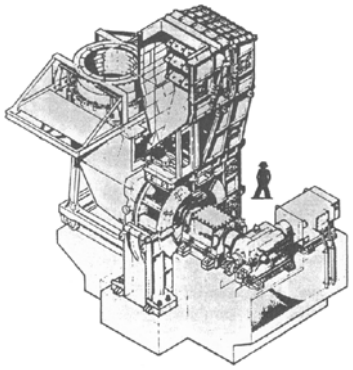

Fig. 1. Rotary impact mill
Rys. 1. Obrotowy młyn udarowy

is designed like a centrifugal fan with radial blades. Pulverisation is by impact on the blades and housing. The mill is basically a housing (mill case) inside which is a wheel with wear-protected blades. This wheel is fitted to a shaft that rotates at a speed according to the kind of mill. A static classifier is fitted at the top of the mill.

These mills are used principally for processing lignites, which are characterised by high moisture content. By means of a suitable supply of hot gas, the product is dried before being fed into the mill.

As it can be seen from the scheme in Figures 1 and 2, coal and the suspension medium (including that contaminated by the fly ash and hot air from the boiler) enter the mill axially and must change direction to a radial one.

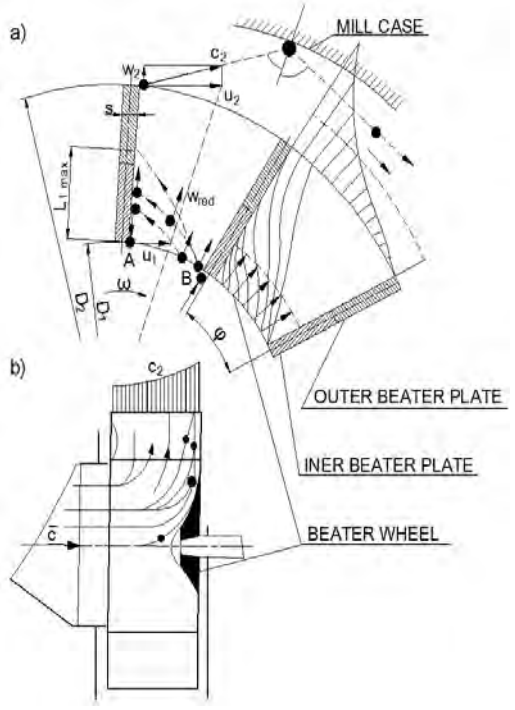

Fig. 2. Scheme of the rotary impact mill: a) Impact area of coal with the beater plate and mill case; b) Coal and suspension medium flow pattern inside the mill. Where: c – velocity distribution, $\bar{c}$ – mean velocity of coal and the suspension medium, D_1, D_2 – inner and outer diameter of the wheel, ω – angular velocity, u_1 – beater plate velocity at point A, u_2 – beater plate velocity at radius $r_2 = D_2/2$, c_2 – coal and suspension medium resultant velocity
Rys. 2. Schemat obrotowego młyna udarowego: a) Obszar oddziaływania węgla z płytą bijaka i obudową młyna, b) Model przepływu węgla i nośnika wewnątrz młyna. Gdzie: c – rozkład prędkości, $\bar{c}$ – średnia prędkość węgla i jego nośnika, D_1, D_2 – wewnętrzna, I – zewnętrzna średnica koła udarowego, ω – prędkość kątowa, u_1 – prędkość liniowa bijaka w punkcie A, u_2 – prędkość liniowa bijaka na promieniu $r_2 = D_2/2$, c_2 – prędkość wypadkowa węgla i nośnika

This is accomplished before entering the working beater wheel. The area of the impact of coal grains with the beater plate depends on the grain entry into the wheel. Theoretically, it can be at any point on the cylinder surface of the wheel of inner diameter D_1, limited by two adjacent plates and the inner width of the wheel. Nevertheless, due to the effect of inertial forces on the grains, the concentration of mass occurs in a third of the wheel width.

If the grains enter the wheel close to the plate of point A, impact on the plate edge (at diameter D_1) will take place. As the entry position translates from point A to B, the longer path directs the grains in a radial direction, while the beater plate approaches. In the region of D_1 to D_1+L_{1max} the inner beater plate will be subjected to the most intensive wear. Two specific types of abrasion-erosion can occur in this region: Gouging erosion, heavy plastic deformation of a surface by hard mineral fragments (e.g. quartz and pyrite) under impact causing deep surface grooving and removal of relatively large wear debris particles [1, 2]. The process is caused by mineral fragments under sufficient contact stress to cause the mineral fragments to fracture. The abrasion also takes the form of scratches on the contacted surface.

In the region up to D_2, the outer plate wear will be less intensive, since only sliding of the grains on the plate surface causes it. This wear is of a different depth, having a wavy appearance due to the effect of the secondary flow of the carrying medium (circulation, non-uniformity of speed profile). In this region, the predominant wear mode is low stress scratching abrasion (sliding-erosion). In this mode, wear occurs mainly by cutting or ploughing by a mineral fragments under contact stress below their crushing strength.

Grinding intensity depends mainly on the impact force of the grain contact with the beater plate and on the number of contacts. Impact force depends on impact speed. In the analysed mill, the peripheral speed was about 100 m/s.

Pulverised coal mixed with a part of combustion air is transported from the mill through the classifier and splitters along fuel pipes to boiler burners at a velocity of about 25m/s. Since the velocity of impacting particles is one of the important parameters governing solid particle erosion wear, the pulverised fuel system is designed to keep the velocity below the above-mentioned value. Then all elements of the pulverised fuel system are exposed to predominantly solid particle erosion wear, but in pipe bends it is more distinctly low angle impingement erosion and low stress scratching abrasion than in other cases [3, 4].

Characterisation of erosive particles

Particle characterisation for an assessment of the abrasion and erosion action must take into account the amount and the mode of the transfer of the kinetic energy of the particles to the worn surface. The energy stored in moving or stressed particles depends on the diameter and density at the points of contact between the particles and the target. Some of the potential or kinetic energy is first

utilised to deform and subsequently to remove material from the surface. The efficiency of the abrasion or erosion mechanism depends on the shape, hardness, and strength of the particles. Hard, high-strength, sharp-edged particles (e.g. quartz and pyrite) are able to transmit relatively high amounts of energy over small areas, thus causing rapid abrasion or erosion wear [5, 6].

The coal substance is a soft, low-strength material (Table 1); therefore, the wear-causing properties of different coals depend largely on the presence of abrasive mineral types (Figure 3).

Table 1. Concentration and hardness of coal constituents [4]
Tabela 1. Udział i twardość składników węgla

Constituent	Approximate concentration	Vickers hardness	Mohs hardness
	(weight percentage)	(kg/mm^2)	-
Soft minerals, Vickers hardness < 100kg/mm^2			
Coal substance	75	10-80	1.5-2.5
Kaolinite	5	30-40	2.0-2.5
Illite	3	20-35	2.0-2.5
Muscovite	3	40-80	2.0-2.5
Medium-hard minerals, Vickers hardness 100-600 kg/mm^2			
Calcite	0.5	100-170	3
Siderite	0.2	370-440	4
Magnesite	< 0.1	370-520	4
Ankerite	0.1	350-490	4
Dolomite	< 0.1	420-580	4
Hard minerals, Vickers hardness > 600 kg/mm^2			
Pyrite	1.5	720-1840	6-7
Quartz	1.5	1100-1560	7
Orthoclase	< 0.1	700-800	6
Kyanite	< 0.1	500-2100	5-8
Topaz	< 0.1	1500-1700	7-8
Alumina	Rare	>2000	9

Table 2. Hardness of coal mineral species and ash constituents
Tabela 2. Twardość składników węgla i popiołu

Species	Amount	Vickers hardness	Mohs hardness
	(weight ercentage)	(kg/mm^2)	-
Coal minerals			
Alumino-silicates	70	20-80	2-2.5
Quartz	15	1200-1300	7
Pyrite	10	1100-1300	6-7
Carbonate	5	150-450	3-4
Pulverised fuel ash			
Glassy spheres with embedded mullite needles and quartz crystalloids	80	550-600	5
Small glassy and large nonspherical quartz particles	10	600-1200	6-7
Spherical particles of iron oxide	5	480-740	5-6

The transformation of coal mineral matter to fly ash in pulverised fuel flames take place in a temperature range of 1700 to 1900K. High temperature and rapid heating cause marked changes in particle size, shape, and hardness (Figure 4 and Table 2); therefore, the flame-imprinted abrasive characteristics of fly ash can be significantly different from those of the original mineral matter. A highly abrasive coal mineral matter, rich in quartz, produces an abrasive ash in which the large quartz particles retain the wear-causing property. If the ash is recirculated with hot air from the boiler, it may considerably increase wear in mills. The scope for combating pulverised fuel and ash impact erosion and abrasion in existing milling systems is rather limited.

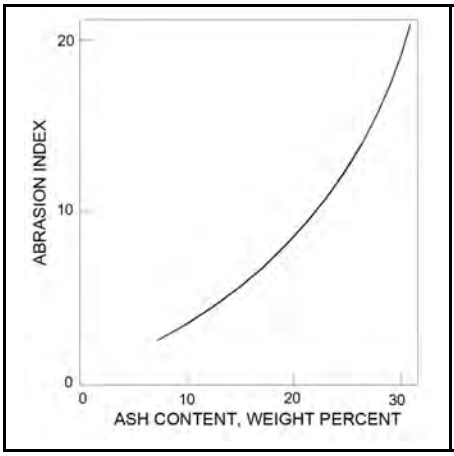

Fig. 3. Increase in abrasion index with ash content
Rys. 3. Wzrost wskaźnika ścieralności w zależności od zawartości popiołu

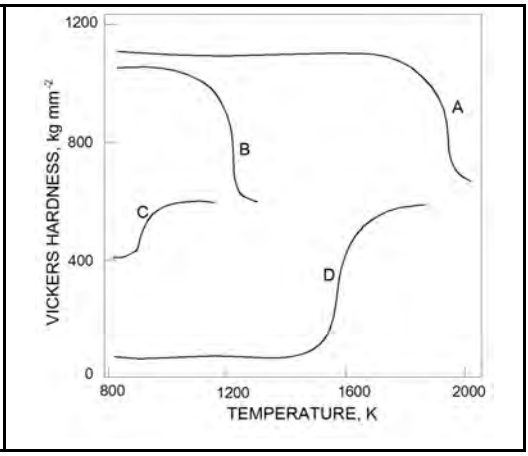

Fig. 4. Change in hardness of coal minerals on heating: A – quartz, B – pyrite, C – siderite, D – alumino-silicates, kaolin, illite
Rys. 4. Zmiana twardości składników węgla z temperaturą: A – kwarc, B – piryt, C – syderyt, D – glinowo-krzemowe, kaolin, illit

Characterisation of materials

In this part of the paper, assessment is made on possible major changes in the pulverised coal-fired system, and the main emphasis is put on possible material choice for the most intensively worn parts such as beater plates, splitters, and pipe bends.

The removal of material from surfaces by coal fragments or pulverised coal fuel is a complex process and varies in intensity depending on material microstructure, mechanical properties of various phases, the hardness of abrasive fragments, and size, shape, and the environment [7]. Removal of material during the abrasive wear processes can occur by cutting or by ploughing [1, 2]. The cutting process is much more efficient and results in more severe wear. The likelihood of cutting by abrasive particles increases with the

sharpness and angularity of the particles. Therefore, quartz particles crushed on the surface of the beater plate will be much more aggressive than other coal components. Since gouging abrasion-erosion normally occurs in the crushing of relatively large pieces of coal, the abrasive wear is usually accompanied by heavy impact and high bending or compressive stresses on the beater plates.

This imposes definite limitations on the choice of ferrous alloys that can be used without premature breakage in this service. Traditionally, the austenitic 12% manganese steels have been the prime choice for beater plates. They have fairly good resistance to gouging abrasion, combined with good toughness and the ability to be heat-treated in heavy sections. However, in some cases, the manganese steels have been at least partially displaced by low-alloy quenched and tempered steels and by martensitic white irons.

Zum Gahr [3] contends that abrasion resistance is influenced by the quantity of carbides in the metal part, the carbide morphology, retained austenite, internal notches, and the matrix structure. These structural components also influence the toughness of the part, something that must ultimately be considered when choosing the material for coal pulverising plates. In materials containing massive carbides, such as high-chromium cast iron, the mean free path between carbides in relation to abrasive particle size is significant to abrasion resistance. The following micro-structural features tend to improve abrasion/erosion resistance: small mean path between carbides, low interface energy, and the ratio of scratch width made by the abrasive to carbide size. In materials having a ferritic matrix with M_3C carbides, silica will penetrate and plough both the matrix and carbide. The M_3C carbide is not hard enough.

Carbides such as $(FeCr)_7C_3$ are much harder than silica and resist ploughing penetration. Pearlitic structures are easily disrupted by silica abrasion. The cementite is deformed and fractured and is torn out of the ferrite phase by the action of silica particles. Materials having massive, hard carbides supported in a relatively soft matrix will tend to wear by the extraction of the matrix material. This is true especially for high stress grinding or for gouging abrasion. There are indications [4] that corrosion plays a role in the wear of coal processing equipment.

The hardness and fracture toughness are very important mechanical properties that influence the abrasive and erosive wear resistance of materials such as high-chrome white cast irons, cast basalt, and high alumina ceramic.

Solid particle erosion is the predominant kind of wear in coal fuel splitters and pipe bends. Knowledge about the mechanism of solid particle erosion wear originates from single particle impingement. Multi-particle impingement, which is experienced in industrial conditions, involves complex phenomena, including a wide range of simultaneous incidence angles, particle interactions, particles embedded in the surface, etc. Several mechanisms of the erosion of materials have been proposed. Some of the main processes involved in erosion wear were summarised by Zum Gahr (Figure 5). Angular particles can remove material by microploughing and/or microcutting when

they strike the target surface at small angles. Temperature effects can be superimposed, due to high impact energies and friction forces induced by adhesion between the particles and the target. The ratio of particle hardness to the hardness of the target plays a role. The ranking order of hard and soft materials can be changed unfavourably in respect to the hard materials with the transition from low to high levels of solid particle erosion wear. Surface cracking becomes important with increasing impingement angle, particle size, particle velocity, and the increasing brittleness of the target material. Erosion rates were observed to be substantially more sensitive to particle size on brittle than on ductile materials (Appendix A).

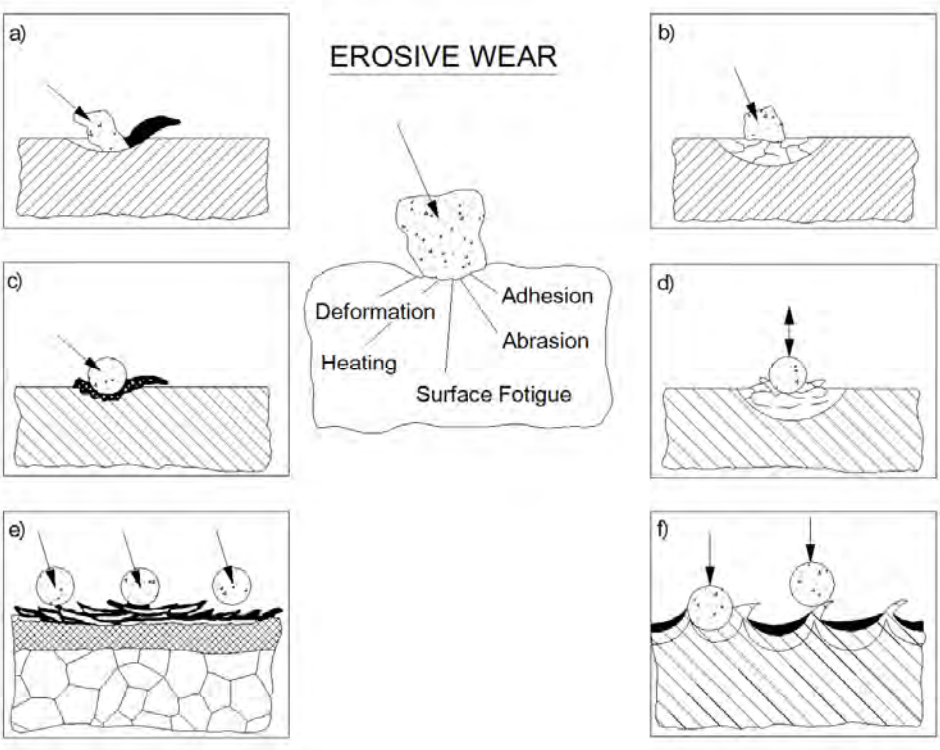

Fig. 5. Processes resulting in wear loss due to single or multiple impact of particles [4]. Where: a) microcutting and microploughing, b) surface cracking (microcracking), c) extrusion of material at the exit end of impact craters, d) surface and subsurface fatigue cracks due to repeated impact, e) formation of thin platelets due to extrusion and forging by repeated impact, f) formation of platelets by a backward extrusion process

Rys. 5. Procesy prowadzące do zużycia z powodu pojedynczego lub wielokrotnego uderzenia cząstek. Gdzie: a) mikroskrawanie i mikrobruzdowanie, b) pęknięcia powierzchniowe (mikropęknięcia), c) wyciskanie materiału na wyjściu z kraterów, d) powierzchniowe i podpowierzchniowe pęknięcia zmęczeniowe z powodu powtarzającego się uderzenia, e) powstawanie cienkich płytek z powodu wyciskania i kucia przez powtarzające się uderzenia, f) powstawanie płytek przez proces wyciskania przeciwbieżnego

The mass loss due to erosion was reported to be proportional to about the square of the velocity of the cause of ductile materials (Appendix A). However, substantially greater velocity exponents up to 5 were reported on brittle materials such as ceramics. Material lips can be produced by oblique impact and are finally detached along shear bands.

Repeated loading cycles by the multiple impact of particles provide the formation of surface or subsurface cracks, which lead finally to the flaking of wear debris. The formation of thin platelets (Figure 5) is favoured by the multiple impact of rounded particles under high angles of incidence. In practice, several of these wear processes can occur simultaneously, depending on the operating conditions and the target material.

Target material properties such as hardness, work hardening, and the capability of deformation, are important physical properties for its resistance to solid particle erosion. Dynamic hardness and work hardening of the target determine the amount of plastic deformation and hence the depth of impact craters at a given impact energy and angle of incidence. The capability of the deformation of the metal during impact loading affects the number of impacts that are required for the formation of wear debris. As a result, a softer metal can show greater erosion resistance than a harder one. Temperature effects can influence wear mechanisms substantially, due to altered microstructures and properties with increasing impact energy or ambient temperature. Chemical effects may be superimposed, depending on the environment (Appendix A).

Experimental testing

Test equipment

It was recognised that the problem of excessive wear is concentrated in three separate parts of the mill system:

a) The rotating impact beater plate,
b) The classifier flaps, and
c) The pipe bends.

Each of these areas is characterised by a different wear mechanism, and the applied testing methods are based on three separate experiments:

1) Simulation of impact abrasion-erosion on the beater plates using raw lignite;
2) Simulation of classifier flap erosion by solid particle erosion using pulverised fuel; and,
3) Simulation of the wear on the pipe bends by means of the spinning erosion wheel.

It is assumed that the problem of the excessive wear is due to the incorrect selection of the material and the aim of the experiments was to find more appropriate materials in each case, although the problem appears to be

compounded by the abrasive quality of the coal and the high recirculation rate of ash. For every three experiments, separate rigs were designed and built.

Experiment 1. Impact-abrasion rig is shown in Figure 6.

Experiment 2. The solid particle erosion equipment was built according to the ASTM designation G76-83 recommendation. The rig is shown in Figure 7.

Experiment 3. Spinning wheel for pipe bend wear is shown in Figure 8.

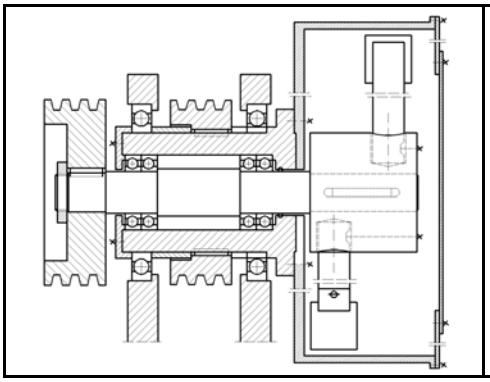

Fig. 6. Schematic drawing of impact-abrasion Equipment, with impact speed $v_i = 100$ m/s
Rys. 6. Schematyczny rysunek urządzenia do badania ścierania udarowego, z prędkością uderzenia $v_i = 100$ m/s

Fig. 7. Erosion tester, nozzle tube and specimen holder
Rys. 7. Tester do badania erozji, dysza i uchwyt próbki

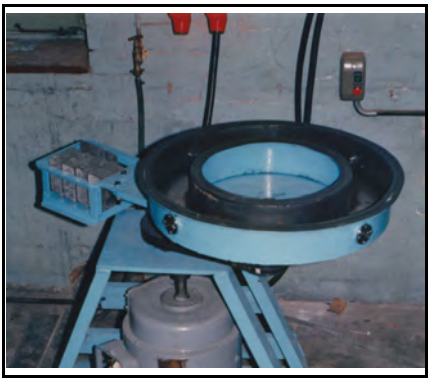

Fig. 8. Overall view of the spinning erosion wheel
Rys. 8. Ogólny widok wirującego koła do badania erozji

Coal and pulverised fuel identification

For abrasion-erosion tests, raw and pulverised lignite from a selected power station were used. Comparison between the raw and pulverised lignite indicates that the ash content is 4-6% higher in the pulverised products than in the raw

lignite [6]. This confirms that additional ash is fed in from the furnace during the grinding process. The hardness of the fly ash and the minerals is considerably higher than that of coal, as tested by microhardness methods [6].

Table 3. Lignite analysis
Tabela 3. Analiza węgla brunatnego

Analysis	Raw Lignite	Pulverised Fuel Upperduct	PF Product
Proximate:			
Moisture %	7.6	8.9	7.7
Volatile %	36.4	32.3	33.3
Ash %	33.6	38.7	40.5
F.C % (by diff.)	22.4	20.1	18.5
Free Silica ($Si0_2$ % in ash)	6.4	6.1	5.8

Experimental results

Simulation of impact-abrasion on the beater plates using raw lignite

In all tests, raw lignite samples were used, M = 500 g. Other test data:

1. Test duration, t = 5 min.
2. Drum rotation, $n_1 = 3\,000\ min^{-1}$.
3. Paddle rotation, $n_2 = 3\,000\ min^{-1}$.
4. Distance between paddle and drum d = 2mm.

Measurements taken:

1. Mass of specimens before test, m_1, g.
2. Mass of specimens after test, m_2, g.
3. Mass lost during test, Δm, g.
4. Pulverised coal during test, fraction below 212μm, PC, g.

Erosion wear was calculated as erosion factor (*EF*)

$$EF = \frac{\Delta m}{M} \cdot 10^6, \qquad \frac{mg}{kg} \tag{1}$$

Hence, relative erosion resistance (ε) was calculated for all materials tested assuming that for the least erosion resistance materials ε = 1.

Final results from these experiments are summarised in Table 4.

Table 4. Results from impact-abrasion experiments
Tabela 4. Wyniki badań ścierania udarowego

No	Material	*EF* mg/kg	ε -
1	25% Cr Cast Iron (Martensitic)	51.72	14.20
2	25% Cr Cast Iron (Austentic)	78.60	9.35
3	12% Cr Tool Steel	275.90	2.66
4	12% Mn Steel	510.30	1.44
5	12% Mn Steel (Highveld)	540.20	1.36
6	High Carbon Tool Steel	734.90	1.00

The experimental results allow the materials to be classified according to their resistance to the type of wear mechanisms which take place on the beater plates. The predominant mechanisms are gouging erosion (front face of specimens) and low-stress scratching abrasion (external side of the specimens).

The results indicate that the life expectancy of the beater plate could be increased by up to 14 times by using the 25 percent chrome cast iron instead of the carbon tool steel originally used or by a factor over 2.6 by using the 12 percent chrome steel.

Simulation of classifier flap erosion by solid particle erosion test using pulverised fuel from a power station

The erosion of classifier flaps in pulverised-fuel lines can be most closely modelled by a particle-gas stream type erosion tester. Erosion tests were performed using the apparatus illustrated in Fig 7. A predetermined mass of pulverised fuel (particle size below 212 μm) from the power station, M = 1 kg was fed into the air stream by means of a vibratory particle feeder. The concentration of particles was kept as close as possible to 1kg/h, although minor fluctuations occurred. The target was cleaned ultrasonically in alcohol, dried, and weighed on a 5-point balance both before and after testing (m_1, m_2). The particle velocity was kept constant (30 ms^{-1}) and was measured using the rotating double disc method developed by Ruff and Ives [7].

Three angles of impingement were used 30°, 60°, and 90°. Scanning electron micrographs were taken for surface examination and erosion mechanism interpretation (Fig. 9). The erosion rate (ER) was finally calculated by equation

$$ER = \frac{m_1 - m_2}{M} \cdot 10^3, \qquad \frac{mg}{kg} \tag{2}$$

Results are presented in Table 5.

Table 5. Summary of solid particle erosion experiment
Tabela 5. Podsumowanie eksperymentu erozji cząstek stałych

No	Target Material	*ER* mg/kg			$\overline{ER}$ mg/kg
		30º	60º	90º	
1	WC-7Co Binder	0.21	0.51	0.02	0.24
2	High Alumina Ceramic	0.42	0.38	0.40	0.40
3	25% Cr Cast Iron (Martensitic)	0.32	1.11	0.78	0.74
4	25% Cr Cast Iron (Austentic)	0.74	1.28	0.61	0.88
5	12% Cr Tool Steel	1.13	1.51	1.76	1.47
6	Roqlast	1.76	2.32	1.47	1.52
7	Mild Steel 43A	1.33	1.92	1.49	1.58
8	High Alumina Ceramic	0.90	2.88	1.49	1.76
9	High Carbon Tool Steel	1.31	2.66	1.32	1.76
10	12% Mn Steel	1.26	2.36	1.72	1.78
11	12 Mn Steel (Highveld)	1.74	2.66	1.92	2.11
12	Cast Basalt	3.87	4.40	5.98	4.75
13	Epoxy System	33.08	23.68	23.58	24.78

The solid particle erosion test allows the materials for the classifier flaps to be evaluated according to their resistance to erosion by pulverised fuel particles. The experiments revealed that instead of 12% Cr tool steel 25% Cr cast iron (martensitic) could be used with almost double durability. The two most erosion resistant materials, namely hardmetal WC-7Co and high alumina ceramic, are both too expensive and too brittle for this type of application. It is quite significant that "Epoxy System" and "Cast Basalt" are both at the bottom of the ranking.

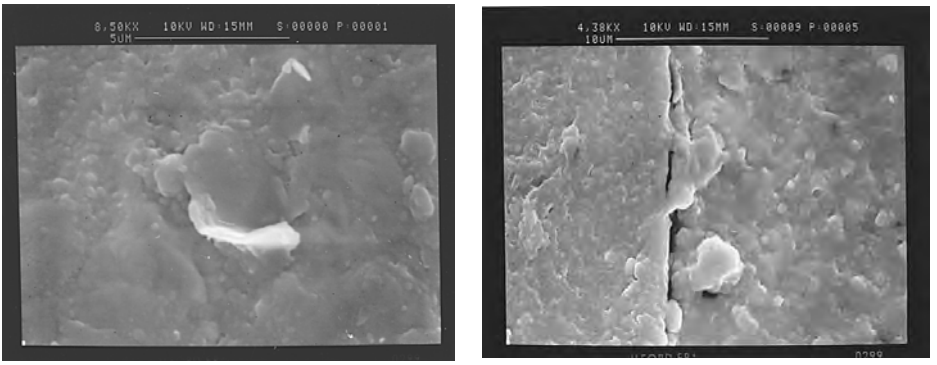

Fig. 9. Extrusion of matrix of the exit end of impact crater and fatigue crack propagation along carbide-matrix interface due to multiple impact on 25% Cr Cast Iron (martensitic)
Rys. 9. Wyciskanie osnowy na wyjściu z krateru i propagacja pęknięć zmęczeniowych na granicy fazy węglika i osnowy z powodu wielokrotnego uderzania na żeliwie stopowym 25% Cr (martenzytycznym)

In order to estimate the difference in the erosiveness between pulverised fuel (PF), which is contaminated by ash, and raw lignite (RAL), the same solid particle erosion procedure was applied using aluminium 6063 as a target specimen. Results are presented in Table 6.

Table 6. Results from comparative erosion test with pulverised and raw coal and aluminium as the target material

Tabela 6. Wyniki porównawcze badania erozji pyłu węglowego i węgla surowego oraz aluminium jako materiał tarczy

Test No	Particle type	Angle of impingement	m_1 g	M_2 G	ER mg/kg
1	PF	60º	6.88198	6.88083	1.15
2	RAL	60º	6.88083	6.88028	0.55
3	RAL	60º	6.88028	6.87928	0.65
4	PF	60º	6.87963	6.87850	1.13
5	PF	90º	6.58895	6.58842	0.53
6	PF	30º	6.59842	6.58627	2.15
7	RAL	90º	6.58461	6.58419	0.42
8	RAL	30º	6.58627	6.58461	1.66

Results indicate that pulverised fuel (PF) from the power station is substantially more erosive than raw lignite (RAL). The mean values of the erosion rate (ER) for PF and RAL are equal to 1.24 mg/kg and 0.82 mg/kg, respectively. As the scanning electron microscope study shows in Figs 10 and 11, this is due to the presence of sharp and hard ash particles in PF.

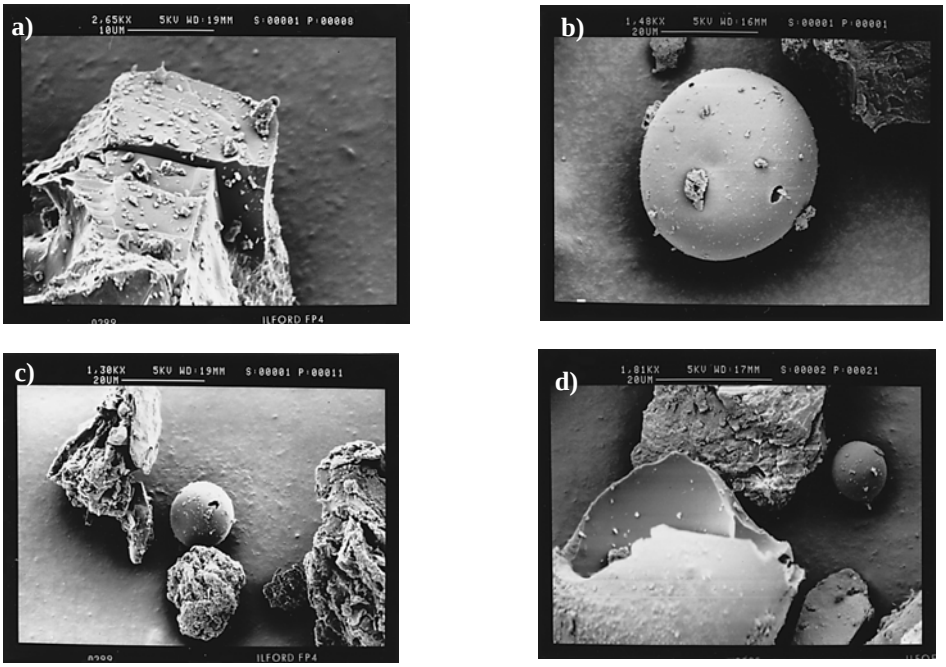

Fig. 10. Scanning electron micrographs showing characteristics feature of mineral particles and flame-heated silicate ash particles in pulverised fuel flame from power station: a) sharp-edged mineral particle; b, c) spheroidized flame-heated silicate ash particle; d) flame ash particle, broken cenosphere

Rys. 10. Mikrofotografie elektronowe skaningowe pokazują cechy charakterystyczne cząstek minerału i nagrzewanych płomieniowo cząstek pyłu żużlowego z elektrowni: a) cząstki minerału posiadające ostrą krawędź; b, c) kuliste wydzielenia nagrzewanych płomieniowo cząstek pyłu żużlowego; d) pęknięte cenosfery pochodzące z popiołu

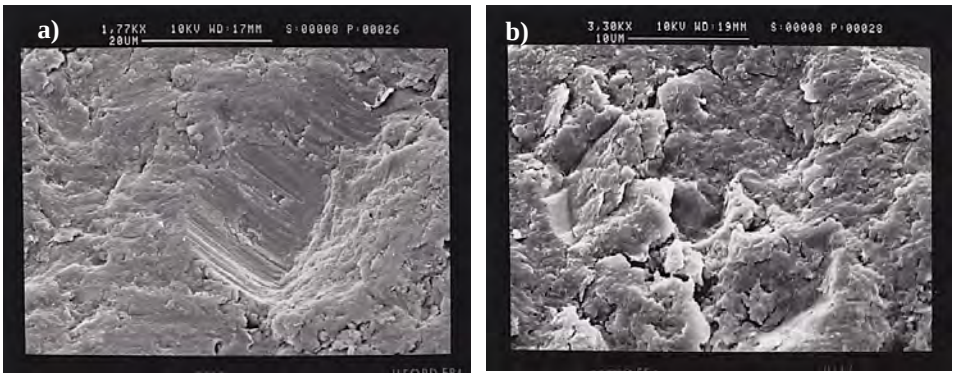

Fig. 11. Scanning electron micrographs showing aluminium target surface after erosion test: a) cutting as result of single impact of sharp particle; b) indentation and surface cracking due to multiple impact

Rys. 11. Mikrofotografie elektronowe skaningowe pokazują aluminiową powierzchnię tarczy po badaniu erozji: a) skrawanie w wyniku pojedynczego oddziaływania ostrej cząstki; b) wgniecenie i pęknięcie powierzchni z powodu wielokrotnego oddziaływania

Simulation of the erosion on the pipe bends by means of spinning erosion loop

The erosion in pipe bends was simulated in the spinning erosion loop (Fig. 8). In order to get uniform and accelerated results, silicon carbide particles (mark 100, 149 μm) were used. In every test, a mass (M = 1 kg) of silicon carbide was kept inside the wheel. The target specimen was cleaned ultrasonically in alcohol, dried and weighed on a 4-point balance both before and after testing (m_1, m_2).

The particle velocity against target was 10 ms^{-1}. Erosion intensity (EI) was calculated using the following equation:

$$EI = \frac{m_1 - m_2}{S \cdot t} \cdot 10^6, \qquad \frac{g}{m^2 h} \tag{3}$$

where:

S – surface area exposed to erosion, mm^2

t – duration of test, h

Erosion intensity (EI) represents the mass loss from a square meter of pipe bend surface during one hour of erosion action. Results are presented in Table 7.

Table 7. Summary of results from pipe bonds erosion tests
Tabela 7. Podsumowanie wyników z badań erozji na łukach rur

No	Target Material	*EI* G/m^2 h	ε -
1	WC - 7Co Binder	2.33	18.80
2	25% Cr Cast Iron (Austenitic)	3.75	11.70
3	High Alumina Ceramic No 1	4.22	10.40
4	25% Cr Cast Iron (Martensitic)	4.29	10.20
5	12% Cr Tool Steel	4.77	9.20
6	High Alumina Ceramic No 2	10.00	4.40
7	12% Mo Steel	10.76	4.08
8	High Carbon Tool Steel	10.78	4.07
9	12% Mn Steel	11.22	3.90
10	Roqlast	17.59	2.50
11	Cast Basalt	22.56	1.90
12	Epoxy System	24.60	1.80
13	Mild Steel 43A	43.90	1.00
14	Aluminium 6063	50.30	0.87

For materials ranking from this part of the research, the relative erosion resistance (ε) was used (Table 7). Relative erosion resistance was calculated assuming that, for material currently used for pipeline production (mild steel) ε = 1. Experiments show that a number of materials have higher erosion resistance than the mild steel. It is recommended that the pulverised fuel pipeline should be protected by means of internal sleeves made of 25% Cr cast iron (ε = 10.2 and ε = 11.7) or 12% Cr tool steel (ε = 4.07) or by tiles made of high alumina ceramic (ε = 10.4).

Conclusions and recommendations

1. The high speed impact-abrasion experiment enabled the materials to be classified according to their resistance to the kind of wear which is taking place on the beater plates surface. Results presented in Table 4 suggest that the life expectancy for the beater plates can be increased up to 14 times using 25% Cr cast iron (martensitic) instead of high carbon tool steel or over 2.6 times by applying 12% Cr tool steel. It is therefore recommended that 25% Cr cast iron be used for the inner beater plate, and 12% Cr tool steel be used for the outer plate, if fracture toughness data and cost consideration justify it.

2. The solid particle erosion experiment simulating classifier flaps wear revealed that the only materials which are significantly more resistant to erosion are 25% Cr cast iron (two times) and high alumina ceramic (four times).

Hardmetal WC-7Co is too expensive to be considered for this application. It is recommended that 25% Cr cast iron be used to make classifier flaps or high alumina ceramic tiles to protect classifiers made of mild steel.

3. Experiments simulating wear conditions on the pipe bends show that a number of materials have higher wear resistance than mild steel which is usually used for pipe production. It is recommended that the pulverised fuel pipeline should be protected by means of internal sleeves made of 25% Cr cast iron or 12% Cr tool steel or by internal tiles made of alumina.

References

[1] Moore M.A.: Abrasive Wear. Fundamentals of Friction and wear of Materials. ASM Materials Science Symposium, 1981, pp. 73-118.
[2] Murray M.J., Mutton P.J., Watson J.D.: Abrasive Wear Mechanisms in Steels. Journal of Lubrication Technology, Vol. 104, 1982, pp. 9-15.
[3] Zum Gahr K.H.: Mircostructure and Wear of Materials. Elsevier, Amsterdam 1987.
[4] Bakker W.T.: Evaluation of Coal Pulverizer Materials. EPRI Research Project Report 1883-2, Palo Alto, 1988.
[5] Skorupa J.J.: Wear of Tube Mill Liners for South African Power Industry. PhD thesis Cape Town. 1989.
[6] Falcon R.M.: Report on an investigation into Abrasion and Wear in Mills and Associated Plant in Amynteon Power Station. September 1989.
[7] Ruff A.W., Ives L.K.: Measurement of solid particle velocity in erosive wear. Wear, Vol. 35 (1975) pp. 195-199.

APPENDIX A

A review of erosion by solid particles

The erosion of materials resulting from the impingement of solid particles is one form of wear that can severely limit of useful life of an element of power plant fuel systems. Erosion can lead to rapid, significant loss of material under certain conditions such as coal processing in power stations under corrosive conditions at elevated temperature [1, 9-11].

Extensive plastic shear is necessary before metal removal occurs but it was not specified when erosive metal loss occurs. A model of steady-state erosion should explain the following general observations, which are expressed in terms of the dimensionless erosion rate, ER (e.g. milligrams of target loss per kg of abrasive).

1. ER varies as $(\text{velocity})^n$ where n is usually in the range from 2.2 to 5.0.
2. A maximum in the erosion rate for ductile metals is at an impact angle of 15° to 30°, or in the case of hardened steel maximum of 60° to 90°.

3. At low impact velocity (v) an incubation time is observed to be inversely proportional to v.
4. Particle size was found to have a significant influence on the erosion of pipe bends [2]. The authors found that sand particle of 70μm mean diameter wore the bends into a pattern of steps or ridges, whereas the 230μm diameter sand particle produced a smooth and round surface. Mills et al [3] found that 70μm particle removed less material that the 230μm particle.
5. Hardness of particles, there is widely held opinion that hard particles are more erosive than softer particles [4, 5].
6. Synergistic effects in erosion. Although the impacting particles used in erosion tests are usually pure and dry, in practice such as impact coal mills the particles are impure, and contain moisture. Small percentages of $Ca(OH)_2$ and water present in abrasives acted as effective intensifier of the erosive wear of metals and alloys [6]. However, with hard and high strength materials such as ceramics, the influence of impurities on erosion was found to be either very low, or to result in less damage.
7. Ruff and Wiederhorn erosion model. Wiederhorn and Lawn [7, 8] assumed that all the kinetic energy of the impinging particle is dissipated in an irreversible plasticity process and thus the following expression for ER was obtained:

$$ER = \alpha H^{0.11} V_0^{2.4} K_C^{-1.3} \rho_p^{1.2} R_p^{3.7}$$

Where: α – constant,
H – hardness of the target material,
V_0 – the particle velocity,
K_C – the fracture toughness of the target material,
ρ_p – density of the impacting particle,
R_p – particle radi

8. Thermal effects in erosion. A substantial temperature rise in the target accompanying an impact. Melting was postulated [7] as playing a significant role in metal loss. Heat is generated in the surface layer in two ways, by surface friction, and by lattice deformation. The tendency to surface melting depends primarily on flow stress, friction coefficient, and the heat required to raise the metal to its melting point, but not on the velocity. The impact of an eroding particle is so quick that the heat generated by deformation does not have time to diffuse away during the impact, provided the particles are over roughly 50μm in diameter [8]. If the surface is initially flat so that the deformation is distributed rather uniformly, the temperature rise is roughly 20-200°C. If the surface is uneven, the temperature rise may be much greater in the asperity struck first. Finally it may be stated that the local temperature

rise plays a critical role in creating the instability that gives the observed extrusion of near surface layer into lips.

References

[1] Shewmon P., Sundarajam G.: The erosion of metals. Ann. Rev. Sci. 1983, 13, pp 301-318.
[2] Mills D., Mason J. S. (1977): Particle size effects in bend erosion. Wear 44, pp. 311-328.
[3] Mills D., Mason J. S., Tong K. N. (1983): The role of penetrative wear in the erosion of pipe bends. Proceedings of the 6th International Conference on Erosion by Liquid and Solid Impact, pp. 58.1-58.7.
[4] Raask E. (1969): Tube erosion by ash impaction. Wear 13, pp. 301-315.
[5] Raask E. (1979): Impact erosion wear caused by pulverized coal and ash. Proceedings of the 5th International Conference by Solid and Liquid Impact, pp. 41-1 - 41-7.
[6] Uuemois H., Kleis I. (1975): A critical analysis of erosion problems which have been little studied. Wear 31, pp. 359-371.
[7] Jennings W. H., Head W. I.: Wear, 40 (1976), pp. 90-112.
[8] Shennon P.G.: Wear, 68 (1981), pp. 253-258.
[9] Hutchings I. M.: Tribology, Friction and Wear of Engineering Materials, Arnold, London, 1992.
[10] Stachowiak G. W. and Batchelor A. W.: Engineering Tribology, Butterworth-Heinemann, Woburn, 2001.
[11] Neale M. J. and Gee M.: Guide to Wear Problems and Testing for Industry. Professional Eng. Publ., London, 2000.

Scientific work executed within the Strategic Programme "Innovative Systems of Technical Support" for Sustainable Development of Economy Operational Programme.

Badania symulacyjne zużycia erozyjnego w węglowych młynach udarowych

S t r e s z c z e n i e

W niektórych elektrowniach opalanych węglem brunatnym pojawia się bardzo duże zużycie w młynach udarowych i związanych z nimi urządzeń, takich jak klapy sortownika, łupiarki i łuki przewodów paliwowych. W przemyśle energetycznym zużycie ścierne i erozyjne są ważnymi czynnikami generującymi koszty podczas transportu węgla surowego, podczas procesu kruszenia węgla, podczas podawania sproszkowanego paliwa do kotłów i podczas transportu popiołu. Opracowano trzy laboratoryjne metody badawcze oraz trzy odrębne testery: a) symulujący proces mielenia i zużycie erozyjne w węglowych młynach udarowych, b) symulujący zużycie erozyjne klap sortownika przez udar cząstek stałych paliwa węglowego, c) symulujący zużycie erozyjne na łukach przewodów paliwa węglowego oraz na rozdzielaczach.

SCIENTIFIC PROBLEMS
OF MACHINES OPERATION
AND MAINTENANCE
4 (164) 2010

WOJCIECH ŻUROWSKI*

Wear research on frictional couples of C80U/145Cr6 under conditions of stabilized friction area temperature

Key words

Tribological wear, wear resistance, dry friction.

Słowa kluczowe

Zużycie tribologiczne, odporność na zużywanie, tarcie suche.

Summary

Research into wear resistance is based on analysing thermodynamic transformations in an open thermodynamic system and is designed to determine conditions under which a system shows the greatest resistance. The verification of theoretical considerations makes possible the utilisation of suitable exploratory positions. At present, a new device has been built to test the resistance of interface systems. In this paper, the design and research possibilities of the new tester are discussed. The device is a modified pin-on-disk system modelling typical working conditions of a disc braking system or a disc clutching system, but with control over the temperature of the friction zone. Beside the mechanical part, the stand is equipped with a cryo-circulator used for setting and stabilising temperatures in the friction zone.

Structurally, the new tester uses a physical model that assumes that the tribological system is able to exchange energy and matter with its environment, where friction is the cause of all transformations in the system and on its boundaries. The friction increases the system's internal energy and its dissipation as heat that compensates for mechanical dissipation, that is, wear.

Data presented in handbooks concerning tribological properties of materials are given for operating conditions in positive temperatures, which may lead to errors when the data are employed to select materials for friction joints working in low temperatures. Our device enables the prediction of low-temperature tribological behaviour of friction couple materials.

The research has proven that there is a precise temperature at which a given matching of materials shows minimum wear, e.g. -25°C for the tribosystem C80U/145Cr6.

* Faculty of Mechanical Engineering, Technical University of Radom, 29 Malczewskiego Street, 26-600 Radom, Poland; e-mail: wojciech.zurowski@pr.radom.pl.

1. Introduction

Research into wear resistance is based on analysing thermodynamic transformations in an open thermodynamic system and is designed to determine conditions under which this system shows maximum resistance. Considering the process of friction, wear, and the issue of resistance to wear at the macroscopic level of matter, the energy balance is accepted as the fundamental starting point. The phenomenological approach results in an analytical description of wear resistance, where microscopic structure and properties of matter are not taken into consideration. The friction coefficient and temperature in the friction area are the parameters set in phenomenological experiments.

A number of tribological research projects by many authors, including most recent publications [1], indicate that it is traditional to accept that friction and wear of elements are affected by set operating parameters of a friction centre (load, sliding velocity, friction distance) as well as uncontrolled (e.g. machine vibrations) and environmental factors (humidity, type of surrounding medium, vacuum, and temperature). This method does not allow the possibility of stabilising, for instance, temperature in the friction area and the friction coefficient itself, which can be quite precisely controlled and stabilised.

Assuming a stabilised friction area temperature and friction coefficient enables one to define the greatest resistance for a given frictional system, that is, the specific work of the friction of the same system. In this case, the specific work of friction is the quotient of the friction work and mass wear of the system (i.e. of both the elements). The remaining parameters of the friction process, that is, pressure, sliding velocity, and friction distance, can be set at random. Thus, optimum parameters of friction can be determined in such a way that the system's resistance is, or approaches, maximum.

The ambient temperature of a frictional centre affects physical and resistance characteristics of sliding materials and the formation of secondary oxide structures [2, 3, 4], which is reflected in the frictional characteristics and wear of sliding elements.

Catalogues presenting tribological properties of materials do not provide temperature ranges for which they were defined and are most often given for operating conditions in positive temperatures. These properties may vary dramatically at low temperatures [5]. Therefore, the data cannot be employed for materials for frictional joints designed to operate at low temperatures.

Engineering practice suggests that the issue of the durability of friction centres at low (below 0°C) temperatures has not been resolved. Oil or plastic lubricants cannot usually be applied to friction centres working at low temperatures, because their solidification points are too high. As a consequence, friction joints are frequently 'dry'. Testing at sub-zero temperatures is required to determine the effects and processes taking place when such friction centres are in

operation. Only then can wear mechanisms be explored and appropriate cooperating materials be selected.

Tribological research at low temperatures requires special apparatus. It was designed and utilised in the 1990s at the Institute of Machine Building, Technical University of Radom [6, 7, 8]. New structures for this type of research have also been developed – TT-3 tester, which is discussed in this paper.

A series of experiments employing the TT-3 have been conducted, some of which are presented in this article. Tribological characteristics of common structural materials were compared at temperatures above and below 0°C. The results may contribute to the development of materials engineering, particularly in the area of modern constructional materials for elements of friction centres operating at low temperatures.

2. Experimental methods

The testing station was designed on the basis of a mathematical model of a tested object which defines resistance to tribological wear, or specific work of wear, as in Equation (1) [6, 8, 9].

$$e_R^x = \frac{1}{-a + b \cdot \Theta} \tag{1}$$

Where: a [g/J] and b [$g \cdot J^{-1} \cdot K^{-1}$] – tribological system constants,
Θ – absolute temperature of surface dF [K].

Testing involved a system of sliding metallic bodies. The object of testing was realised, like in earlier testers, as a system of rings – slider. The ring is the rotating element of the frictional joint. Two fixed sliders, samples whose flat surface is in contact with the ring, were applied as well. The sample material can be selected for each separate matching so that the effect of physical properties, chemical composition, hardness, and structure of the material on increased wear resistance can be assessed. A sample made of both metallic and other materials can be used. The flow diagram of the control and measurement system is illustrated in Figure 1, and a diagram of the device is shown in Figure 2.

A system of two samples that are symmetrically pressed against a disc is a good model of coupling systems and provides for even distribution of loading. Sample loads are internal forces of the loading system. The system guarantees equal loading of both the samples and facilitates the measurement of the friction force and, if necessary, the measurement of the total linear wear of the samples.

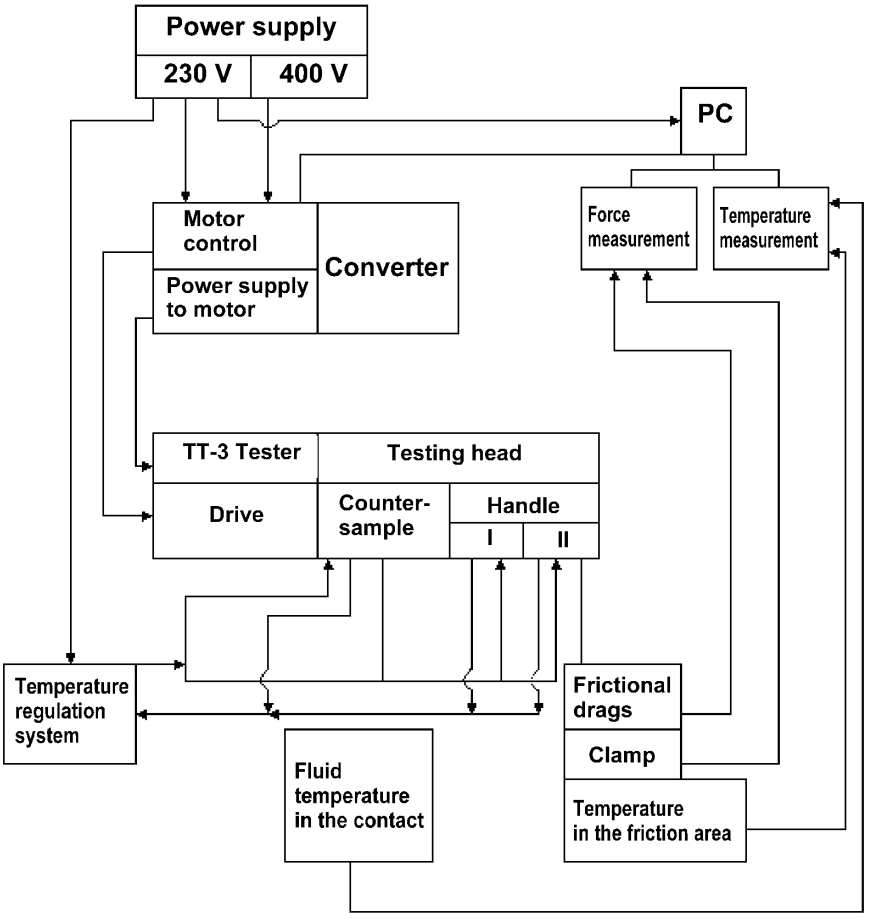

Fig. 1. Flow diagram of the control and measurement systems
Rys. 1. Schemat blokowy układów sterowania i pomiaru: PC – komputer, I i II – uchwyty próbek

The friction couple comprises sliders, made of a selected material, and a ring of 145Cr6 steel of hardness 63 HRC. This design solution enables the application of rings made of both steel and steel covered with layers that increase resistance to wear. The ring is a rotational element, and it is fixed to a disc containing a cooling system and powered by an electric motor including a rotation regulator and a planetary gear. A Stoeber type PA312ED servomotor assembly was employed. Rotational velocities of the discs are regulated by a controller that is connected to a personal computer. A CF-40 circulator was used to stabilise the disc's temperature. The sliders – surface area F = 5, 15 or 25 mm^2 (sliders of surfaces in the range 3 - 25 mm^2 may be utilised) and thickness 0.5 mm – are mounted in dedicated copper clamps. The clamps help to build an isothermal limit 0.5 – 0.1 mm away from the friction area (Fig. 3).

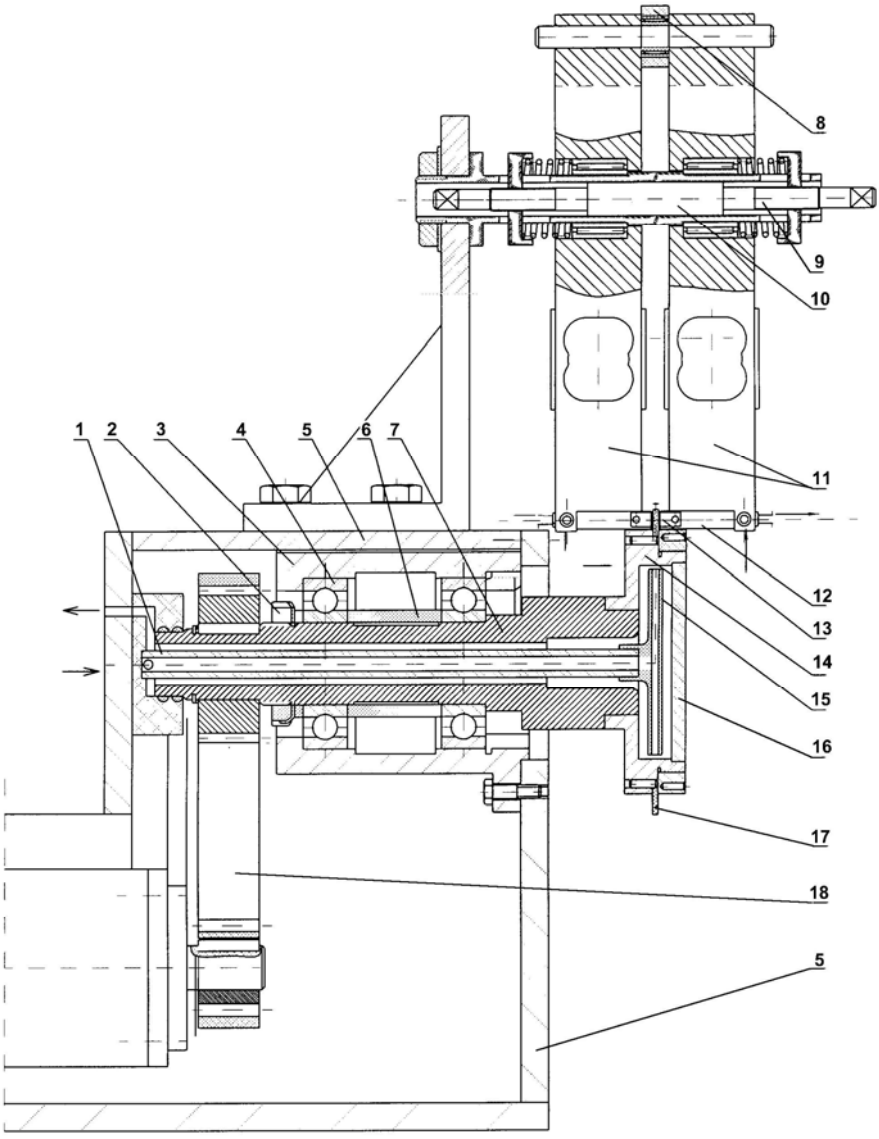

Fig. 2. Diagram of TT-3 tester: 1 – cooling pipe, 2 – lock nut, 3 – bearing sleeve, 4 – ball bearing, 5 – body, 6 – distancing sleeve, 7 – cylinder, 8 – mainstay of the moment of friction measurement, 9 – Roman screw, 10 – sliding sleeve of the clamp against the sample, 11 – extensometer bridge of loading, 12 – clamp of the sample, 13 – sample, 14 – cooling disc, 15 – internal cooling disc, 16 – cover of the cooling disc, 17 – countersample, 18 – driving cogbelt

Rys. 2. Schemat konstrukcyjny testera TT-3: 1 – doprowadzenie cieczy chłodzącej, 2 – nakrętka zamykająca, 3 – tuleja nośna, 4 – łożysko, 5 – korpus, 6 – tuleja dystansowa, 7 – wałek, 8 – opora przetwornika pomiaru momentu tarcia, 9 – śruba rzymska, 10 – tuleja ślizgowa, 11 – przetwornik tensometryczny obciążenia, 12 – uchwyt próbki, 13 – próbka, 14 – tarcza chłodząca, 15 – wewnętrzna tarcza chłodząca, 16 – pokrywa tarczy chłodzącej, 17 – przeciwpróbka, 18 – pasek zębaty napędu

A slider is fitted in the clamp socket using a screw. The end of an iron-constantan thermocouple, in physical contact with the slider, is fitted in the clamp. Cooling fluid is fed and drained via a duct inside the copper clamp.

Temperature characterising the isothermal limit is measured by means of the iron-constantan thermocouple. The measurement is executed during the friction; therefore, the impact of friction heat and heat exchange via the CF-40 circulator is taken into account. The sliders and the clamp are mounted in a head that allows for pressure regulation.

The tester's loading assembly consists of a dynamometer in the form of a Roman screw. A tensometric force measurement sensor on the dynamometer enables accurate setting of the intended pressure.

A tensometric friction force measurement system connected to a measurement card is used to measure friction resistance.

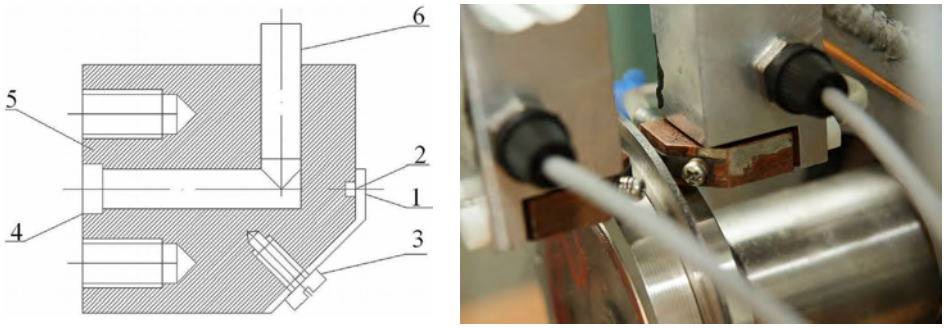

a) b)

Fig. 3. Couple fixing clamp: a) drawing of the clamp 1 – slider, 2 – thermocouple, 3 – screw to fasten the slider in the clamp, 4 – fluid supply pipe, 5 – copper clamp, 6 – fluid drain pipe, b) view of the clamp - wire endings of the pressure force measurement system and screws fixing the couples can be seen

Rys. 3. Uchwyt do mocowania próbek: a) rysunek uchwytu 1 – ślizgacz, 2 – termoelement, 3 – wkręt mocujący ślizgacz w uchwycie, 4 – przewód doprowadzający płyn, 5 – uchwyt miedziany, 6 – przewód odprowadzający płyn, b) widok uchwytu (widoczne wyprowadzenia przewodów układu pomiaru siły docisku i śruby mocujące próbki)

The wear of the sample and the countersample are measured by high-precision scales with an accuracy of 0.01 mg. Before the measurements, the samples were ground under a loading equal to the anticipated measurement loading. Based on earlier experiments [8], the grinding time was set at 3600 s. Depending on a tested friction couple, the sliding velocity was adjustable in the range 0 - 2 m/s.

The Cryo-Compact CF40 circulator was manufactured by Julabo Labortechnik. This device helps to supply fluids at constant temperatures to external circuits. The circulator can provide temperatures within the range of –40 to +150°C, a temperature stability of ±0.03°C, and a flow velocity of 15

L/min. The control system is equipped with a microprocessor controller to provide for high temperature stability. Thermal S oil designed for use within the temperature range of –50 - +150°C serves as the coolant.

A polycarbonate climatic chamber can also be mounted on the friction system head when testing is conducted below ambient temperature.

A felt sweep-off gear is used for controlled removal of friction products from the friction area and the resultant stabilisation of friction resistance. The friction coefficient was maintained at 0.4±0.04 for the duration of the test.

3. Results

Wear resistance was tested under conditions of dry friction and oxidative in order to establish the temperature (referred to as characteristic temperature) at which a given matching of materials displays greater resistance to tribological wear. The following assembly was tested: C80U steel in various conditions of heat treatment in association with hardened 145Cr6 steel (63HRC). Characteristics of the materials are provided in Tables 1 and 2.

C80U is a cold-work tool steel. Structures of both normalised and heat-treated C80U steel were tested.

145Cr6 is a cold-work tool steel, oil-hardened and with stable dimensions once hardened, resistant to abrasion.

Table 1. Characteristics of slider and ring materials
Tabela 1. Charakterystyka materiałów ślizgaczy (pozycje 1÷2) i pierścienia (3)

No.	Material	Condition of heat treatment	Hardness	Chemical composition, %
1	C80U steel (slider)	normalised	27 HRC	C – 0.81 Mn – 0.3 Si – 0.27 Ni – 0.05 Cr – 0.16
2		hardened and tempered at 160°C	55HRC	
3	145Cr6 steel (ring)	hardened	63 HRC	C – 1.4 Mn – 0.59 Si – 0.28 Ni – 0.08 Cr – 1.6 V – 0.17

Table 2. Structures of C80U and 145Cr6 steels
Tabela 2. Opis struktur stali C80U i 145Cr6

Material	View of the structure	Description of the structure
normalised C80U steel		Pearlitic structure: pearlite of low dispersion and with partly visible spheroidisation process
C80U tempered at 160°C/1h	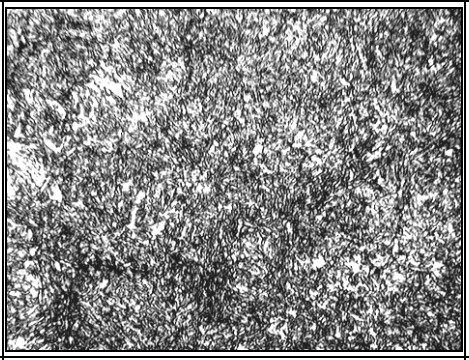	Martensitic structure (low-tempered martensite): martensite of a fine acicular structure
145Cr6 hardened 63 HRC	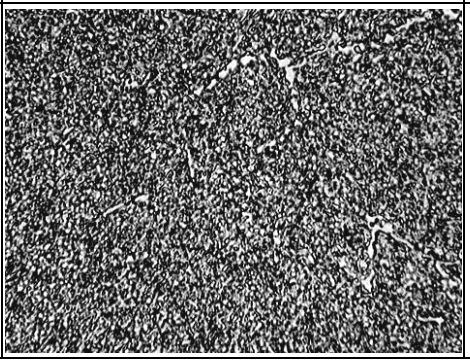	Structure of fine-acicular (cryptoacicular) martensite with low quantity of very fine carbides $(Fe,Cr)_3C$

Research into the characteristic temperature described in [6, 8, 10, 11, and 12] has indicated friction process parameters for selected matchings of engineering metals. The effects of temperature, pressure, and sliding velocity on the specific work of wear have been detected and characterised. According to results of optimisation experiments, it was determined to test wear resistance in the friction zone's temperature range of –25 - +15°C, with a constant friction coefficient, sliding velocities and pressures provided in the respective papers.

Specific work of wear was calculated from the formula:

$$e_R^x = \frac{\mu \cdot N \cdot v \cdot t}{\Delta m_c} \quad [\text{J/g}] \tag{2}$$

where: μ – friction coefficient, N – load [N] , v – sliding velocity [m/s], t – testing time [s], Δm_c – variation of the system's mass [g].

Each measurement was repeated six times and statistically developed. Sample results of the measurements are illustrated in Figures 4 and 5.

The temperature of increased resistance (+10°C), obtained in earlier measurements, was confirmed concerning the couple C80U(norm)/145Cr6 (Fig. 4) as well. However, a new range of increased resistance was found for this matching. This was obtained for -25°C and caused specific work of wear to grow from approx. 45 MJ/g to approx. 109 MJ/g, that is, by 240%. Values of characteristic temperatures and their corresponding wear resistances are summarised in Table 3. This means that the originally determined temperature of increased resistance, though defined correctly, applied solely to the range for which the sliding pair had been tested before. The new value is merely an approximation. As Figure 4c clearly shows, once the temperature of the friction zone falls below –25°C, the specific work of wear may be even greater. In addition, it appears possible that the resistance to wear may vary cyclically as dependent on the temperature of the friction zone.

Table 3. Maximum specific work of wear for tested matchings
Tabela 3. Wartości maksymalne pracy właściwej zużycia dla badanych skojarzeń

Matching	Characteristic temperature, °C	Specific work of wear, MJ/g
C80U(norm)/145Cr6	–25	109
C80U(160)/145Cr6	–25	22

Wear measurements of heat-treated C80U demonstrated (Fig. 5) a significant dependence of resistance obtained for a given temperature of the friction area on the material structure. Matching of heat-treated C80U that is tempered at 160°C and has a structure of pearlite of low dispersion and with partly visible spheroidisation process proved the worst. The resistance was approx. 20% less than that of normalised C80U.

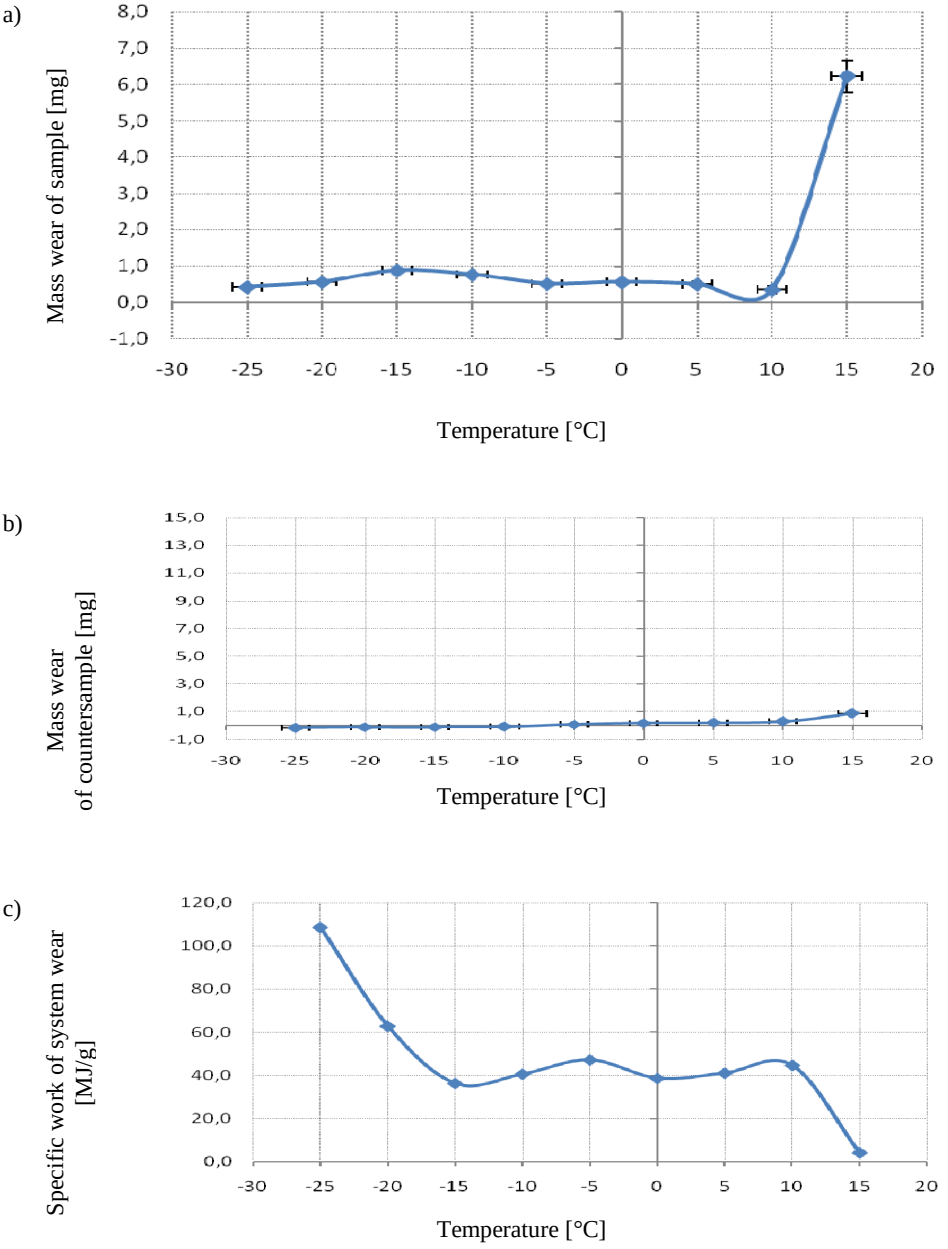

Fig. 4. Testing of the wear resistance of C80U(norm)/145Cr6(63 HRC) friction couple as a function of friction area's temperature: a) mass wear of the sample, b) mass wear of the countersample, c) specific work of the system's wear (p = 0.98 MPa, v = 0.8 m/s, μ = 0.4)

Rys. 4. Badanie odporności na zużywanie pary trącej C80U/145Cr6(63 HRC) jako funkcji temperatury strefy tarcia: a) zużycie masowe próbki, b) zużycie masowe przeciwpróbki, c) praca właściwa zużycia układu (p = 0,98 MPa, v = 0,8 m/s, μ = 0,4)

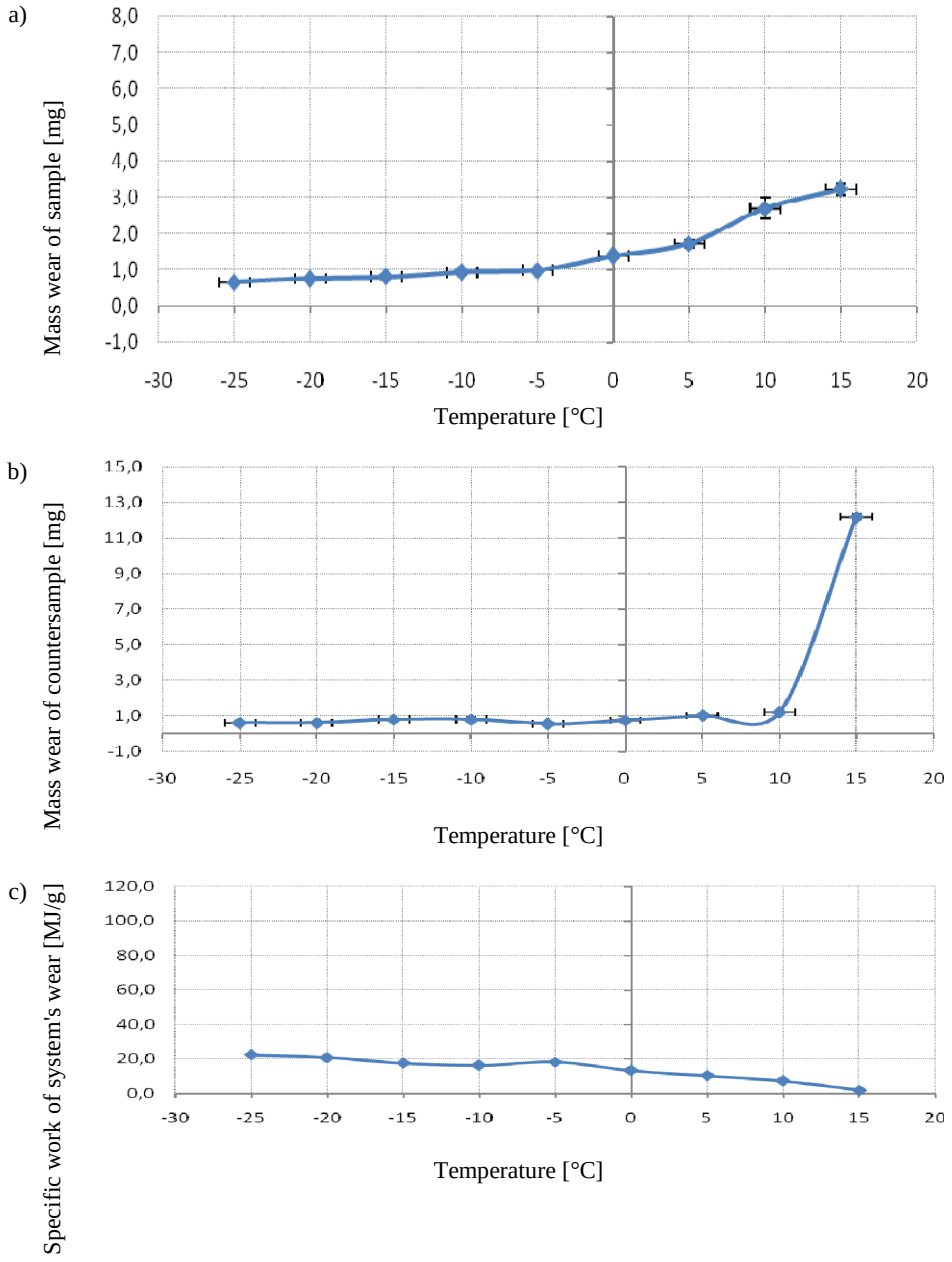

Fig. 5. Testing of the wear resistance of C80U(160)/145Cr6(63 HRC) friction couple as a function of friction area's temperature: a) mass wear of the sample, b) mass wear of the countersample, c) specific work of the system's wear (p = 0.98 MPa, v = 0.8 m/s, μ = 0.4)

Rys. 5. Badanie odporności na zużywanie pary trącej C80U(160)/145Cr6 (63 HRC) jako funkcji temperatury strefy tarcia: a) zużycie masowe próbki, b) zużycie masowe przeciwpróbki, c) praca właściwa zużycia układu (p = 0,98 MPa, v = 0,8 m/s, μ = 0,4)

4. Discussion

The mathematical model of the tested object (Equation 1) is correct until the characteristic temperature in the friction couple is reached. The tribosystem changes after that point are a result of phase transitions in the material. The systemic constants, *a* and *b*, are then modified. A characteristic temperature can again be determined in this altered system. It will be different. This cyclical nature is graphically presented in Figure 6. The new temperature was lower than the original temperature in the case of the systems under discussion. Since the range of the friction area temperatures included in the testing was limited (–25 - +15°C), it cannot be determined if the effect will recur at still lower temperatures.

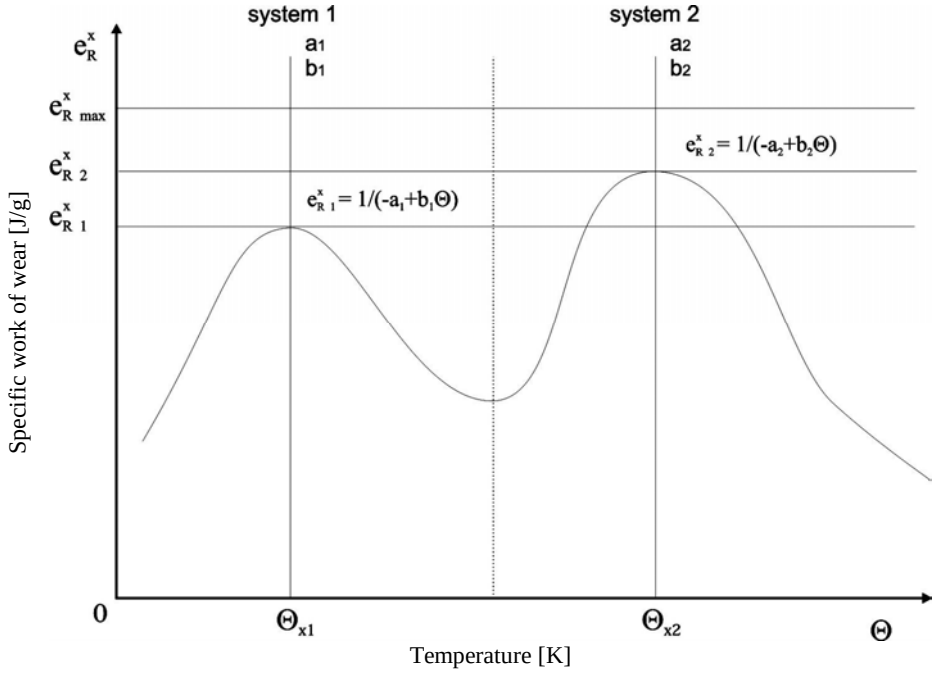

Fig. 6. Schematic representation of the possible cyclical nature of wear resistance increases. The maximum specific work of wear that can be obtained in the given system is marked
Rys. 6. Schematyczne przedstawienie możliwego występowania lokalnych maksimów odporności na zużycie (zaznaczono maksymalną pracę właściwą zużycia teoretycznie możliwą do uzyskania w danym systemie)

A measurable depositing of particles onto cooperating elements was noted in most cases. In the figures, this is shown as a negative mass wear of both sample and countersample. Such depositing may have occurred (and was most likely to occur) also where mass increments were not recorded. In these

circumstances, material particles migrated between the cooperating surfaces, as discussed in a transfer model in [8]. Mössbauer spectral analysis helped to detect nanometric particles and particles of the native material (ferrite and martensite) among the wear products, which further confirms this possibility. Presence of austenite, on the other hand, indicates the presence of the countersample particles.

The presence of nanoparticles, a result of abrasion in the system, can help consolidate the material [13] and change the degree of the heterogeneity of mechanical properties. It can therefore be expected that the refinement of structure will, to a greater or lesser extent, modify both the weight and operation of the particular component mechanisms of the consolidation, i.e. solution, deformation, dislocation, substructure, with foreign phase particles, and from grain boundaries. Above all, grain refinement from micro- to nanometric scale improves resistance properties.

The mechanism of the material's phase transitions during the friction needs to be clarified. Results of Mössbauer spectral analysis point to diffusive impregnation of ferrite with carbon as an effect of plastic-elastic interactions at the contact of the rough surfaces of cooperating elements. Heat effects at the friction contact also play a certain role, although they are not decisive owing to intense collection of heat from the friction contact. Principles of tribosystem self-organisation described by Kostecki [14] appear to be a key reference for the clarification of the issue under discussion. Kostecki cites the formation of secondary structures by frictional depositing of metals as an example of a practical application of the self-organisation.

5. Conclusions

Testing by means of the tester TT-03 leads to the following conclusions:

- For each material matching, there is a characteristic temperature (negative or positive) at which an increased (approaching maximum) resistance of a given system to wear is obtained.
- Variations of dependence of wear resistance on a friction area temperature are unique features of a given material matching and depend on the chemical composition and structure of the materials.
- Further physicochemical and material testing is necessary to explain a number of potential dependencies (chemical composition, micro hardness, structure).

References

[1] Mańkowska A., Michalczewski R., Szczerek M., Wulczyński J.: Low-temperature characteristics of steel friction couples. Tribologia, (2010), No. 1 pp.77÷92.

[2] Quinn T.F.J., Sullivan J.L., Rowson D.M.: Origins and development of oxidational wear at low ambient temperatures. Wear, (1984), No. 94 pp. 175÷191.
[3] Straffelini G., Trabucco D., Molinari A.: Oxidative wear of heat-treated steels. Wear. (2001), No. 250, pp. 485÷491.
[4] So H., Yu D.S., Chuang C.Y.: Formation and wear mechanism of tribooxides and the regime of oxidational wear of steel. Wear. (2002), No. 253, pp. 1004÷1015.
[5] Ostrovskaya Ye.L., Yukhno T.P., Gamulya G.D., Vvedenskij Yu.V., Kuleba V.I.: Low temperature tribology at the B. Verkin Institute for low temperature physics & engineering (historical review). Tribology International, (2001), No. 34, pp. 265÷276.
[6] Żurowski W.: Energetyczny aspekt wzrostu odporności metali na zużywanie w procesie tarcia technicznie suchego. Rozprawa doktorska, Politechnika Świętokrzyska, Kielce, (1996).
[7] Żurowski W.: Stanowiska do badań maksymalnej odporności układów metali na zużywanie tribologiczne. Politechnika Radomska. Scientific Publications. Mechanical Engineering, (2002), No. 1, pp. 172÷185.
[8] Żurowski W.: Wear resistance maximization of frictional interface systems (in Tribology 2008). SAIT, Pretoria. 2008. ISBN: 978-0-620-38082-9.
[9] Sadowski J., Żurowski W.: Thermodynamische Aspekte über die Verschließbeständigkeit von Metallen. Tribologie und Schmierungstechnik, (1992) No. 3, pp. 152÷158.
[10] Sadowski J. Żurowski W.: Badania maksymalnej odporności układów ciał metalicznych na zużywanie tribologiczne. Cz. I. Teoretyczno-eksperymentalne podstawy maksymalizacji odporności na zużywanie tribologiczne. Inżynieria Powierzchni nr 4/2000, IMP – Warszawa, s. 46÷51.
[11] Sadowski J., Żurowski W.: Badania maksymalnej odporności układów ciał metalicznych na zużywanie tribologiczne. Cz. II. Badania eksperymentalne maksymalnej odporności na zużywanie tribologiczne i wybranych cech warstwy wierzchniej. Inżynieria Powierzchni nr 1/2001, IMP – Warszawa. s. 41÷55.
[12] Sadowski J., Żurowski W.: Sposób zmniejszania zużycia tribologicznego elementów trących. Patent polski No. 1767118, B1, F16N 29/00, Warszawa 1999.
[13] Muszka K.: Wpływ rozdrobnienia struktury na mechanizmy umocnienia stali niskowęglowych umacnianych plastycznie. Rozprawa doktorska. AGH, Kraków 2008.
[14] Kostecki B.I.: Basic conditions of tribological system self-organization. Tribologia, 1988, No. 4, pp. 4÷14.

Badania zużycia skojarzenia tarciowego C80U/145Cr6 w warunkach stabilizacji temperatury w strefie tarcia

S t r e s z c z e n i e

Badania odporności na zużywanie opierają się na analizie przemian termodynamicznych zachodzących w systemie termodynamicznym otwartym. Celem opisanych w artykule badań jest stwierdzenie, w jakich warunkach układ trący uzyskuje największą odporność. Weryfikację rozważań teoretycznych umożliwia wykorzystanie odpowiednich stanowisk badawczych.

Wykonane zostało nowe urządzenie służące do badań odporności układów sprzęgających. W artykule omówiono jego konstrukcję oraz możliwości badawcze. Jest to zmodyfikowany układ typu trzpień-tarcza modelujący typowe warunki pracy tarczowego mechanizmu hamulcowego lub sprzęgłowego, ale z wymuszeniem temperatury strefy tarcia. Oprócz części mechanicznej

stanowisko wyposażone jest w kriocyrkulator służący do ustalania i stabilizowania temperatury w strefie tarcia.

Założenia konstrukcyjne nowego testera opierają się na modelu fizycznym zakładającym, że system tribologiczny jest w stanie wymieniać energię i materię z otoczeniem, przy czym przyczyną wszelkich przemian zachodzących w systemie i na jego granicach jest praca tarcia. Wywołuje ona wzrost energii wewnętrznej układu, a także jej dyssypację na sposób ciepła kompensująca dyssypację mechaniczną, czyli zużywanie.

Dane zawarte w katalogach materiałowych dotyczące właściwości tribologicznych materiałów podawane są dla warunków pracy w temperaturach dodatnich, co może być błędne w przypadku ich wykorzystania przy doborze materiałów na pary tarciowe przeznaczone do pracy w niskich temperaturach. Urządzenie pozwala na sporządzenie niskotemperaturowych charakterystyk tribologicznych par tarciowych.

W wyniku przeprowadzonych badań wykazano, że istnieje temperatura, w której dane skojarzenie materiałowe wykazuje minimum zużycia, np. dla skojarzenia C80U/145Cr6 jest to 25°C.

SCIENTIFIC PROBLEMS
OF MACHINES OPERATION
AND MAINTENANCE
4 (164) 2010

HENRYK TOMASZEK [*], MICHAŁ JASZTAL[**]

Outline of a method for fatigue life determination for selected aircraft's elements

Key words

Fatigue life, Paris' equation, constant and variable amplitude loading.

Słowa kluczowe

Trwałość zmęczeniowa, równanie Parisa, stało- oraz zmiennoamplitudowe widmo obciążenia.

Summary

This paper describes a method for the evaluation of the fatigue life of a structural component of an aircraft for constant and variable amplitude loading, using deterministic description of fatigue crack growth based on Paris equation with corrective coefficients. The coefficients take into consideration crack and element geometry and phenomena connected with variable amplitude loading effects. Final equations for fatigue life calculations were carried out for two special cases: when the exponent of the Paris formula is $m = 2$ and $m = 4$. Examples show the application of the method and indicate numerical verification of the mathematical model.

[*] Air Force Institute of Technology, Księcia Bolesława 6 Street, 01-494 Warsaw, Poland.
[**] Military University of Technology, Kaliskiego 2 Street, 00-908 Warsaw, Poland, mjasztal@wat.edu.pl, tel. +48 22 683 77 89.

1. Introduction

This paper assumes that crack l_o occurs in a given structural element during operation, and it increases under variable loading to admissible (safety) length l_d. The crack growth process, approached in a deterministic way, has been described with the Paris formula in the following form:

$$\frac{dl}{dN} = C(\Delta K)^m \tag{1}$$

where: ΔK – range of stress intensity factor,
C, m – material constants,
N – variable which represent number of load cycles.

According to equation (1), structural element fatigue life can be express by the following equation:

$$N_{l_d} = \int_{l_0}^{l_d} \frac{1}{C(\Delta K)^m} dl \tag{2}$$

The above-mentioned integral (2) is sometimes hard to solve. Troubles are caused by the coefficients, which are dependent on actual crack length. Mathematical model consists the coefficients which improve accuracy but on the other hand makes analytical solution difficult. An example of this coefficient is a variable described as M_k which specifies the influence of crack location and dimensions in relation to structural element dimensions on crack growth velocity. Admissible crack length l_d can be described with use of the stress intensity factor in the following form:

$$K = M_k \sigma \sqrt{\pi l} \tag{3}$$

Stress intensity factor (3) becomes a quantity of a critical value K_c when the crack length and the stress takes critical values l_{kr} and σ_{kr} respectively. Then it is called “resistance of the material to cracking”.

$$K_c = M_k \sigma_{kr} \sqrt{\pi l_{kr}} \tag{4}$$

Exceeding the critical value of the crack length usually leads to a catastrophic damage to the component. If a factor of safety is introduced, one can find the admissible value of the crack. The computational formula takes the following form:

$$l_d = \frac{K_c^2}{kM_k^2\sigma_{kr}^2\pi} \tag{5}$$

where: k – factor of safety.

2. Fatigue life of selected structural elements under constant amplitude loading

Equation (1) in the developed form is as follows:

$$\frac{dl}{dN} = UCM_k^m(\Delta\sigma)^m\pi^{\frac{m}{2}}l^{\frac{m}{2}} \tag{6}$$

where: U – empirical function of crack closure contribution to crack growth relates to stress ratio R,
$\Delta\sigma$ – the range of stress in one cycle $\Delta\sigma = \sigma_{max} - \sigma_{min}$,
M_k – geometrical coefficient (Fig. 1) defined for specified geometry by relation [1]:

$$M_k = 1 - 0{,}1\left(\frac{l}{w}\right) + \left(\frac{l}{w}\right)^2 \tag{7}$$

w – structural element dimension in the direction of crack growth.

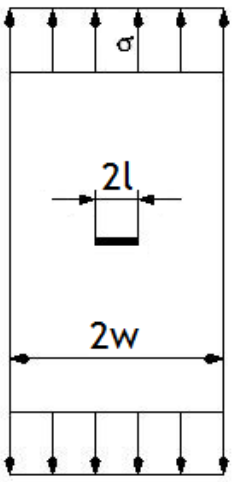

Fig. 1. Element geometry with central crack
Rys. 1. Geometria elementu z centralnym pęknięciem

Notation of the coefficient M_k was assumed in the following form:

$$M_k = a + bx + cx^2 \tag{8}$$

where: $x = l,\ a = 1,\ b = -\frac{0{,}1}{w},\ c = \frac{1}{w^2}$.

Taking the above-mentioned assumption into account, Equation (6) takes the following form:

$$\frac{dx}{dN} = UC(a + bx + cx^2)^m (\Delta\sigma)^m \pi^{\frac{m}{2}} x^{\frac{m}{2}} \tag{9}$$

The indefinite integral has the following form:

$$\int \frac{dx}{(a+bx+cx^2)^m x^{\frac{m}{2}}} = \int UC(\Delta\sigma)^m \pi^{\frac{m}{2}} dN \tag{10}$$

Hence, fatigue life of the structural element for assumed type of load is as follows:

$$N = \frac{1}{UC(\Delta\sigma)^m \pi^{\frac{m}{2}}} \int_{l_0}^{l_d} \frac{dx}{x^{\frac{m}{2}}(a + bx + cx^2)^m}$$

For $R = a + bx + cx^2$ the equation has the form:

$$N = \frac{1}{UC(\Delta\sigma)^m \pi^{\frac{m}{2}}} \int_{l_0}^{l_d} \frac{dx}{x^{\frac{m}{2}}(R)^m} \tag{11}$$

Calculation of Integral (11) in analytical form is difficult. Hence, the fatigue life description was carried out for two special cases: when the exponent of the Paris formula is $m = 2$ and $m = 4$.

Fatigue life determination for $m = 2$

Formula (11) for $m = 2$ takes the following form:

$$N = \frac{1}{UC(\Delta\sigma)^2 \pi} \int_{l_0}^{l_d} \frac{dx}{xR^2} \tag{12}$$

where: $R = (a + bx + cx^2)$.

Indefinite integral [2]:

$$\int \frac{dx}{xR^2} = \frac{1}{2a^2} ln \frac{x^2}{R} + \frac{1}{2aR}\left(1 - \frac{b(b+2cx)}{\Delta}\right) - \frac{b}{2a^2}\left(1 + \frac{2ac}{\Delta}\right)\int \frac{dx}{R} \quad (13)$$

Integral $\int \frac{dx}{R}$ has following solution [2]:

$$\int \frac{dx}{R} = \begin{cases} \frac{-2}{\sqrt{-\Delta}} arctgh \frac{b+2cx}{\sqrt{-\Delta}} & \text{dla } \Delta < 0 \\ \frac{-2}{b+2cx} & \text{dla } \Delta = 0 \\ \frac{2}{\sqrt{\Delta}} arctg \frac{b+2cx}{\sqrt{\Delta}} & \text{dla } \Delta > 0 \end{cases} \quad (14)$$

where: $\Delta = 4ac - b^2$.

For the assumption that $\Delta > 0$ Indefinite Integral (13) takes the form:

$$\int \frac{dx}{xR^2} = \frac{1}{2a^2} ln \frac{x^2}{R} + \frac{1}{2aR}\left(1 - \frac{b(b+2cx)}{\Delta}\right) - \frac{b}{2a^2}\left(1 + \frac{2ac}{\Delta}\right)\frac{2}{\sqrt{\Delta}} arctg \frac{b+2cx}{\sqrt{\Delta}} \quad (15)$$

Calculating the definite integral:

$$\int_{l_0}^{l_d} \frac{dx}{xR^2} = \left[\frac{1}{2a^2} ln \frac{{l_d}^2}{R(l_d)} + \frac{1}{2aR(l_d)}\left(1 - \frac{b(b+2cl_d)}{\Delta}\right) - \frac{b}{2a^2}\left(1 + \frac{2ac}{\Delta}\right)\frac{2}{\sqrt{\Delta}} arctg \frac{b+2cl_d}{\sqrt{\Delta}}\right] -$$

$$\left[\frac{1}{2a^2} ln \frac{{l_0}^2}{R(l_0)} + \frac{1}{2aR(l_0)}\left(1 - \frac{b(b+2cl_0)}{\Delta}\right) - \frac{b}{2a^2}\left(1 + \frac{2ac}{\Delta}\right)\frac{2}{\sqrt{\Delta}} arctg \frac{b+2cl_0}{\sqrt{\Delta}}\right] \quad (16)$$

where: $R(l_d) = (a + bl_d + c(l_d)^2)$; $R(l_0) = (a + bl_0 + c(l_0)^2)$

The fatigue life of the element for $m = 2$ can be obtained from the following:

$$N = \frac{1}{UC(\Delta\sigma)^2\pi}\int_{l_0}^{l_d} \frac{dx}{xR^2} \quad (17)$$

where: integral $\int_{l_0}^{l_d} \frac{dx}{xR^2}$ is described by Equation (16).

Fatigue life determination for *m* = 4

The main task in this case is to the calculation of indefinite integral:

$$\int \frac{dx}{R^4 x^2}$$

Calculating Integral (18):

$$\int \frac{dx}{R^4x^2} = \frac{1}{3a^5}\left(-\frac{3a}{x} + \frac{a^3\left(b^3-3abc+b^2cx-2ac^2x\right)}{(-b^2+4ac)\left(a+x(b+cx)\right)^3} - \right.$$

$$\frac{a^2\left(3b^5-22ab^3c+35a^2bc^2+3b^4cx-20ab^2c^2x+22a^2c^3x\right)}{(b^2-4ac)^2\left(a+x(b+cx)\right)^2} +$$

$$\left.\left(\frac{3a\left(-3b^7+34ab^5c-124a^2b^3c^2+134a^3bc^3-3b^6cx+32ab^4c^2x-104a^2b^2c^3x+76a^3c^4x\right)}{(b^2-4ac)^3\left(a+x(b+cx)\right)}\right) -\right.$$

$$\frac{12\left(b^8-14ab^6c+70a^2b^4c^2-140a^3b^2c^3+70a^4c^4\right)arctg\left[\frac{b+2cx}{\sqrt{-b^2+4ac}}\right]}{(-b^2+4ac)^{7/2}} - 12b\cdot log(x) + 6b\cdot$$

$$\left. log\left(a+x(b+cx)\right)\right) \tag{18}$$

Finally, applying a similar procedure like for *m* = 2 one can determine the fatigue life of the structural element for the Paris formula exponent *m* = 4.

3. Fatigue life of selected structural elements under variable amplitude loading

In this model, further assumptions are as follows:

1. Aircraft structural element works during operation under variable loading.
2. Fatigue loading of the component is determined with some spectrum of loads, set up using a pattern of loading in the standard flight of aircraft.
3. Spectrum of loads is determined as follows:
   - The load spectrum consist of N_c cycles.
   - Load cycles can be ordered in L stress levels and each level has maximum stress values $\sigma_1^{max}, \sigma_2^{max}, \ldots, \sigma_L^{max}$.
4. The number of maximum stress values repetitions in the load spectrum is as follows:
   σ_1^{max} occurs n_1 times, σ_2^{max} occurs n_2 times, …, σ_L^{max} occurs n_L times.

The number of specified load level repetitions during a standard flight of the aircraft is as follows: $N_c = \sum_{i=1}^{L} n_i$.

5. The minimum stress value at the specified load levels is described by the following formula:

$$\sigma_{i,śr}^{min} = \frac{\sigma_{i,1}^{min} + \sigma_{i,2}^{min} + \cdots + \sigma_{i,n_i}^{min}}{n_i}, \text{ where } i = 1,2, \ldots, n_i.$$

6. Table 1 shows the maximum and minimum stress levels and the frequency of stress levels appearing in the spectrum:

Table 1. Maximum σ_i^{max} and minimum $\sigma_{i,śr}^{min}$ stress values in the cycles, and frequencies of their appearing in the spectrum P_i

Tabela 1. Zestawienie maksymalnych σ_i^{max} and minimum $\sigma_{i,śr}^{min}$ wartości naprężeń w cyklach oraz częstości ich występowania P_i

σ_i^{max}	σ_1^{max}	σ_2^{max}	…	σ_i^{max}	…	σ_L^{max}
$\sigma_{i,śr}^{min}$	$\sigma_{1,śr}^{min}$	$\sigma_{2,śr}^{min}$	…	$\sigma_{i,śr}^{min}$	…	$\sigma_{L,śr}^{min}$
P_i	$P_1 = \frac{n_1}{N_c}$	$P_2 = \frac{n_2}{N_c}$	…	$P_i = \frac{n_i}{N_c}$	…	$P_L = \frac{n_L}{N_c}$

7. Table 2 presents stress ratio coefficients and empirical function U of the crack closure contribution to crack growth as related to stress ratio $\hat{R}_i$:

Table 2. Stress ratios $\hat{R}_i$ and empirical coefficients of influence on crack growth U_i

Tabela 2. Zestawienie współczynników asymetrii cyklu oraz współczynników uwzględniających ich wpływ na prędkość pękania

cykle i	1	2	…	*i*	…	*L*
$\hat{R}_i$	$\hat{R}_1$	$\hat{R}_2$	…	$\hat{R}_i$	…	$\hat{R}_L$
U_i	U_1	U_2	…	U_i	…	U_L

where: $\hat{R}_i = \frac{\sigma_{i,śr}^{min}}{\sigma_i^{max}}$, $U_i = \propto_1 + \propto_2 \hat{R}_i + \propto_3 \hat{R}_i^{\,2}$; $\propto_1, \propto_2, \propto_3$ – empirical coefficients.

8. Table 3 consist of stress range levels:

$$\Delta\sigma_i = \sigma_i^{max} - \sigma_{i,śr}^{min}$$

Table 3. Range of stress $\Delta\sigma_i$ and frequencies of their appearing in the spectrum P_i
Tabela 3. Zestawienie wartości zakresu zmian naprężeń $\Delta\sigma_i$ oraz częstości ich występowania P_i

$cycle\ types$	1	2	…	i	…	L
$\Delta\sigma_i$	$\Delta\sigma_1$	$\Delta\sigma_2$	…	$\Delta\sigma_i$	…	$\Delta\sigma_L$
P_i	P_1	P_2	…	P_i	…	P_L

9. Table 4 consist of retardation coefficients C_i^P for specified levels which takes into consideration the influence of overload cycles on crack growth rate:

$$\Delta\sigma_{i,ef} = C_L^P \Delta\sigma_i$$

where: C_i^P – retardation coefficients.

Table 4. Range of effective stress $\Delta\sigma_{i,ef}$ which takes into consideration effect of overload cycles
Tabela 4. Zestawienie wartości zakresu zmian naprężeń efektywnych $\Delta\sigma_{i,ef}$ uwzględniających występowanie cykli przeciążających

$cycle\ types$	1	2	…	i	…	L
$coefficients$	C_1^P	C_2^P	…	C_i^P	…	C_L^P
$\Delta\sigma_{i,ef}$	$\Delta\sigma_{1,ef}$	$\Delta\sigma_{2,ef}$	…	$\Delta\sigma_{i,ef}$	…	$\Delta\sigma_{L,ef}$

The crack growth process, approached in a deterministic way, has been described with the Paris formula in (1). For the above-mentioned assumptions, Formula (1) for *i*-th type of load cycles has following form:

$$\frac{dl}{dN} = C U_i M_k^m \left(\Delta\sigma_{i,ef}\right)^m \pi^{\frac{m}{2}} l^{\frac{m}{2}} \tag{20}$$

Taking into consideration all types of load cycles, Formula (20) has the following form:

$$\frac{dl}{dN} = C\pi^{\frac{m}{2}} \left(\sum_{i=1}^{L} P_i\, U_i \left(\Delta\sigma_{i,ef}\right)^m\right) M_k^m l^{\frac{m}{2}} \tag{21}$$

Assuming that

$$l = x;\ M_k = R;\ R = (a + bx + cx^2)$$

Then

$$\frac{dx}{dN} = C\pi^{\frac{m}{2}} \left(\sum_{i=1}^{L} P_i\, U_i \left(\Delta\sigma_{i,ef}\right)^m\right) (a + bx + cx^2)^m x^{\frac{m}{2}} \tag{22}$$

The integration of equation (22) produces the following fatigue life formula:

$$N = \frac{1}{C\pi^{\frac{m}{2}}\left(\sum_{i=1}^{L} P_i U_i \left(\Delta\sigma_{i,ef}\right)^m\right)} \int_{l_0}^{l_d} \frac{dx}{x^{\frac{m}{2}} R^m} \tag{23}$$

Equation (23) provides the possibility of the fatigue life calculation for structural elements with use of a variable amplitude loading description, which take into consideration L load types.

Using these results one can derive a formula for the fatigue life calculation of a structural element for the Paris formula exponent $m = 2$ or $m = 4$.

4. Final remarks and a computational example

The method was verified by predicting the crack behavior and fatigue life estimation for steel sheet subjected to variable amplitude load program. The specimens geometry given in Fig. 2 were cut out from the sheet. Subsequently, a through-thickness central hole of 5 mm in diameter, was cut inside each specimen. The central hole had on each side a through-thickness saw cut of 2.5 mm length and an initial pre-crack of 2.5 mm length, the total length of the initial crack was equaled to $2l = 20$ mm. The hole served as crack initiator.

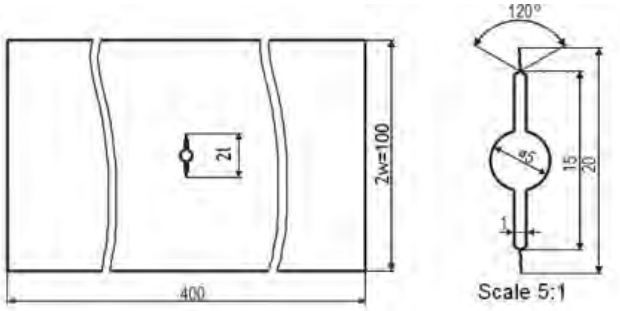

Fig. 2. Geometry of specimen
Rys. 2. Geometria próbki

The calculation was carried out for a variable amplitude load spectrum. The characteristic of the spectrum is presented in Table 5. The table contains maximum stress σ_i^{max}, average minimum stress $\sigma_{i,śr}^{min}$ and effective stress range values $\Delta\sigma_{i,ef}$ for the established 7 load levels with frequency of stress levels appearing in the spectrum. Furthermore, the table contains stress ratio coefficients $\hat{R}_i$ and empirical function U_i of crack closure contribution to crack growth relates to stress ratio:

$$U_i = 0{,}55 + 0{,}33\hat{R}_i + 0{,}12\hat{R}_i^{\,2}$$

The calculation was carried out with use of following material constants:

$$m = 2$$
$$C = 8 \cdot 10^{-10}.$$

Table 5. Quantities which describe loading spectrum
Tabela 5. Wielkości charakteryzujące widmo obciążeń

Load level i	1	2	3	4	5	6	7
Number of cycles	1	5	4	10	30	50	140
σ_i^{max} [MPa]	186	159	141	129	112	93	72
$\sigma_{i,śr}^{min}$ [MPa]	-28	-13	8	17	23	27	27
Coefficient $\hat{R}_i$	-0.1505	-0.0818	0.0567	0.1317	0.2053	0.2903	0.375
Stress range $\Delta\sigma_{i,ef}$ [MPa]	214	172	133	112	89	66	45
Empirical function U_i	0.5030	0.5238	0.5691	0.5955	0.6228	0.6559	0.6906
Load level contribution into load spectrum P_i	0.0042	0.0208	0.0167	0.0417	0.125	0.2083	0.5833

Furthermore, the calculation of fatigue life was carried out for crack growth from initial crack length l_0 = 10 mm to admissible crack length l_d = 27 mm. The admissible crack length was calculated using Formula (5). Retardation coefficient C_i^P which takes into consideration the influence of overload cycles on crack growth rate was assumed as $C_i^P = 1$. Finally, Formula (23) was used for the calculation fatigue life for m = 2:

$$N_{l_d} = \frac{1}{C\pi\left(\sum_{i=1}^{L} P_i\, U_i\left(\Delta\sigma_{i,ef}\right)^2\right)} \int_{l_0}^{l_d} \frac{dx}{xR^2}$$

Integral described by Formula (16):

$$\int_{l_0}^{l_d} \frac{dx}{xR^2} = \left[\frac{1}{2a^2} ln \frac{{l_d}^2}{R(l_d)} + \frac{1}{2aR(l_d)}\left(1 - \frac{b(b+2cl_d)}{\Delta}\right)\right.$$
$$\left. - \frac{b}{2a^2}\left(1 + \frac{2ac}{\Delta}\right)\frac{2}{\sqrt{\Delta}} arctg \frac{b+2cl_d}{\sqrt{\Delta}}\right]$$
$$- \left[\frac{1}{2a^2} ln \frac{{l_0}^2}{R(l_0)} + \frac{1}{2aR(l_0)}\left(1 - \frac{b(b+2cl_0)}{\Delta}\right)\right.$$
$$\left. - \frac{b}{2a^2}\left(1 + \frac{2ac}{\Delta}\right)\frac{2}{\sqrt{\Delta}} arctg \frac{b+2cl_0}{\sqrt{\Delta}}\right]$$

where: $R(l_d)=(a + bl_d + c(l_d)^2)$; $R(l_0)=(a + bl_0 + c(l_0)^2)$; $\Delta = 4ac - b^2$.

For the geometry specified in Fig. 2 $a = 1, b = -\frac{0,1}{w}$, $c = \frac{1}{w^2}$, where element width w = 50 mm

On the basis of the above-mentioned formula, the authors made a fatigue life calculation for structural elements with use of variable amplitude loading description included in Table 5. As a result of the calculation, value $N_{l_d} = 114000$ cycles is the fatigue life expressed by number of cycles.

This method has the advantage of taking into consideration physical phenomenon connected with variable amplitude loading and variable geometrical coefficient M_k. On the basis of this confirmation, this method may be of practical use for structure's element fatigue life assessment. This method can be extended in the future by solution for various Paris exponent m values.

5. Literature

[1] Kocańda S., Szala J., *Podstawy obliczeń zmęczeniowych*, PWN, Warszawa 1985.
[2] Ryżyk J.H., Gradsetyn J.S., *Tablice całek, sum, szeregów i iloczynów*, PWN, Warszawa 1964.
[3] Tomaszek H., Żurek J., Jasztal M., *Prognozowanie uszkodzeń zagrażających bezpieczeństwu lotów statków powietrznych*, Wydawnictwo naukowe ITE, Radom 2008.
[4] Kocańda D., Tomaszek H., Jasztal M., *Predicting fatigue crack growth and fatigue life under variable amplitude loading*, Fatigue of Aircraft Structures - Monographic Series Issue 2010 - Institute of Aviation Scientific Publications, Warsaw 2010.
[5] Schijve J., *The significance of fractography for investigations of fatigue crack growth under variable-amplitude loading*, Fatigue Fract Eng Mater Struct 22 (1999).

Zarys metody oceny trwałości wybranych elementów konstrukcji statku powietrznego

S t r e s z c z e n i e

W artykule zaprezentowano sposób analitycznego wyznaczenia trwałości zmęczeniowej elementów konstrukcyjnych dla przypadku obciążenia cyklami jednorodnymi oraz dla zmiennego widma obciążenia. Opis deterministyczny rozwoju pęknięcia oparto na zależności Parisa zawierającej współczynniki korekcyjne uwzględniające geometrię elementu oraz geometrię pęknięcia, a także zjawiska związane z oddziaływaniem zmiennego widma obciążenia. Zależności końcowe na trwałość zmęczeniową zostały wyznaczone dla dwóch przypadków szczególnych, gdy wykładnik równania Parisa m = 2 oraz m = 4. Przedstawiony przykład obliczeniowy pozwolił na przeprowadzenie weryfikacji liczbowej opracowanego modelu oraz zobrazował aplikacyjny charakter opracowanej metody.

SCIENTIFIC PROBLEMS
OF MACHINES OPERATION
AND MAINTENANCE
4 (164) 2010

STANISŁAW MROZIŃSKI*, JÓZEF SZALA*

Problem of cyclic hardening or softening in metals under programmed loading

Key words

Fatigue life, cyclic properties, cyclic softening and hardening, fatigue tests.

Słowa kluczowe

Trwałość zmęczeniowa, cykliczne własności, cykliczne osłabienie lub umocnienie, testy zmęczeniowe.

Summary

Problem of cyclic hardening or softening in metals and their alloys has been known for over 40 years. Despite such a long period of time there is lack of the of universal models describing these processes. The basis of their valuation are experimental tests carried out under constant amplitude sinusoidal loadings. The tests can be performed under constant stress amplitude or constant strain amplitude. These conditions are not equivalent for the range of loadings, where the law of the linear relation of stress from strain is not valid. The problem of the cyclic hardening or softening in metals and their alloys becomes significantly complex in the case of variable amplitude loadings, typical for operating loadings of construction elements.

In the paper there was described the investigating of cyclic properties of three alloys: PA7 aluminium alloy strongly hardening cyclically, 30HGSA alloy steel strongly softening cyclically and C45 constructional steel which, depending on loading level, undergoes cyclic softening or cyclic hardening. The tests were carried out under programmed loadings with gradually increasing stress amplitude.

* University of Technology and Life Sciences in Bydgoszcz, al. prof. S. Kaliskiego 7, 85-796 Bydgoszcz, Poland.

1. Introduction

Fatigue in metals and their alloys is very complex process which depends on many factors and very difficult to describe [1-2]. In spite of nearly 200 years of intensive research and over 90000 publications (1995 year data according to Science Direct base) there was not developed an universal description of fatigue process so far. Fatigue calculations methods of construction elements are based on low- cycle properties of materials which are determined experimentally according to proper standards [3]. Lack of stability of cyclic properties of metals leads to serious problems in their description, usually in the form of fatigue characteristics (Wöhler, Manson – Coffin [4, 5] and Ramberg-Osgood [6] curves).

The question of cyclic properties stabilization of metals was widely analysed in the paper [7]. The earlier mentioned characteristics are determined in stress (Wöhler *S-N* curves) or strain approach (Manson-Coffin ε_a -$2N_f$ curves and Ramberg-Osgood σ-ε curves).

Wöhler curves are used for calculations in the area of so called high- cycle fatigue (HCF), where elastic strains of the material are dominant in the area of fatigue cracks initiation, Manson-Coffin and Ramberg-Osgood curves, on the other hand, are applied in the calculations in the area of low – cycle fatigue (LCF), where plastic strains are dominant in the crack area.

As the standard of qualification of the mentioned HCF and LCF areas the plasticity limit R_e is accepted, which in the case of metals is determined in the static tensile test. This limit does not correspond with the conditions of cyclic loading and is a weak criterion [8-10]. Another doubt is concerned with the assumption that under constant amplitude loadings (constant stress amplitude σ_a or constant total (ε_{ac}) or plastic (ε_{ap}) strain amplitude) there is observed stabilization of cyclic properties. As it was proved in the paper [4] cyclic properties of metals are the momentary properties – they are different in individual periods of fatigue process. The lack of stabilization is strongly visible in the case of variable amplitude loading, where every fluctuation of loading value leads to the change of cyclic properties of metals. In the case of random loadings, which are predominant under operating loadings, the change of the loading value (stress or strain) takes place “cycle after cycle”.

The recognition of the changes of cyclic properties under variable amplitude loadings which are located in HCF and LCF area is the main cognitive and utilitarian aim of this paper. An additional aims are:

- to prove the weakness of accepting plasticity limit R_e as the criterion of the loading qualification to HCF and LCF area,
- fatigue life determination under programmed loading,
- comparative analysis of the chosen mechanical parameters determined under monotonic and cyclic loadings.

2. Test description

The valuation of cyclic properties of the tested metals was based on stress-strain hysteresis loop parameters recorded during the tests from the first till the last cycle both under constant amplitude and programmed loading.

Program of the tests included five – step loading with the period of program including ten cycles (Fig. 1a). Tests were performed with the use of specimens made of C45 steel, 30HGSA steel and PA7 aluminium alloy (Fig. 1b). These materials differed significantly in their cyclic and monotonic properties.

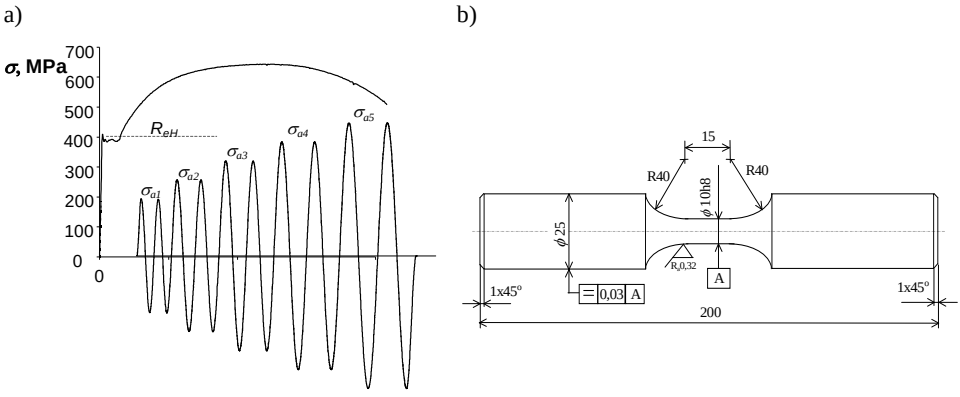

Fig. 1. Test description: a) loading program, b) specimen for the fatigue tests
Rys. 1. Opis badań: a) program obciążenia, b) próbki do badań zmęczeniowych

Diagrams of static tensile tests of the specimens made of the accepted materials were presented in Fig. 2 and strength parameters determined on their base in Table 1.

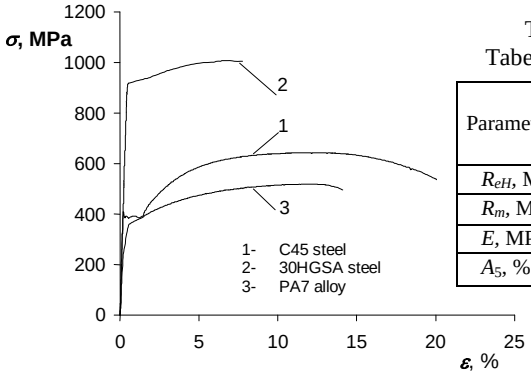

Table 1. Static tests results
Tabela 1. Wyniki prób statycznych

Parameter	Material		
	C45 steel	30HGSA steel	PA7 alloy
R_{eH}, MPa	446.3	936.7	321.7
R_m, MPa	713.3	1030	514.7
E, MPa	215000	207000	75000
A_5, %	22	9,5	16

Fig. 2. Diagrams of static tensile tests
Rys. 2. Wykresy rozciągania próbek

Constant amplitude loadings were performed on five levels of total strain ε_{ac} = const. On each level there were performed three fatigue tests. Hysteresis loops in respective periods of fatigue process were recorded. As the criterion of the fatigue test ending the occurig of deformation of hysteresis loop arm in the half – cycle of squeezing (occuring of the twist) was accepted. Sampling time of the loading force and strain signals was equal 0.025 s which at frequency of loading f = 0.2 Hz allowed for description of hysteresis loop with 200 points. Tests parameters under constant amplitude loadings are presented in Table 2.

Table 2. Parameters of constant amplitude loadings
Tabela 2. Parametry obciążeń stałoamplitudowych

Scheme of the program	Parameters	
	C45 steel, 30HGSA steel	PA7 alloy
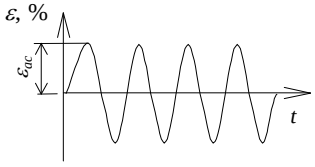	ε_{ac} = 0.35% ε_{ac} = 0.5% ε_{ac} = 0.8% ε_{ac} = 1.0% ε_{ac} = 2.0% f = 0.2 Hz	ε_{ac} = 0.50% ε_{ac} = 0.65% ε_{ac} = 0.80% ε_{ac} = 1.0% ε_{ac} = 1.5% f = 0.2 Hz

Controlling parameter during the tests under programmed loading was the force converted into stress. The rate of the stress growth was equal 50 MPa·s^{-1}. For each sequence of programmed loading three fatigue tests were performed, just like under constant amplitude loading. During the tests under programmed loadings momentary values of the loading force and strain for the whole chosen loading blocks with the volume of n_o = 10 cycles were recorded. Program of loadings was carried out by the way of repeating the program blocks until failure. Values of the stress amplitudes on individual steps of tested materials were given in Table 3.

Table 3. Parameters of programmed loadings
Tabela 3. Parametry obciążeń programowanych

Material	Stress amplitude on the step σ_{ai}					
	σ_{a1}	σ_{a2}	σ_{a3}	σ_{a4}	σ_{a5}	σ_{a6}
30HGSAsteel	510	570	630	690	750	810
C45 steel	200	260	320	380	440	-
PA7 alloy	325	350	375	425	450	475

3. Tests results

The examples of hysteresis loops for one strain amplitude level ε_{ac} = 0,8% were shown in Fig. 3. To make the diagrams more transparent there were drawn only three characteristic loops for each material: 1 - for the first cycle, 2 - for the cycle from the half - life of the specimen and 3 - for the cycle corresponding with the total life.

a)

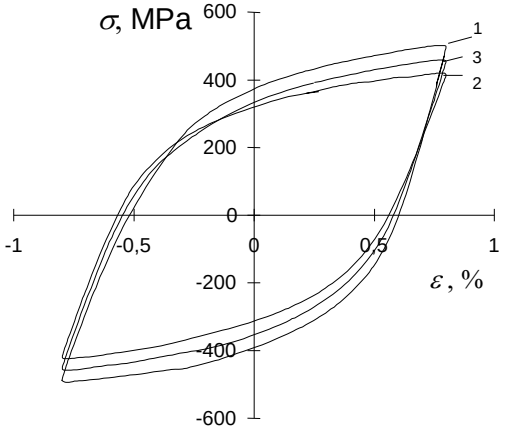

b)

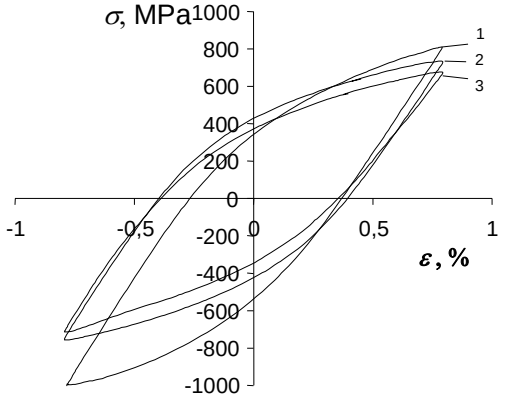

c)

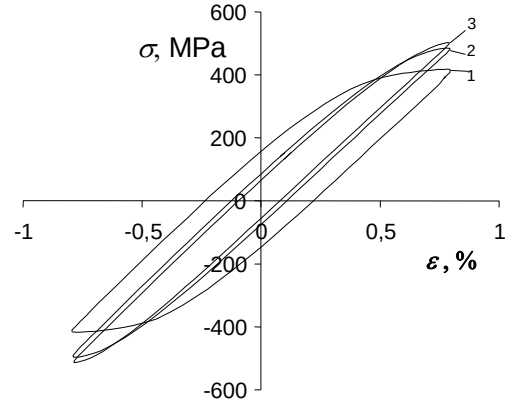

Fig. 3. Examples of the hysteresis loop taken from the begining (1), from the middle (2) and from the end (3) of fatigue life: a) specimens of 30HGSA steel, b) specimens of PA7 alloy, c) specimens of C45 steel

Rys. 3. Przykładowe pętle histerezy z początku (1), środka (2) i końca (3) okresu trwałości: a) próbki ze stali 30HGSA, b) próbki ze stopu PA7, c) próbki ze stali C45

Location and shape of the chosen hysteresis loops show the significant differences of the cyclic properties of the tested materials in the context of cyclic hardening or softening. General view of the fluctuations of hysteresis loop parameters on all accepted levels of total strain amplitude (Table 2) was presented in Fig. 4 and the list of average life values in Table 4.

Table 4. Fatigue life under constant amplitude loadings
Tabela 4. Trwałość w warunkach obciążeń stałoamplitudowych

Material	Strain amplitude ε_{ac}, %						
	0,35	0,5	0,65	0,8	1,0	1,5	2,0
C45	21167	4952	-	995	567	-	127
30HGSA	25417	5500	-	1467	830	-	133
PA7	-	3767	702	192	97	28	-

The course of the example diagrams for C45 steel and PA7 alumunium alloy presented in Fig. 4 allows for the quantitative valuation of hardening or softening phenomenon of the tested materials and, moreover, it enables the valuation of the accepted assumption concerning the cyclic properties stabilization periods of the materials during fatigue calculations. The above issue will be described in the analysis of tests results (point 4).

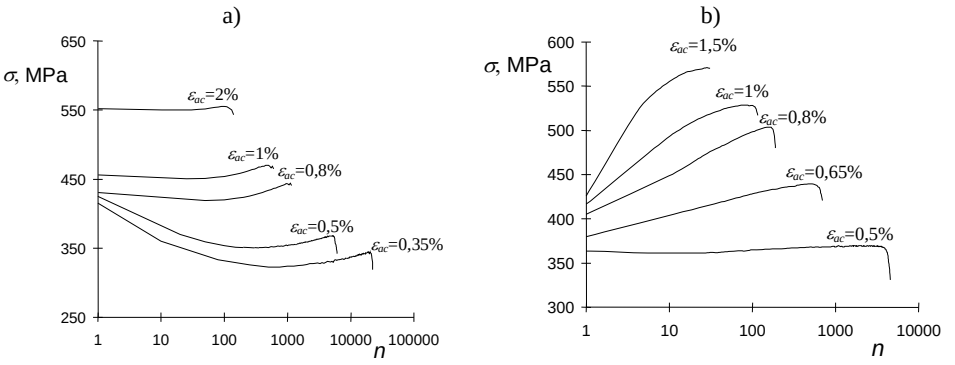

Fig. 4. σ_a values in the relation to the cycles number of constant amplitude loading: a) specimens of C45 steel, b) specimens of PA7 aluminium alloy
Rys. 4. Wartości σ_a w zależności od liczby cykli obciążenia stałoamplitudowego: a) próbki ze stali C45, b) próbki ze stopu aluminium PA7

More complex hardening and softening processes occur in the case of variable amplitude loading: programmed or random. It was illustrated in Fig. 5-7 by drawing the chosen hysteresis loops for the first block of programmed loading and for the block recorded in the half – life. Results for C45 steel were shown in Fig. 5, for 30 HGSA steel in Fig. 6 and for PA7 aluminium alloy in Fig. 7.

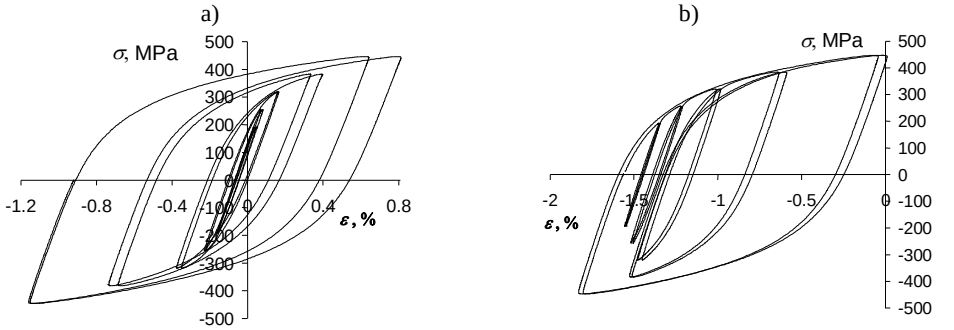

Fig. 5. Hysteresis loops obtained under programmed loadings of C45 steel specimens: a) first block of loading program, b) block from the half - life
Rys. 5. Pętle histerezy uzyskane w warunkach obciążeń programowanych próbek ze stali C45: a) pierwszy blok programu obciążenia, b) blok z połowy trwałości

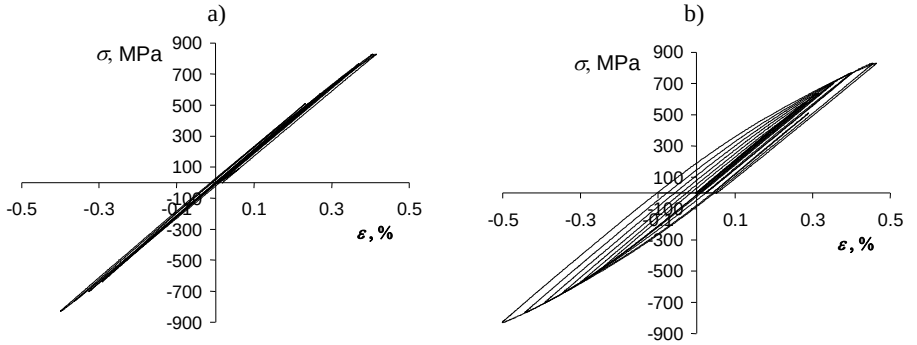

Fig. 6. Hysteresis loops obtained under programmed loading of 30HGSA steel specimens: a) first block of loading program, b) block from the half – life
Rys. 6. Pętle histerezy uzyskane w warunkach obciążeń programowanych próbek ze stali 30HGSA: a) pierwszy blok programu obciążenia, b) blok z połowy trwałości

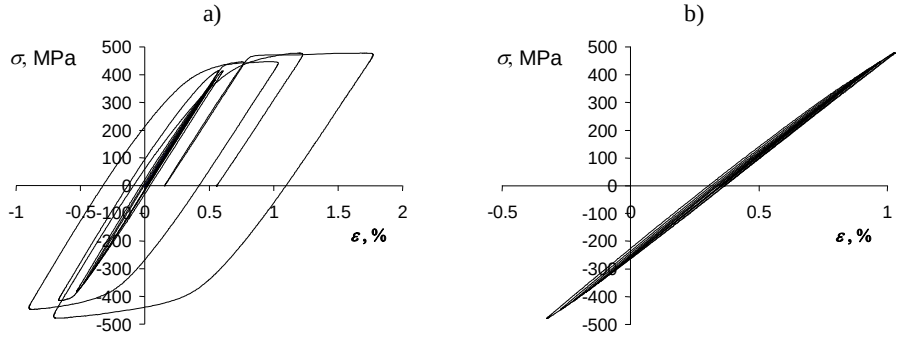

Fig. 7. Hysteresis loops obtained under programmed loading of PA7 alloy specimens: a) first block of loading program, b) block from the half – life
Rys. 7. Pętle histerezy uzyskane w warunkach obciążeń programowanych próbek ze stopu PA7: a) pierwszy blok programu obciążenia, b) blok z połowy trwałości

Basing on the diagrams presented in Fig. 5-7, it can be found that under programmed loading with the force (converted into stress) as controlled parameter there occurs the cyclic creeping phenomenon, which significantly, negatively influences the analysis of tests results. It is visible in the case of C45 steel (Fig. 5) and PA7 aluminium alloy (Fig. 7). In considered tests fatigue life was also determined. These data were presented in Table 5.

Table 5. Fatigue life under programmed loadings
Tabela 5. Trwałość zmęczeniowa w badaniach programowanych

Material	Fatigue life N	
	Number of blocks	Number of cycles
Stal C45	98	979
Stal 30HGSA	31	305
Stop PA7	139	1388

Fatigue life results given in Table 5 can be used in experimental verification of the calculation methods. Because of the limited volume of this paper these methods are not described here.

4. Analysis of obtained results

4.1. Constant amplitude loadings

Basing on the tests results presented in point 3 it is possible to determine cyclic strain diagrams σ-ε (Ramberg-Osgood) and fatigue diagrams ε_a -$2N_f$ (Manson-Coffin) applied in fatigue calculations in low- cycle fatigue (LCF) area. These diagrams were presented in Fig. 8-10. On each of these drawings there was placed diagram of cyclic strain at the background of monotonic tensile test diagram (figures a) and fatigue diagrams (figures b).

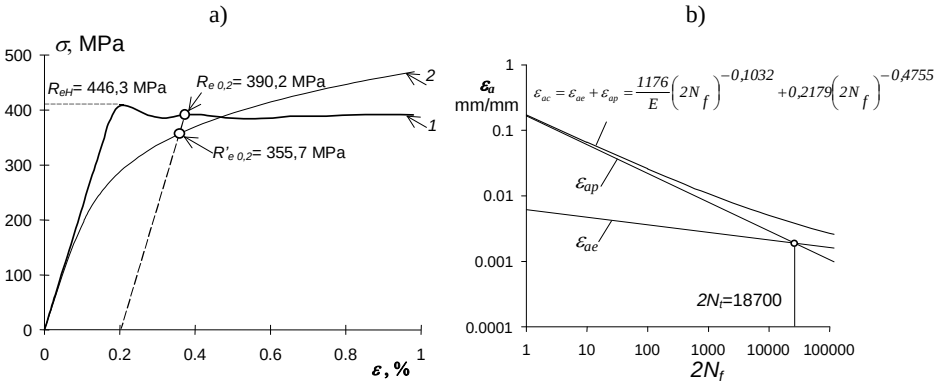

Fig. 8. C45 steel: a) diagram of the monotonic tensile test – 1 and cyclic strain diagram – 2, b) fatigue diagram

Rys. 8. Stal C45: a) wykres monotonicznego rozciągania – 1 i wykres cyklicznego odkształcenia – 2, b) wykres zmęczeniowy

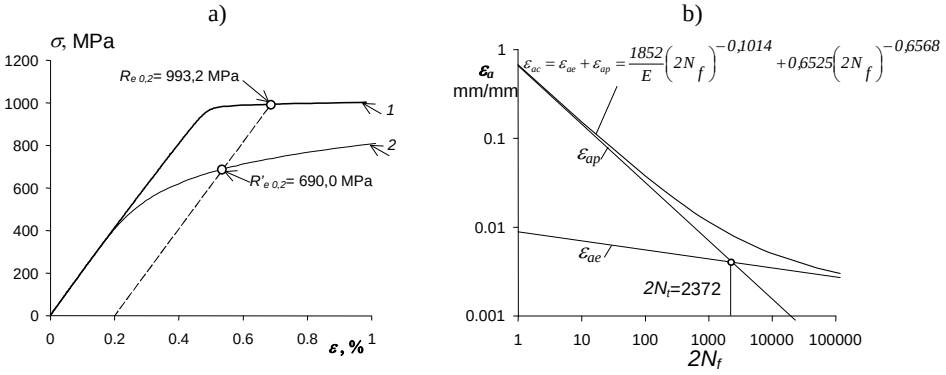

Fig. 9. 30 HGSA steel: a) diagram of the monotonic tensile test – 1 and cyclic strain diagram – 2, b) fatigue diagram

Rys. 9. Stal 30 HGSA: a) wykres monotonicznego rozciągania – 1 i wykres cyklicznego odkształcenia – 2, b) wykres zmęczeniowy

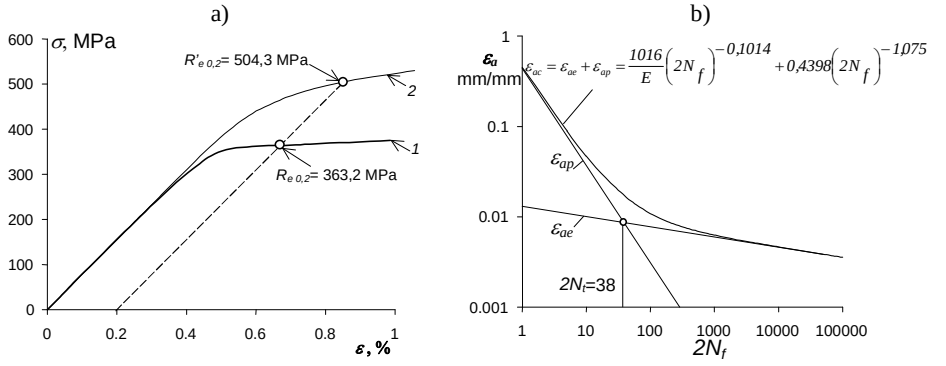

Fig. 10. PA7 alloy: a) diagram of the monotonic tensile test – 1 and cyclic strain diagram – 2, b) fatigue diagram

Rys. 10. Stop PA7: a) wykres monotonicznego rozciągania – 1 i wykres cyklicznego odkształcenia – 2, b) wykres zmęczeniowy

The examples of hysteresis loops presented in Fig. 3 and especially fluctuations of hysteresis loop parameters on all strain levels accepted in the tests which are presented in Fig. 4 demonstrate the lack of full stabilization of cyclic properties of tested materials. This fact seriously complicates determination of cyclic strain diagram (σ-ε) and fatigue diagram (ε_a-$2N_f$). Mentioned diagrams, shown in Fig. 8-10, were determined on the base of parameters of hysteresis loop recorded in fatigue half-life.

An analysis of the influence of hysteresis loop parameters fluctuations in different periods of fatigue process on the course of (σ-ε) and (ε_a-$2N_f$) diagrams were presented in paper [4]. It results from that analysis that cyclic properties of metals are "momentary" properties and depend on fatigue degree of these metals. Not considering this fact in calculations may lead to serious discrepancies between calculations and tests results.

4.2. Criterion of low-cycle fatigue

In fatigue calculations of the construction elements in the case of plastic strains occuring in the areas of fatigue cracking there are applied methods using cyclic strain diagrams (σ-ε) and fatigue diagrams (ε_a-$2N_f$) corresponding with low-cycle fatigue (LCF) area. As the criterion of low-cycle fatigue the following condition is widely accepted:

$$\Delta\sigma \leq 2R_e \text{ for } R=-1 \text{ or } \sigma \leq R_e \text{ for } R \neq -1 \tag{1}$$

In the case when there is no distinct plasticity limit R_e, the stress value is accepted for which plastic strain is equal 0.2% ($\sigma = R_{e0.2}$). Basing on the data given in Fig. 8-10 it can be found that differences between plasticity limit R_e or $R_{e0,2}$ and cyclic plasticity limit $R'_{e0,2}$ are considerable and depend on that if material undergoes cyclic hardening or softening. It results from Fig. 8a that C45 steel for the amplitude $\sigma_a \leq R_e$ undergoes cyclic softening then for $\sigma_a > R_e$ undergoes cyclic hardening. Value of cyclic plasticity limit $R'_{e0.2}$ = 355.7 MPa is lower from plasticity limit R_{eH} = 446.3 MPa.

In the case of 30 HGSA steel which, as it results from Fig. 9a, undergoes strong cyclic softening these values are equal respectively $R_{e0,2}$ = 993.2 MPa and $R'_{e0,2}$ = 690.0 MPa. Cyclic plasticity limit $R'_{e0,2}$ of this steel is much lower than plasticity limit $R_{e0,2}$.

Different situation is in the case of strongly hardening PA7 aluminium alloy (Fig. 10a) for which $R_{e0.2}$ = 363.2 MPa and $R'_{e0,2}$ = 504.3 MPa, so the cyclic plasticity limit $R'_{e0.2}$ is much higher than plasticity limit $R_{e0.2}$.

It results from the above comparison that accepting plasticity limit R_e or $R_{e0.2}$ as the criterion of valuation of low-cycle fatigue area is burdened with considerable error for two reasons:

- accepting in the fatigue analyses the values of parameters, including plasticity limit, from monotonic tensile tests is unreliable because of the course of failure processes diversification,
- lack of possibility to determine the relation between the values of plasticity limit R_e (or $R_{e0.2}$) and cyclic plasticity limit $R'_{e0.2}$ makes it difficult to work out the criterion of low-cycle fatigue area on the base of R_e (or $R_{e0.2}$) value, so more reasonable is accepting $R'_{e0.2}$ as the criterion value.

4.3. Programmed loadings

LCF area loadings with stress as controlled parameter generate, beside the fatigue damage effect, the phenomenon of cyclic creeping, which was shown in point 3 while discussing results of programmed loading tests. Cyclic creeping demands verification of boundary plastic strain condition in calculation of construction elements and these problems are not considered in this paper.

Interesting from the point of view of fatigue calculations is the question of the relationship of programmed loading hysteresis loop to the diagrams of cyclic strain. In order to compare the location of cyclic strain diagrams (3) and hysteresis loops the centring of the loops to the begining of coordinate system was made. Results of these actions were presented in Fig. 11 for C45 steel, in Fig. 12 for 30HGSA steel and in Fig. 13 for PA7 alloy. For the illustrations there were chosen loops which correspond with the lowest values of amplitudes (Fig. 11a, Fig. 12a, Fig. 13a) and with the highest values of amplitudes (Fig. 11c, Fig. 12c, Fig. 13c) according to Table 3. In order to illustrate hardening and softening processes under programmed loading there were drawn hysteresis loops from the first block of program (marking – 1) and from the middle block corresponding with fatigue half-life (marking – 2).

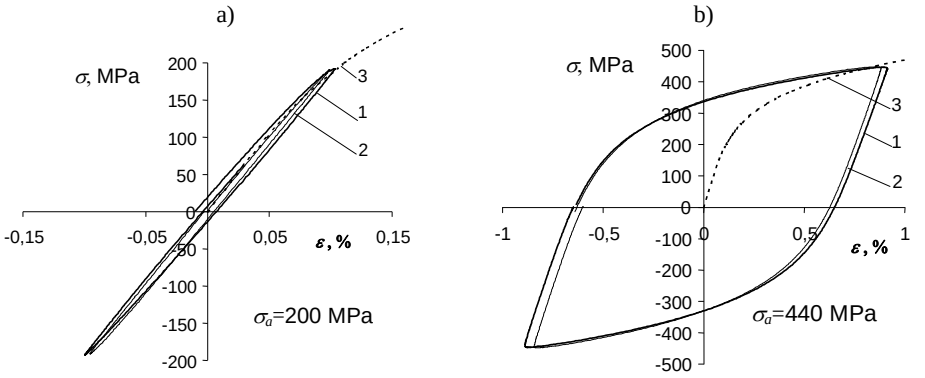

Fig. 11. Hysteresis loops obtained for C45 steel specimens under programmed loadings on the background of cyclic strain diagram

Rys. 11. Pętle histerezy uzyskane dla próbek ze stali C45 w warunkach obciążeń programowanych na tle wykresu cyklicznego odkształcenia

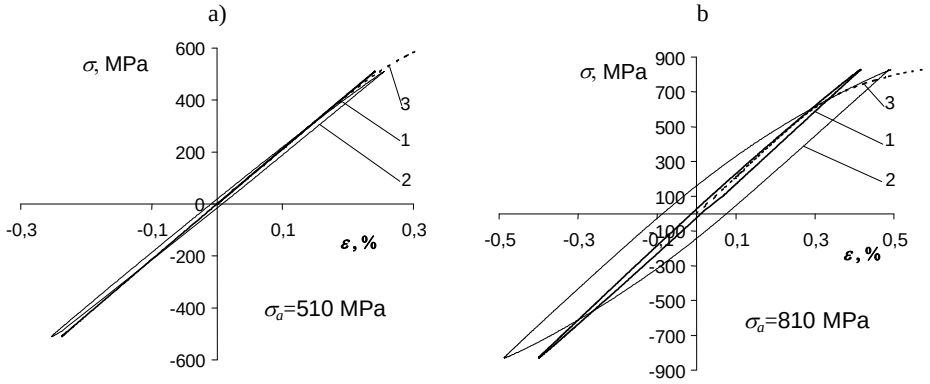

Fig. 12. Hysteresis loops obtained for 30 HGSA steel specimens under programmed loadings on the background of cyclic strain diagram

Rys. 12. Pętle histerezy uzyskane dla próbek ze stali 30 HGSA w warunkach obciążeń programowanych na tle wykresu cyklicznego odkształcenia

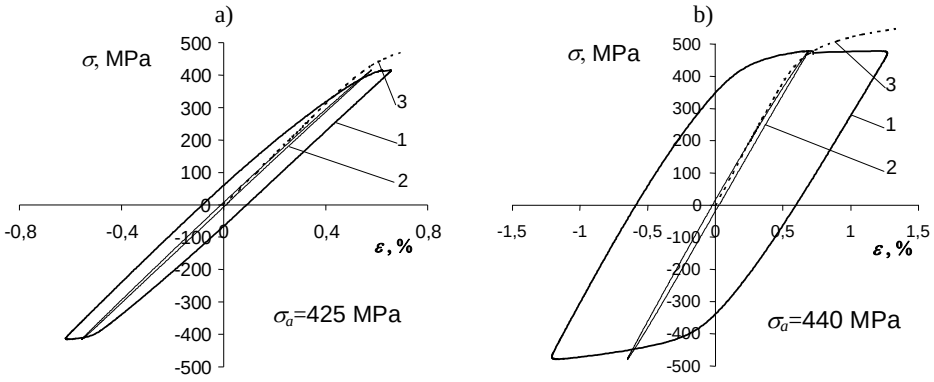

Fig. 13. Hysteresis loops obtained for PA7 aluminium alloy specimens under programmed loadings on the background of cyclic strain diagram
Rys. 13. Pętle histerezy uzyskane dla próbek ze stopu aluminium PA7 w warunkach obciążeń programowanych na tle wykresu cyklicznego odkształcenia

In all mentioned cases the apexes of hysteresis loop (from fatigue half-life) were approximately located on cyclic strain diagrams. The above observation has fundamental significance in fatigue life calculations of construction elements which are based on local stresses and strains method because it enables the transformation of diagrams of variable in time stress or stress programs into diagrams of variable in time strain or strain programs. This transformation is essential because it is necessary to use fatigue diagrams (ε_a-$2N_f$) in LCF area calculations.

Presented observation also proves that it is possible to use the method of gradually increasing cyclic loading in determination of cyclic strain diagram with the use of single specimen and with stress (stress amplitude) as controlled parameter.

5. Conclusions

1. Methods of fatigue life calculations in low-cycle fatigue area demand that one should know fatigue characteristics in the strain or energy approach. In the strain approach they are cyclic strain diagrams (σ-ε) and fatigue diagrams (ε_a-$2N_f$). In these calculations the transformation of loadings in the form of variable in time stresses into strain courses is necessary. Analysis of tests results showed that in the case of variable amplitude stress programs this transformation can be performed with the use of cyclic strain diagram.
2. The comparison of the properties determined under monotonic loading with the cyclic properties of the tested metals alloys showed considerable

differences of these properties which were generated by cyclic hardening (PA7 aluminium alloy) or softening (30HGSA steel). In the case of C45 steel after initial softening there took place considerable cyclic hardening of the material.

3. The basic parameter, important from the point of view of fatigue calculations, is plasticity limit and elasticity module. Comparison of tensile tests diagrams and cyclic strain diagrams showed the high agreement of elasticity module and essential differences in the values of plasticity limit and cyclic plasticity limit.
4. Analysis of the tests results showed that plasticity limit of metals R_e used for determination of low-cycle fatigue area is an approximate criterion, which do not correspond with the process of failure in metals under cyclic loading.
5. The suitable parameters accepted as the valuation criterion of low-cycle fatigue area are these which are related to the cyclic properties of metals, for example cyclic plasticity limit determined from cyclic strain diagram which is necessary in fatigue calculations of construction elements under loadings generating local plastic strains.

The paper was presented at the VI International Symposium of Materials and Constructions Failure Mechanics in Augustów in 2011 and was published in Polish language in "Acta Mechanica et Automatica" quarterly vol. 5 no. 3 (2011), publication of Faculty of Mechnical Engineering of Bialystok Univeristy of Technology.

This article was created on the base of tests results funded by MNiSzW in the framework of the project NN 503222139.

References

[1] Kocańda S., *Zmęczeniowe pękanie metali*. WNT, Warszawa 1985.
[2] Kocańda S., Kocańda A., *Niskocyklowa wytrzymałość zmęczeniowa metali*. PWN, Warszawa 1989.
[3] Kocańda S., Szala J., *Podstawy obliczeń zmęczeniowych*. PWN, Warszawa 1997.
[4] Manson S.S., Behaviour of materials under conditions of thermal stress. NACA TN – 2933, 1953.
[5] Coffin L.F., A study of the effects of cyclic thermal stresses on a ductile metal. Trans. ASME 76, 1954, 931-950.
[6] Ramberg W., Osgood W.R., Description of stress-strain curves by three parameters. NACA, Tech. Note 402, 1943.
[7] Mroziński S., *Stabilizacja własności cyklicznych metali i jej wpływ na trwałość zmęczeniową*. Wydawnictwo Uczelniane Uniwersytetu Technologiczno-Przyrodniczego w Bydgoszczy, Rozprawy Nr 128, 2008.
[8] Duyi Y., Zhenlin W., *A new approach to low cycle fatigue damage based on exhaustion of static toughness and dissipation of cyclic plastic strain energy during fatigue*. International Journal of Fatigue 23, 2001, 679-687.

[9] Duyi Y., Zhenlin W., *Change characteristics of static mechanical property parameters and dislocation structures of 45# medium carbon structural steel during fatigue failure process.* Materials Science & Engineering A297, 2001, 54-61.
[10] Szala J., Ligaj B., Szala G., *Wytrzymałość wstępnie cyklicznie obciążonych próbek ze stopu aluminium D16CzATW*. XIX Sympozjum Zmęczenie i Mechanika Pękania, Pieczyska k. Bydgoszczy, 2002, 373-382.
[11] Procedury FITNET (*Fitness - for - service NETwork*).

Zagadnienie cyklicznego umocnienia lub osłabienia metali w warunkach obciążenia programowanego

S t r e s z c z e n i e

Zjawisko cyklicznego umocnienia lub osłabienia metali i ich stopów jest znane od ponad 40 lat. Mimo tak długiego okresu badań brak jest ogólnego opisu uniwersalnych modeli tych zjawisk. Podstawą w ich ocenie są badania doświadczalne prowadzone w warunkach obciążeń sinusoidalnych stałoamplitudowych. Wyróżnia się badania ze stałą amplitudą naprężenia lub stałą amplitudą odkształcenia. Warunki te nie są równoważne w zakresie obciążeń, w których nie obowiązuje prawo liniowej zależności naprężenia od odkształcenia. Zagadnienie cyklicznego umocnienia lub osłabienia metali oraz ich stopów istotnie komplikuje się w przypadku zmiennoamplitudowych obciążeń, które są charakterystyczne dla obciążeń eksploatacyjnych elementów konstrukcyjnych.

W pracy opisano badania własności cyklicznych trzech stopów metali: stopu aluminium PA7 silnie umacniającego się cyklicznie, stali stopowej 30HGSA- podlegającej silnemu cyklicznemu osłabieniu oraz stali konstrukcyjnej C45, która w zależności od poziomu obciążenia ulega cyklicznemu osłabieniu lub cyklicznemu umocnieniu. Badania przeprowadzono w warunkach programowanych obciążeń ze stopniowo rosnącą amplitudą naprężenia.